



AMERICAN UNIVERSITY OF BEIRUT

SEISMIC PERFORMANCE ENHANCEMENT OF STEEL  
BOLTED MOMENT CONNECTIONS

by  
SANA NAJIB EL KALASH

A dissertation  
submitted in partial fulfillment of the requirements  
for the degree of Doctor of Philosophy  
to the Department of Civil and Environmental Engineering  
of the Faculty of Engineering and Architecture  
at the American University of Beirut

Beirut, Lebanon  
July 2019

AMERICAN UNIVERSITY OF BEIRUT

SEISMIC PERFORMANCE ENHANCEMENT OF STEEL  
BOLTED MOMENT CONNECTIONS

by  
SANA NAJIB EL KALASH

Approved by:

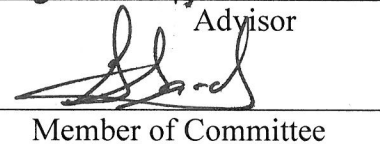
Dr. Salah Sadek, Professor  
Department of Civil and Environmental Engineering

  
Chair of Committee

Dr. Elie Hantouche, Assistant Professor  
Department of Civil and Environmental Engineering

  
Advisor

Dr. George Saad, Associate Professor  
Department of Civil and Environmental Engineering

  
Member of Committee

Dr. Camille Issa, Professor  
Department of Civil and Environmental Engineering  
Lebanese American University

  
Member of Committee

Dr. Antoine Gergess, Professor  
Department of Civil and Environmental Engineering  
University of Balamand

  
Member of Committee

Date of thesis defense: July 30, 2019

AMERICAN UNIVERSITY OF BEIRUT

THESIS, DISSERTATION, PROJECT RELEASE FORM

Student Name: El Kalash Sana Nejib  
Last First Middle

Master's Thesis       Master's Project       Doctoral Dissertation

I authorize the American University of Beirut to: (a) reproduce hard or electronic copies of my thesis, dissertation, or project; (b) include such copies in the archives and digital repositories of the University; and (c) make freely available such copies to third parties for research or educational purposes.

I authorize the American University of Beirut, to: (a) reproduce hard or electronic copies of it; (b) include such copies in the archives and digital repositories of the University; and (c) make freely available such copies to third parties for research or educational purposes  
after : **One --- year from the date of submission of my thesis, dissertation, or project.**  
**Two --- years from the date of submission of my thesis, dissertation, or project.**  
**Three --- years from the date of submission of my thesis, dissertation, or project.**

  
Signature

31/10/2019  
Date

## ACKNOWLEDGMENTS

I would like to acknowledge and thank my advisor, Dr. Elie Hantouche. His expertise, dedication and enthusiasm were essential in the successful development of this research work. I appreciate his constant support and valuable critics which helped me develop my research skills, and knowledge throughout the time spent at the American University of Beirut.

My recognition and gratitude are addressed to my committee members for their constant support and instructive comments: Dr. Salah Sadek, Dr. George Saad, Dr. Camille Issa, and Dr. Antoine Gergess.

Furthermore, I would like to gratefully acknowledge the financial support provided by the American University of Beirut Research Board under the PhD Scholarship and by the Lebanese National Council for Scientific Research under the AUB/CNRS-L PhD Scholarship 2017.

Finally, I would like to express gratitude to my family and friends for their support in the pursuit of my degree.

# AN ABSTRACT OF THE DISSERTATION OF

Sana Najib El Kalash for Doctor of Philosophy  
Major: Civil and Environmental Engineering

Title: Seismic performance enhancement of steel bolted moment connections

The damage of steel structures caused by recent earthquakes motivated the structural engineering profession to change the prescriptive design guidelines to accommodate for the performance-based seismic design approach. One of its characteristics is that steel structures are expected to go from the linear response to the non-linear response before failure. Thus, the pre-yielding as well as the post-yielding behavior of steel connections is of interest to the structural engineering community. The goal of this research is to investigate innovative techniques to enhance the seismic performance and to lower the fabrication cost of eight-bolt double Tee and extended endplate connections through experimental work and analytical modeling. Despite all the experimental tests and the analytical models conducted on double Tees and extended endplates, very few investigated the influence of the column flange size (thin, medium, and thick), bolt arrangement (circular and rectangular), and omission of continuity plates and stiffeners on the seismic performance. Most importantly, the prying phenomenon caused by the significant bending of the connection (*primary* prying for the circular bolt configuration) and the column flange (*secondary* prying) in bolted connections was not experimentally investigated in the literature and not yet included in the current prequalified connections for steel moment frames for seismic applications - *ANSI/AISC 358-16*. Those prying induced forces in the tension bolts might cause unexpected failure of the connection leading to collapse of moment resisting frames and thus need to be accounted for in the design process.

To address the abovementioned shortcomings, first, seven specimens are conducted on double Tee connections subjected to monotonic and cyclic loading. The results of these tests are used to develop stiffness and strength models that predict the behavioral characteristics of the column flange/connection system. This aims at including the *secondary* prying strength check and associated column failure mode to the *ANSI/AISC 358-16* to ensure a safe design. Second, eight specimens are conducted in extended endplate connections with circular bolts configuration subjected to monotonic and cyclic loading. The data collected from the experimental study and finite element (FE) parametric modeling lead to the development of a strength model that predicts the capacity of extended endplate connections with circular bolts configuration including prying effect. The circular bolt configuration enhances the ductility and energy dissipation of the connection and ensures an equal distribution of tensile forces among all bolts. Also, design guidelines, that include total prying check, are proposed for extended endplate connections with circular

bolts configuration to be incorporated in future *ANSI/AISC 358*. Third, FE fracture models that incorporate material damage and plasticity are developed, calibrated, and validated against the experimental results of this research and from the literature. The current building design codes are limited to predicting the response of steel structures up to yielding and no consideration for predicting the post-yielding behavior is yet proposed. Thus, the FE fracture model predicts the post-ultimate strength and ductility required in seismic applications. Also, all failure modes are covered whether fracture initiates in the base or bolt material due to tensile and/or shear loadings. This included failure in the connection (column flange, endplate, bolts, etc.) or in the beam section (alternate block shear, net section fracture). Fourth, full scale extended endplate connections with circular bolt configuration with reduced beam section (ranging from W18 to W24) are designed and virtually tested, using FE analysis, subjected to cyclic loading. The connections satisfy the requirements for both intermediate and special moment resisting frames.

This research aims at improving the seismic response of double Tee and extended endplate connections at a lower fabrication cost. Also the fracture modeling constitutes a first step towards developing new design guidelines for failure after first component fracture.

# CONTENTS

Page

ACKNOWLEDGMENTS .....	v
ABSTRACT .....	vi
ILLUSTRATIONS .....	xiii
TABLES .....	xvii

Chapter

I. INTRODUCTION AND LITERATURE REVIEW .....	1
A. Introduction .....	1
B. Literature review .....	5
II. GOALS AND OBJECTIVES .....	19
III. SECONDARY PRYING OF COLUMN FLANGE IN TEE- CONNECTIONS: EXPERIMENTAL INVESTIGATION AND MECHANICAL MODELING .....	22
A. Experimental program.....	23
1. Component test .....	23
2. Component test results .....	27
a. Interior and exterior bolt force.....	31
b. Energy dissipation .....	34
B. Mechanical model .....	35
1. Bolt mechanical model .....	39
2. Failure modes .....	40



a.	Bolt fracture .....	40
b.	Column flange partial yielding followed by bolt fracture 40	
c.	Mixed mode .....	41
d.	Flange mechanism .....	41
3.	Model performance .....	41
C.	FE modeling .....	43
1.	Geometric and force boundary conditions .....	43
2.	Material Properties .....	43
3.	Model discretization .....	44
a.	Analytical modeling.....	44
b.	Energy dissipation .....	45
D.	Conclusions .....	46
<b>IV.</b>	<b>PRYING EFFECT IN UNSTIFFENED EXTENDED ENDPLATE CONNECTION WITH CIRCULAR BOLTS CONFIGURATION .....</b>	<b>49</b>
A.	Experimental program.....	49
1.	Component tests .....	49
2.	Component results .....	54
a.	Failure modes.....	54
b.	Load-displacement.....	54
c.	Bolt force .....	56
B.	FE validation .....	59
1.	Description of the connection model.....	59
2.	Comparison of FE predictions with experiments .....	60
C.	FE parametric study.....	61
1.	Description of the connection model.....	61

2. Results .....	62
D. Strength model .....	64
1. F1: Endplate flexural mechanism and B1 and B2 fracture.....	66
2. F2: Column flange/endplate flexural mechanism and B4 fracture	67
3. F3: Column flange flexural mechanism and B4 fracture .....	68
4. Total prying forces .....	68
E. Design procedure and example.....	69
F. Conclusions.....	72
<b>V. METHODOLOGY AND APPLICATION OF DUCTILE FRACTURE MODELING ON BOLTED STEEL CONNECTIONS .....</b>	<b>74</b>
A. Introduction .....	74
B. Methodology of FE fracture modeling in <i>ABAQUS</i> .....	75
1. Ductile damage .....	75
2. Shear damage.....	76
3. Material Definition .....	77
4. Damage Evolution .....	78
5. Methodology.....	79
C. Material calibration .....	80
1. SMCS .....	80
2. Hooputra .....	83
D. Validation.....	84
1. Geometric, force boundary, and material properties .....	84
2. Model discretization .....	86
3. Comparison of FE predictions with experiments .....	87

a.	El Kalash and Hantouche [64] .....	87
b.	El Kalash and Hantouche [69] .....	90
c.	Coelho et al. [65] .....	93
d.	Piluso and Rizzano [66] .....	95
e.	Kiamesh [67] .....	97
f.	Massimo et al. [13] .....	99
g.	Sun et al. [68] .....	101
E.	Conclusions .....	103
<b>VI.</b>	<b>FE FRACTURE MODELING APPLICATION: ALTERNATE BLOCK SHEAR IN BEAMS.....</b>	<b>105</b>
A.	FE fracture model.....	107
1.	Numerical results.....	107
a.	Geometric, force boundary, and material properties.....	107
b.	Model discretization.....	108
c.	Comparison of FE predictions with experiments .....	108
B.	Conclusions .....	111
<b>VII.</b>	<b>SEISMIC PERFORMANCE OF FULL SCALE EXTENDED ENDPLATE CONNECTIONS WITH CIRCULAR BOLTS CONFIGURATION AND RBS .....</b>	<b>112</b>
A.	Design Procedure .....	113
1.	Prequalification limits .....	116
2.	Endplate and bolt design .....	118
3.	Column-side design .....	122
4.	Circular bolt pattern.....	124
5.	Reduced beam section - RBS .....	126
B.	FE modeling .....	127
1.	Description of the connection model.....	127

2. Results .....	128
<b>VIII. SUMMARY, CONCLUSIONS, AND RECOMMENDATIONS .....</b>	<b>135</b>
A. Summary and conclusions.....	135
B. Recommendations .....	137
<b>BIBLIOGRAPHY .....</b>	<b>138</b>
Appendix	
<b>I. APPENDIX A .....</b>	<b>147</b>
<b>II. APPENDIX B .....</b>	<b>155</b>
A. W21x62 beam section.....	155
1. Prequalification limits .....	155
2. Endplate and bolt design .....	156
3. Column-side design .....	159
4. Circular bolt pattern.....	160
5. Reduced beam section - RBS .....	162
B. W18x55 beam section .....	164
1. Prequalification limits .....	164
2. Endplate and bolt design .....	165
3. Column-side design .....	168
4. Circular bolt pattern.....	169
5. Reduced beam section - RBS .....	171

## ILLUSTRATIONS

Figure	Page
1. Moment-rotation curve.....	3
2. Moment-rotation curve of typical connections.....	3
3. Typical double Tee connection: (a) Profile view of connection, (b) Front view of column, (c) Top view of connection.....	9
4. (a) Test setup and instrumentation, (b) Experimental setup.....	26
5. Load-Total flange displacement: (a) TM1, (b) TC1, (c) TM2.....	28
6. Load-Total flange displacement: (a) TC2, (b) TM3 and TC3, (c) TM4	29
7. Load-Total flange displacement: monotonic specimens.....	31
8. Interior bolt force vs. applied load.....	33
9. (a) Column flange geometry, (b) Decision tree for half of the column flange.....	36
10. Load-Total flange displacement: Mechanical model (MM) vs. Experiment (Exp.).....	42
11. Bolt force-Load of TM2: Mechanical model (MM) vs. Experiment (Exp.): (a) Interior bolt, (b) Exterior bolt.....	43
12. Load-Total flange displacement of rolled section: Mechanical model (MM) vs. FE.....	45
13. (a) Typical eight-bolt unstiffened extended endplate connection (b) Experimental setup.....	51
14. Test specimen.....	51
15. Load-Total displacement: Experiment vs. FE (a) Monotonic tests, (b) Cyclic tests.....	56
16. Bolt-force distribution- Experiment (exp.) vs. FE: (a) M2 (b) M5.....	57
17. Comparison of failure in experiment vs. FE: column flange mechanism	60
18. Load-Total displacement of FE parametric study.....	62

19.	Bolt-force distribution in FE parametric study: (a) for thick column flange specimens, (b) for thin column flange specimens.....	64
20.	Elements representation: (a) Endplate, (b) Column.....	66
21.	Endplate yield line mechanism.....	72
22.	Material Components [53].....	78
23.	A992: (a) Coupon 1 - mesh, (b) Coupon 1 - deformed shape, (c) stress vs. strain, (d) stress-triaxiality vs. strain at fracture.....	82
24.	El Kalash and Hantouche [64] –Load-displacement: Exp. vs. FE: (a) Monotonic, (b) Cyclic.....	88
25.	El Kalash and Hantouche [64] – Failure mode: Exp. vs. FE: (a) TM1, (b) TM2, (c) TM3, (d) TM4.....	90
26.	El Kalash and Hantouche [65] – Load-displacement: Exp. vs. FE: (a) Monotonic, (b) Cyclic.....	91
27.	El Kalash and Hantouche [65] – Failure mode: Exp. vs. FE: (a) M1, (b) M3-Column side, (c) M3-Endplate side, (d) M4.....	93
28.	Coelho et al. [66] – Load-displacement: Exp. vs. FE.....	94
29.	Coelho et al. [66] – Failure mode: Exp. vs. FE: (a) WT1g, (b) WT61b.....	95
30.	Piluso and Rizzano [67] – Load-displacement: Exp. vs. FE.....	96
31.	Piluso and Rizzano [67] – Failure mode: Exp. vs. FE: (a) A1, (b) B1, (c) C1, (d) D1.....	97
32.	Kiamanesh [68] – Load-displacement: Exp. vs. FE.....	98
33.	Kiamanesh [68] – Failure mode: Exp. vs. FE.....	98
34.	Massimo et al. [13] – Load-displacement: Exp. vs. FE.....	99
35.	Massimo et al. [13] – Failure mode: Exp. vs. FE: (a) Test 1, (b) Test 2, (c) Test 3.....	100
36.	Sun et al. [70] – Load-displacement: Exp. vs. FE.....	101
37.	Sun et al. [41] – Failure mode: Exp. vs. FE: (a) T1-test 3 (b) T2-test 3	102

38.	(a) Typical block shear failure path and (b) alternate block shear failure path in W beam section connected to thick plate.....	107
39.	Load-Displacement: Experiment (Exp.) vs. FE fracture: (a) MC1, (b) MC2, (c) MC3, and MC4.....	109
40.	Experiment vs. FE fracture paths: (a) ABS and (b) NSF.....	110
41.	Eight-bolt extended endplate connection with circular bolts configuration and RBS.....	115
42.	Connection details: W24x76.....	116
43.	Mesh and boundary conditions.....	127
44.	Moment-rotation: W24x76 beam.....	129
45.	Moment-rotation: W21x62 beam.....	130
46.	Moment-rotation: W18x55 beam.....	131
47.	Von Mises stress contours: (a) W24x76-beam, (b) W24x76-plate, (c) W21x62-beam, (d) W21x62-plate, (e) W18x55-beam, (f) W18x55-plate	134
48.	A572-50 & S355: (a) stress vs. strain, (b) stress-triaxiality vs. strain at fracture.....	147
49.	A36 & S275: (a) stress vs. strain, (b) stress-triaxiality vs. strain at fracture	148
50.	A490 & Grade 10.9: (a) stress vs. strain, (b) stress-triaxiality vs. strain at fracture.....	149
51.	A325 & Grade 8.8: (a) stress vs. strain, (b) stress-triaxiality vs. strain at fracture.....	150
52.	A572-50 & S355: (a) stress vs. strain, (b) stress-triaxiality vs. strain at fracture.....	151
53.	A36 & S275: (a) stress vs. strain, (b) stress-triaxiality vs. strain at fracture	152
54.	A490 & Grade 10.9: (a) stress vs. strain, (b) stress-triaxiality vs. strain at fracture.....	153
55.	A325 & Grade 8.8: (a) stress vs. strain, (b) stress-triaxiality vs. strain at fracture.....	154

56.	Connection details: W21x62.....	163
57.	Connection details: W18x55.....	172



## TABLES

Table		Page
1.	Test results.....	25
2.	Energy dissipation till first component failure.....	46
3.	Test parameters and results.....	53
4.	Parametric study tests matrix.....	61
5.	Strength model results.....	69
6.	Design example: summary of results.....	70
7.	Calibration of steel material.....	83
8.	Experiments details.....	86
9.	Tests geometrical characteristics.....	115

TO MY BELOVED FATHER

# CHAPTER I

## INTRODUCTION AND LITERATURE REVIEW

### A. Introduction

Current interest in performance-based design approach is being driven by a need for safety, economy, and flexibility. Particularly, providing safety of structures subjected to extreme events requires the engineer to design for and predict the post-yield forces and deformations of the steel framed connections. When it comes to steel structures, current design standards are limited to the pre-ultimate state of the structure ignoring all behavioral characteristics of steel material post-ultimate till full fracture. This research is part of an ongoing research to characterize the behavior of steel connections, including fracture, to ultimately improve existing design codes.

Beam-end-framing steel connections are used to connect beams and columns in steel structures. Two types of connecting elements are used in practice: welds and bolts. Fully welded steel moment connections, previously thought to be adequate for seismic applications, caused numerous failures during the 1994 Northridge and 1995 Kobe earthquakes. Subsequent investigations revealed that welded connections have several problems mainly characterized by low rotational ductility and weak connection performance under cyclic loadings. Alternative bolted moment connections, having low installation cost and high reliability, were needed to be investigated. The *Federal Emergency Management Agency, FEMA, 350* [1], prequalified several bolted connections for use in seismic applications. Bolted connections have been used for decades and have performed well in past earthquakes. Using bolted connections throughout the

structure provides a high level of redundancy and a level of stiffness comparable to that of fully welded connections.

The *ANSI/AISC 358-16* [2] defines moment resisting frames (MRFs) as frames that are designed to withstand inelastic deformations. Three types of steel MRFs exist: Ordinary Moment Frames (OMF), Intermediate Moment Frames (IMF), and Special Moment Frames (SMF). SMFs are designed to withstand significant inelastic deformations in their members and connections when subjected to high seismic loading. Steel connections associated with SMFs are expected to attain high stiffness, strength, and ductility characteristics. Connections used in SMFs must be prequalified prior to their use. The prequalification is based on a modest number of experiments that meet the requirements as per *ANSI/AISC-341-16* [3]. Eight-bolt double Tee and extended endplate connections have been included in the *ANSI/AISC 358-16* [2] prequalified connections manual due to their satisfactory seismic performance that met the prequalification requirements for SMFs.

A comprehensive characterization of the behavior of connections is the moment-rotation curve. A typical moment-rotation curve is shown in Fig. 1. Three main characteristics are shown: strength, stiffness, and ductility [4]. When considering strength, connections are classified as either full or partial strength depending on whether they are capable of transferring the full plastic moment of the connection beam element. With regard to stiffness, connections are classified as fully restrained, partially restrained, and simple connections depending on their service load stiffness. Finally connections are classified as brittle or ductile and certified for use in OMF, IMF, or SMF based on their ability to reach and sustain certain plastic rotational demands.

Moment-rotation curves of typical bolted steel connections are presented in Fig. 2. Double Tee and extended endplate connections are both classified as adequate for use in both IMFs and SMFs by the *ANSI/AISC 358-16* [2].

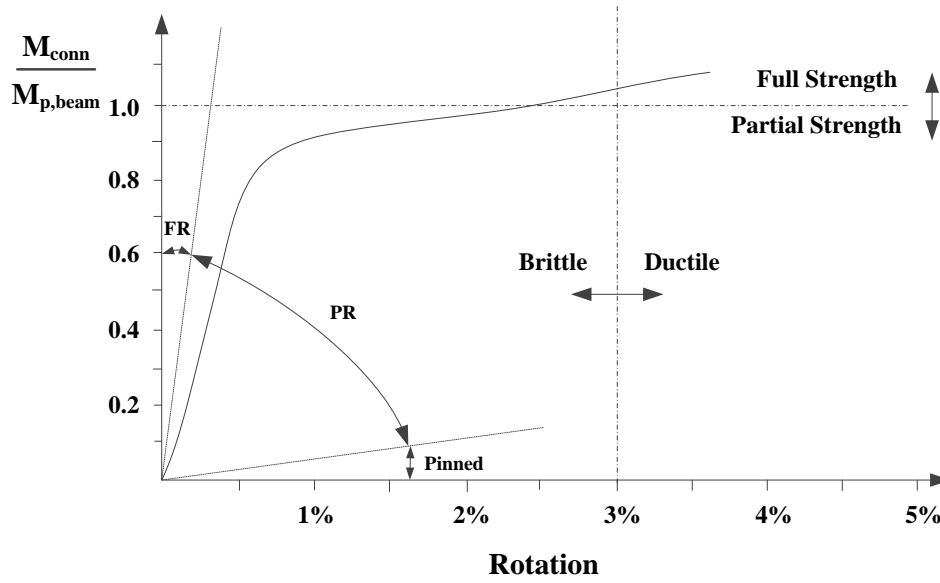


**Figure. 1.** Moment-rotation curve

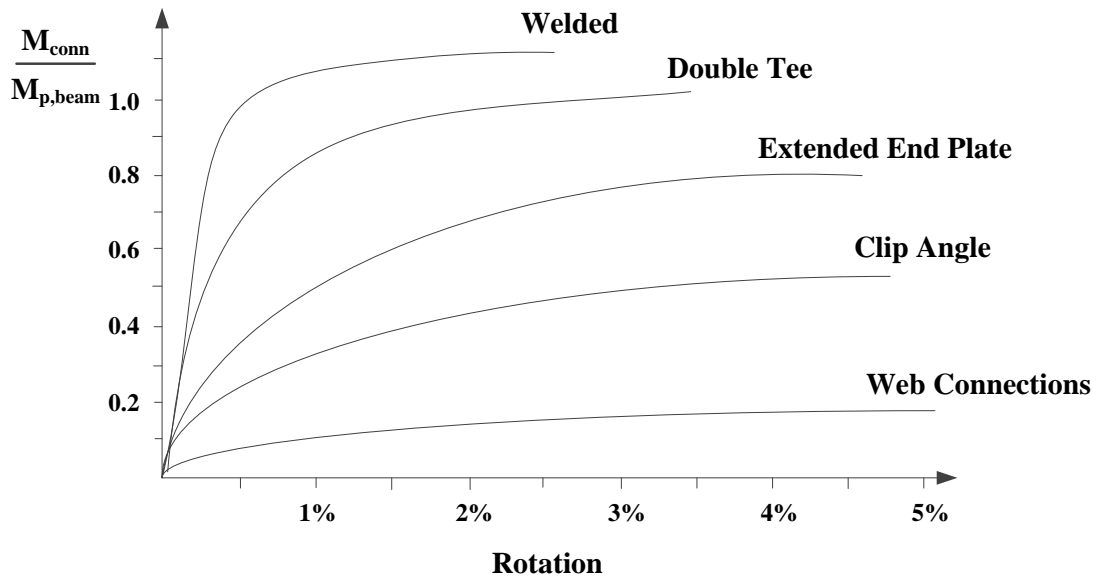


**Figure. 2.** Moment-rotation curve of typical connections

Accurate design of steel moment connections requires a proper prediction of the moment-rotation curve. This can be done using experimental tests, FE modeling, or analytical modeling. The experimental tests are the most accurate methods of predicting the moment-rotation curve of a connection; however, it is the most expensive and time consuming. Hence, limited experimental tests are usually done to calibrate and validate the remaining methods. The FE modeling is an efficient and accurate method to study the behavior of steel moment connections in the research domain. However, it is time consuming and complex when it comes to design engineers. For this purpose, researchers have come up with an analytical method that allows engineers to develop rationally the behavior of steel moment connections. That is, stiffness model, also known as the component method in the *Eurocode 3 part1-8* [5]. In this approach, the individual components of the connection are modeled by linear or nonlinear springs. Each of these springs is assigned a corresponding stiffness and then added to the system. All abovementioned methods are used in this research to investigate the double Tee and extended endplate connections not only under monotonic but also under cyclic (seismic) loading.

As previously mentioned, the current seismic design philosophy is shifting towards the performance-based design approach where ductile components of the structure are expected to undergo considerable cyclic plastic deformation to dissipate the energy released during a seismic event. The material stress-strain curve and fracture limit characteristics have a significant influence on the ability of these structural components to undergo large inelastic deformations. Furthermore, the stress-strain curve in the necking section decreases gradually instead of decreasing to zero rapidly. This implies that the steel material in the necking section still has load carrying capacity until the final fracture occurs. Also, most metals used in structures experience large plastic deformations before fracture occurs. Therefore, the prediction of ductile crack

formation (fracture initiation) appears to be an essential factor in the engineering design practice. Hence, it is important to be able to predict the fracture characteristics to incorporate them into the design and analysis procedures. For these reasons, explicit FE fracture modeling is used instead of the conventional implicit FE modeling to predict the steel moment connections response till full fracture. The developed FE fracture models predict the post-ultimate strength and ductility of connections required in seismic applications.

## **B. Literature review**

The purpose of this research is to investigate innovative techniques to ultimately enhance the seismic performance and lower the fabrication cost of both eight-bolt double Tee and extended endplate connections through experimental, FE fracture, and analytical analyses. The literature review focuses on both moment connections and on the fracture modeling.

In moment connections, continuity plates are often used to stiffen the column flange and web. However, detailing columns without continuity plates reduces the fabrication cost. Furthermore, in areas of high seismic risk, it is recommended to avoid welding in regions of potentially low notch toughness in wide flange sections and the corners of the continuity plates are required to be clipped [1, 3]. The *ANSI/AISC 358-16* [2] explicitly states in *the commentary section 13.5* that further research is needed before the requirement of including continuity plates can be relaxed. Thus, an investigation is required to study the effect of continuity plates' omission in double Tee moment connections subjected to seismic loading.

Bolted rolled double Tee moment connections have undergone extensive experimental and analytical investigations for the past two decades resulting in their prequalification in the *ANSI/AISC 358-16* [2] for use in seismic areas. The design approach is based on plastic hinging in the beam when used in SMFs or in combination with shear yielding of the column panel zone

when used in OMFs [1]. When addressing the column in double Tee moment connections, the following limit states are accounted for in the design procedure: flange flexural yielding, web yielding, web crippling, and panel zone shear failure.

One of the major behavioral characteristics associated with double Tee moment connections is the prying effect. Prying forces are defined as the additional tensile forces added to the tension bolts due to the flexural bending of the plates they are connected to. Prying can be divided into two types: (1) *primary* prying when the Tee flange undergoes flexural deformation and (2) *secondary* prying when the column flange undergoes bending [6]. The induced flexural deformation can cause unexpected failure of tension bolts leading to failure of the connection. All existing design codes consider the column flange as rigid where almost no deformation exists either by supplying thick column flange or by providing continuity plates. As mentioned earlier, *ANSI/AISC 358-16* [2] explicitly states that providing continuity plates eliminates the need to check for *secondary* prying.

Ductility-based design is being introduced into design codes to reduce the fabrication cost of steel moment connections while achieving the required seismic performance of structural members. The practice is to allow some inelastic deformations to occur in various elements of a connection to enhance its ductility and energy dissipation capacities without sacrificing its strength. In moment connections, continuity plates are often used to stiffen the column flange and web in order to resist large forces transmitted by the beam flange and to provide more ductile connection performance. However, detailing columns without continuity plates reduces the fabrication cost. Also, as mentioned earlier, in areas of high seismic risk, it is recommended to avoid welding in regions of potentially low notch toughness in wide flange sections and the corners of the continuity plates are required to be clipped as per *ANSI/AISC 341-10* [3] and the



*National Institute of Standards and Technology, NIST* [7]. As a result of omitting continuity plates in columns, column flange bending may cause *secondary* prying forces [2]. Thus, it is important to quantify the *secondary* prying forces in designing double Tee moment connections as an alternative of providing continuity plates, specifically for column flange thickness less than that of the Tee flange. And larger bolt diameter can be used to account for the additional forces caused by the flexural deformation of the column flange.

Extensive experimental, FE, and analytical research dealt with the characterization of the monotonic and cyclic behavior of double Tee moment connections. Strength and mechanical models were proposed and validated against experimental and FE results [8, 9, 10, 11, 12]. All developed models dealt only with *two-bolted* thin and medium thickness Tees associated with thicker column flanges. For such connections, three failure modes are defined: (1) full Tee flange yielding, (2) Tee flange yielding at the K-zone followed by bolt fracture, and (3) pure bolt fracture. However, in SMFs thick flange double Tee connections are needed with deep girders to resist the large moment expected. This may lead to a connection where the Tee flange is thicker than the column flange. All existing models focused on thin to medium thickness double Tees connected to rigid columns. A modification of existing models was needed to accurately predict the response of thick double Tee connections. Hantouche et al. [6, 8] proposed strength and stiffness models for thick Tees whereby partial yielding of the Tee flange occurs followed by bolt fracture. The authors also investigated numerically the effect of column flange deformation associated with thick double Tee connections in which the column flange is thinner than the Tee flange. It was concluded that, if continuity plates are supplied in columns, *secondary* prying becomes negligible [2, 6]. Moreover, the authors proposed a mechanical-based model to predict the behavior of thick double Tees including *primary* and *secondary* prying forces. However, no

experimental work was performed and their proposed model was limited to a mixed mode failure in the column flange where full plastification at the K-zone is followed by interior bolt fracture. For this reason, an experimental work is performed and a mechanical model is developed in this research to cover all failure modes encountered in column flange/bolt system associated with thick double Tee moment connections.

Limited research work has been performed on the behavior of columns in thick double Tee connections. In such connections, the column flange is *four-bolted* as opposed to the Tee flange which is *two-bolted* (Fig. 3). In spite of the extensive studies performed on the double Tee connections, the research of past decades has almost neglected looking at column flange with four bolts per row. Pisarek and Kozłowski [9] conducted two experimental tests on double Tees having four bolts per row subjected to monotonic loading. The authors proposed a strength model to predict the behavior of *four-bolted* Tees based on the virtual work method and a mechanical-based model that was limited to predicting the initial stiffness. Demonceau et al. [10] conducted experimental tests on extended endplates with four bolts per row. The authors suggested modifications to the strength model proposed by *Eurocode 3* [5] which is applicable to Tees with two bolts per row. More recently, Massimo et al. [13] studied the behavior and failure mechanisms of double Tee connections with four bolts per row under monotonic loading using FE analysis and validated their results against three experimental tests. The aforementioned literature has several limitations specifically in characterizing column flange associated with thick double Tee connections. In fact, only monotonic behavior of Tees with four bolts per row was investigated experimentally. Furthermore, interior and exterior tension bolts were assumed to carry equal forces in developing the strength and mechanical-based models which does not reflect the true behavior as per *ANSI/AISC 358-16 commentary section 13.5* [2]. Also, only initial

stiffness of the connection was predicted. Finally, the associated secondary prying forces that may lead to the unexpected failure of the connection were not investigated. No extensive cyclic experimental tests and no current design guidelines are available to characterize the behavior of four-bolted Tees despite their availability in structural applications. That is, the behavior of four-bolted Tees subjected to monotonic and cyclic loading is needed to be included in the standard codes.

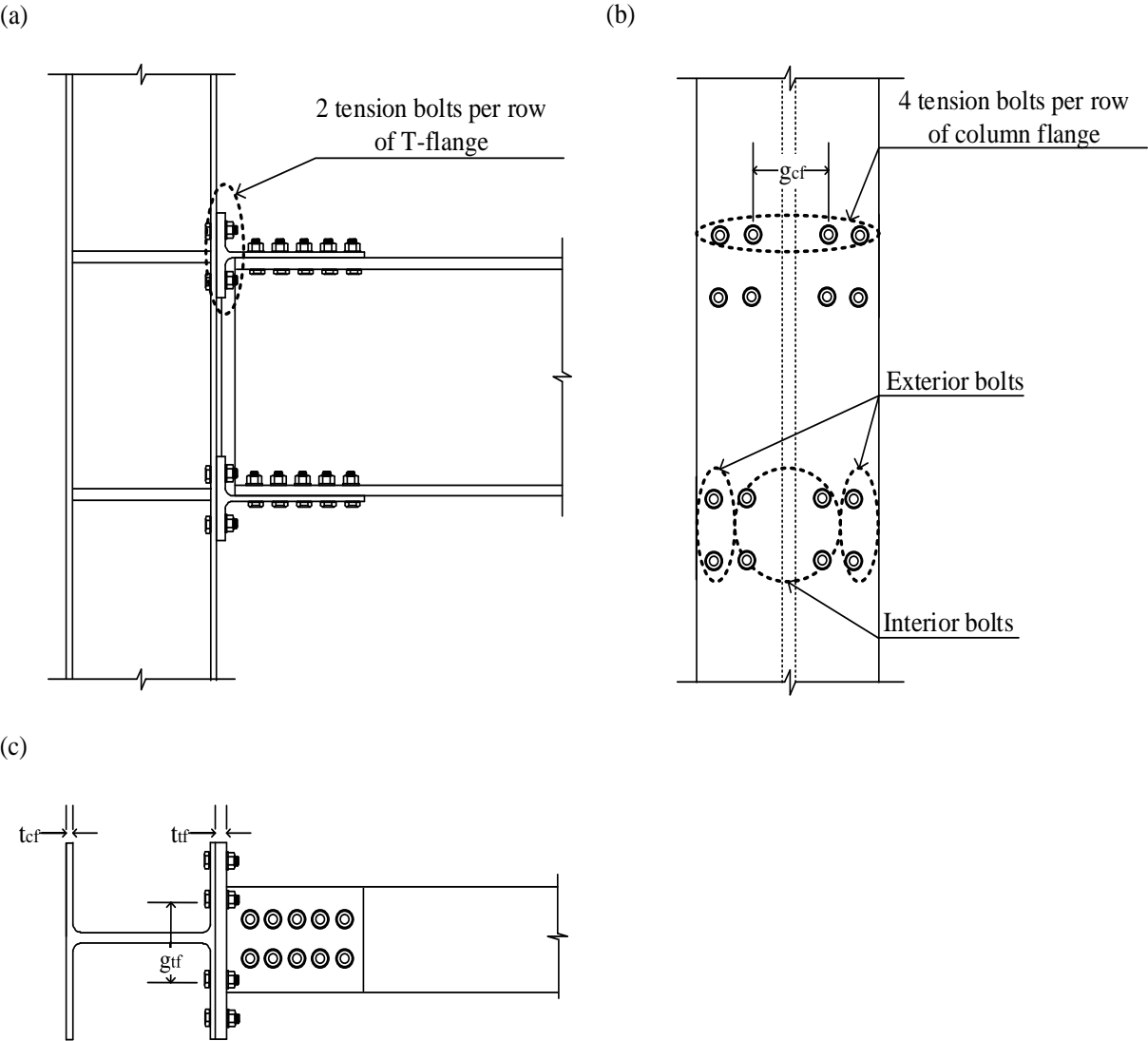


**Figure 3.** Typical double Tee connection: (a) Profile view of connection, (b) Front view of column, (c) Top view of connection

Besides double Tee moment connections, extended endplate connections are highly used in practice due to their satisfactory seismic performance. In fact, four-bolt stiffened/unstiffened and eight-bolt stiffened extended endplate connections are prequalified for use in SMF in both the *ANSI/AISC 358-16* [2] and *Eurocode 3 part 1.8* [5] design guidelines due to their large inter-story drift rotation capacities and associated ductile failure modes. Ongoing extensive analytical and experimental research is being performed to enhance the strength and ductility capacities of moment connections such as extended endplates using innovative solutions.

For beams with significant plastic moment capacity, eight-bolt extended endplate connection, as opposed to four-bolt extended endplate connection, must be used to develop the high moment capacity required between the column flange and endplate to exceed the moment capacity of the beam. Extensive FE, experimental, and analytical research have been performed on eight-bolt stiffened extended endplate [14, 15, 16, 17] to show that such connections perform well under high seismic loading. The performed research covers the strength, ductility, energy dissipation capacity, and all failure modes of such connections.

In the prequalified eight-bolt stiffened extended endplate connection, stiffener plates are welded between the end plate and the beam flanges: (1) to strengthen the extended portion of the end plate, (2) to force plastic hinging of the beam to occur away from the connection region, and (3) to promote uniform distribution of beam flange forces to the tension bolts. However, it is shown from experimental results in the literature that rupture of beam flange at the toe of the stiffener occurs due to the high stress concentration in this region [1]. For this reason, it is necessary to improve the seismic performance of the eight-bolt stiffened extended endplate connection.

One of the proposed connection enhancement techniques consisted of removing the stiffeners to eliminate the stress concentrations available in the conventional eight-bolt stiffened extended endplate connection. Also, to allow for an equal distribution of forces in the bolts, a connection with a circular bolt configuration was proposed.

Kiamanesh et al. [12] were the first to propose a circular bolt distribution to improve the seismic performance of eight-bolt unstiffened extended endplate connections. The authors performed one component experiment on the monotonic behavior of T-stubs with circular bolt configuration. Also, they studied the effect of various bolt diameters and endplate thicknesses on the bolt-force distribution in eight-bolt unstiffened connections having circular and rectangular bolt configurations using FE analysis. It was concluded that the circular distribution of tension bolts enhances the moment capacity, reduces pinching, and increases the energy dissipation capacity of the connection. Similarly, Schweizer [18] performed one full scale experiment to study the effect of circular bolt configuration on the cyclic behavior of eight-bolt unstiffened extended endplate connection. It was mainly concluded that an even distribution of beam flange force between all eight bolts can be achieved with the circular orientation of tension bolts. Hantouche and Mouannes [19] studied, using FE analysis, the effect of bolt configuration (circular or rectangular) and column flange thickness on the prying phenomenon (*primary* and *secondary*) encountered in eight-bolt unstiffened extended endplate connections having circular and rectangular bolt configurations. Also, the authors developed strength and stiffness models to predict the failure capacity and the response characteristics of such connections. Most recently, Morrison et al. [20] compared, using FE, the cyclic behavior of eight-bolt unstiffened extended endplate connection having circular bolt configuration to the conventional eight-bolt stiffened extended endplate connection. It was concluded that improved strength and post-yielding

stiffness are achieved as well as more uniform bolt-force distribution when having a circular bolt arrangement. The authors concluded that although thicker endplates may be required, the fabrication cost of the proposed connection is still less than that of the conventional one.

Despite all experimental tests and analytical models conducted on eight-bolt unstiffened extended endplate connections having circular bolt configuration as a method of enhancing the seismic performance of the stiffened moment connection, all researchers stressed out the need to perform additional experimental tests to prove the validity of the circular arrangement of tension bolts. Also, the influence of column size (thin, medium, and thick) on the response of eight-bolt unstiffened extended endplate connections with circular bolt configuration and the associated secondary prying forces were investigated using FE analysis only [19].

As previously mentioned, experimental tests are the most accurate method to predict the behavioral characteristics of steel bolted moment connections. However, the great cost and time efforts associated with this method requires researchers to seek more effective methods of analysis with acceptable accuracy. For this purpose, FE modeling is used to widen the bank of data available. All the previously mentioned FE analyses on double Tees and extended endplates were performed till first component yielding. However, it is important to predict moment connections response post-ultimate especially in seismic applications as mentioned earlier. Hence, FE fracture modeling is required to: (1) model the behavior of bolted moment connections pre-ultimate and post-ultimate, (2) predict the different limit states and failure modes, (3) predict the ductility and energy dissipation capacities of moment connections. For this purpose, the focus of the analytical modeling in this research is on FE fracture modeling.

Ductile fracture is the sequential process of necking, micro-voids formation, coalescence of micro-voids to form a crack (crack grows  $90^\circ$  to applied stress), crack

propagation by shear deformation, and fracture [21]. Crack formation, nucleation, growth, and linkage are very complex processes that depend on several factors most importantly are the material type, the geometry of the system under consideration, and the loading conditions.

McClintock [22] studied the void growth and coalescence process of plastic material and discovered the inverse proportionality between the strain at fracture and the hydrostatic tensile stress which is the mean of the principle stresses. Later on, Rice and Tracey [23] studied the behavior of spherical voids in elastic perfectly plastic materials and highlighted the high dependency between the rate of growth of micro-voids and the stress triaxiality in a material. The developed model (known as *Void Growth Model, VGM*) predicts the strain at fracture as a function of the void radius and stress triaxiality. Afterwards, Hancock and Mackenzie [24] based their ductile fracture model on the *VGM*. They developed a material-dependent relationship between the strain at fracture and the stress triaxiality only. They introduced the toughness index,  $\alpha$ , and the material parameter,  $\beta$ . This model marked the beginning of a new era for the uncoupled ductile fracture models and is known as the *Stress Modified Critical Strain* model (*SMCS*). Almost a decade later, Johnson and Cook [25] developed a cumulative fracture model based on the results of experimental tests on steel, copper, and iron. They concluded that fracture highly depends on hydrostatic stress but not much on strain rate and temperature. Hooputra [26] investigated the effect of shear stresses on void propagation. It was shown from experimental results of tensile, compressive, and shear tests that the strain at fracture is not only related to tensile stresses, but also to shear stresses.

In previous studies on void nucleation and coalescence the focus was on experimental and complex numerical models to try and understand the process of crack formation. Kanvinde and Deierlein [27, 28] compared the *VGM* and the *SMCS*. Both models were found to be accurate

with the latter model being easier to apply and covering a range of varying stress triaxiality. The authors also calibrated the toughness index,  $\alpha$ , and the characteristic length,  $l^*$ , over which the macro-crack propagates. Wierzbicki et al. and Bao [29, 30] performed a detailed study on ductile crack formation in tensile aluminum specimens. Myers et al. [31] also calibrated the steel material for use in the *SMCS* model. The authors noted the independency between  $\alpha$  and the specimen geometry. Wang et al. [32] compared the traditional and the ductile fracture mechanics for steel connections. The authors calibrated the steel material for use in the *VGM* and *SMCS* models and it was found that the traditional fracture mechanics approach is conservative in predicting failure due to fracture. Kiran and Khandelwal [33] developed a new micromechanical approach for ductile fracture simulation in which hardening of structural steel is accounted for. Cai [34] calibrated the A992 steel material for use in ductile fracture models when subjected to elevated temperatures. Jia et al. [35, 36] studied the effect of combined shear and tension on the ductile failure of structural steel material through experimental and FE studies. Also, they proposed a new ductile fracture model based on the *VGM* in which the material deterioration due to fracture propagation is taken into account. The proposed model is validated against pure shear and combined tension and shear cyclic loading tests on structural steels.

Ductile fracture models are incorporated in the FE software *ABAQUS*. Oh et al. [37] applied the *SMCS* model into *ABAQUS* using a user-defined subroutine. The proposed method is then validated against experimental results on pipes. Zhou et al. [38] validated the *SMCS* model against steel moment connections subjected to cyclic loading in *ABAQUS*. The authors included the fracture model in a user subroutine. Although no pictures were reported for the fractured model, comparison between experimental and FE results showed the accuracy of the model. More recently, Jia and Kuwamura [39, 40] developed a ductile fracture model based on the *VGM*



that can be easily applied in FE studies. The authors first proposed a method to determine the true stress-strain of materials including necking. Second, they developed the ductile fracture model and a damage accumulation variable based on Miner's rule. Third, they validated this model against FE simulations developed in *ABAQUS* for both monotonic and cyclic loadings. Kang et al. [41] studied the variation of two ductile fracture parameters of the *VGM* (material parameter  $\alpha$  and equivalent displacement at failure  $u_{eq}^f$ ) with the increasing stress triaxiality. FE results of the proposed ductile parameters agreed with experimental results of coupon tests. Wen [42] proposed a new ductile fracture model that includes the effect of shear stresses. The author included the model into *ABAQUS* via a user-defined subroutine and validated it against various steel connections subjected to monotonic and cyclic loadings. Also Wang et al. [43] proposed a new ductile fracture model and applied it to *ABAQUS* via a user-defined subroutine.

While fracture has been successfully predicted in steel coupon tests, very scarce research has been conducted to apply the developed and calibrated fracture models to predict the response of steel bolted moment connections. Furthermore, researchers have used different approaches into calibrating the proposed models which lead to discrepancies in the values of the fracture parameters for the same steel grade. Also, since the way voids nucleate, grow and link to form macrocracks is different for different materials, structures, and loading conditions; a combination of fracture criteria is needed to predict the response of moment connections. Thus, in this research, the *SMCS* and *Hooputra* ductile fracture models are applied in *ABAQUS* tackling various failure modes and limit states of bolted moment connections subjected to both tensile and shear loading conditions. A common method to calibrate both models is used and the generated fracture parameters are used in predicting the response post-ultimate.

The aim of this research is to improve the seismic performance of double Tees and extended endplates at a lower fabrication cost. Thus, in the light of the highlighted shortage in the corresponding literature:

- First, the results of a series of seven component tests on column flange/thick Tee connected back-to-back are presented and discussed providing all possible failure modes and yielding mechanisms encountered in the column flange. The component tests are subjected to both monotonic and cyclic loadings and cover the range of thin, medium, and thick column flanges connected to thick Tees. A proposed mechanical model is developed and is able to predict the strength, stiffness, ductility, and all possible failure modes of the column flange.
- Second, the behavior of eight-bolt extended endplate connection with circular bolts configuration under monotonic and cyclic loadings is experimentally investigated. The results of a series of component experimental tests and FE simulations are used to develop a strength model to predict the connection capacity and prying forces. The effect of the column flange thickness, the endplate thickness, and the bolt diameter on the connection performance and the prying forces are investigated. Based on the experimental and FE results, a design procedure and an example are proposed.
- Third, a methodology is presented to guide researchers to model the FE fracture of steel material subjected to combined tensile and shear loadings using the two built-in ductile damage models in ABAQUS (the Stress Modified Critical Strain (SMCS) and the Hooputra models). Then, several steel base material grades including A992, A572-50, A36 and A325 and A490 bolt material are calibrated for use in both ductile damage models (SMCS and Hooputra). Also, FE fracture models that incorporate

material damage and plasticity are developed and validated against experimental results, available in the literature, of double Tee and extended endplate connections subjected to monotonic and cyclic loadings.

- Fourth, the alternate block shear (ABS) failure in steel beams is investigated using FE fracture analysis. ABS might be a potential failure mode of beams in bolted connections subjected to pure tensile forces. The results of a series of four specimens are modeled in ABAQUS. FE fracture simulations, including tensile and shear fracture modeling, are developed to predict the experimental results after first component failure. The Rice and Tracey and the Hooputra models are associated with all steel materials to model their ductile damage under tensile and shear loading, respectively.
- Fifth, the behavior of full scale extended endplate connections with circular bolts configuration is investigated using FE analysis to widen their applicability in seismic areas. Despite all experimental tests and analytical models conducted so far on extended endplate connections with circular bolts configuration, the seismic performance of full scale extended endplates with circular bolts configuration is yet to be determined. To address the above-mentioned shortcoming, three full scale connections with medium to deep beam sections are designed and tested under a cyclic loading using FE analysis. A reduced beam section (RBS) is adopted to account for the beam flange stiffener removal. Results of these tests are used to: (1) validate the design recommendations of the newly proposed connection, and (2) classify the proposed connection for use in IMFs and SMFs.

### **C. Dissertation layout**

Chapters I, and II present the introduction, literature review, and goals and objectives of this research. The current chapter presents the dissertation layout. Chapter IV describes the experimental and analytical investigation of component eight-bolt double Tee connections subjected to monotonic and cyclic loadings. Chapter V describes the experimental, FE, and analytical investigation of component eight-bolt extended endplate connections with circular bolt configuration. Chapter VI describes a methodology, material calibration, and experimental validation of FE fracture models of steel base and bolt material subjected to monotonic and cyclic loading conditions. Chapter VII describes an application of the developed fracture model to steel beam sections that failed in ABS. Chapter VIII describes the analytical investigation of full scale eight-bolt extended endplate connections with circular bolt configuration and RBS. Chapter IX presents the summary, conclusions and recommendations of the research conducted. Appendices A and B present detailed results that are referenced in the chapters.

## CHAPTER II

### GOALS AND OBJECTIVES

The main goal of this research is to propose and investigate innovative techniques to enhance the seismic performance and reduce the fabrication cost of two bolted moment connections: eight-bolt double Tee and eight-bolt unstiffened extended endplate with circular bolt configuration through experimental and analytical analyses.

To achieve the above goal, the following objectives have been identified for this study:

1. Perform experimental tests on double Tee connections:
  - i) Seven component tests on column flange/thick double Tee connection system are designed and tested under cyclic (three specimens) and monotonic (four specimens) loadings.
  - ii) To examine the behavioral characteristics of the column flange associated with thick double Tee connection, the component tests are designed to have failure in the column flange/bolt system.
  - iii) *Secondary* prying effect are investigated, thus continuity plates are omitted in all but one control specimen.
2. Develop a mechanical model for double Tee connections:
  - i) A mechanical-based model is proposed to predict the force-deformation, bolt force variation, and failure mode of eight-bolt thick Tee connected to varying thickness column flange.
3. Perform experimental tests on extended endplate connections:

- i) Eight component tests on eight-bolt extended endplate connection system with circular bolt configuration are designed and tested under cyclic (three specimens) and monotonic (five specimens) loadings.
  - ii) To study the potential performance enhancement of the eight-bolt extended endplate connection: beam flange stiffeners are omitted and tension bolts are distributed in a circular pattern configuration and the column flange thickness is varied.
  - iii) Propose design guidelines with design examples for the extended endplate connection assembly with circular bolts configuration for use in high seismic areas.
4. Develop a strength model for extended endplate connections:
- i) Propose a new strength-based model to predict the failure load of extended endplates with circular bolt configuration for all possible failure modes in the endplate/column flange/bolt system.
5. Develop FE fracture models:
- i) Using the FE software package *ABAQUS*, calibrate the A992, A572-50, A36, S355, S275, A490, and A325 base and bolt steel material in order to model the fracture of steel material due to tensile and shear loadings.
  - ii) Reproduce the response of the tested connections pre-yielding and post-yielding using FE fracture analysis and predict all possible limit states and failure modes in bolted steel moment connections available in the literature.
  - iii) Apply the proposed FE fracture model to reproduce the response of beams in steel connections that fail in ABS.
6. Design and test full scale extended endplate connections:

- i) Propose a detailed design method for the eight-bolt extended endplate connection with circular bolt configuration and RBS.
- ii) Test the proposed connection under cyclic loading using FE analysis.
- iii) Classify the extended endplate with circular bolt configuration and RBS as adequate for use in IMFs and/or SMFs.

## CHAPTER III

### SECONDARY PRYING OF COLUMN FLANGE IN TEE- CONNECTIONS: EXPERIMENTAL INVESTIGATION AND MECHANICAL MODELING

The aim of this chapter is to investigate experimentally the effect of column flange on the monotonic and cyclic responses of thick double Tee moment connections detailed with and without continuity plates. Seven component tests (four monotonic and three cyclic) varying the column flange thickness connected back-to-back to thick Tee connections, are performed in the *Structural and Materials Laboratory* at the *American University of Beirut*. Also, a mechanical based model is proposed to predict the behavior of thin, medium, and thick column flange sections connected to thick double Tee connections. The proposed model is then validated against the experimental results. It is noted that the model accounts for the deformation of column flange, stem, and bolt system assuming no significant deformation of the Tee flange since it is rigid. It is noted that although an FE analysis provides additional dataset to simulate the behavior of column flange in thick Tee connections; however, the focus of this chapter is on conducting an experimental investigation and on developing a mechanical design model of column flange behavior including secondary prying effect. That is, eliminating the computational and time efforts associated with FE analysis. The results of this research provide a dataset to develop new design guidelines for double Tee moment connections detailed without continuity plates. This constitutes a significant change from the current practice which specifies that continuity plates be supplied for seismic applications.



## A. Experimental program

### 1. Component test

Seven component tests on column flange/thick double Tee connection system were designed and tested under cyclic (three specimens) and monotonic (four specimens) loadings. Component Tees (S355 steel) connected back-to-back, using eight tension bolts (grade 8.8), were tested to examine the behavioral characteristics of the column flange associated with thick double Tee connection. The component tests were subjected to axial load based on expected beam flange force in actual full strength moment connection and were designed to have failure in the column flange/bolt system to study the *secondary* prying effect.

All specimens had a Tee flange thickness of 40 mm (minimum design thickness to eliminate *primary* prying) associated with HEM450 (W18x175) beam. The Tee sections used were built-up sections since they can be designed to be stronger, stiffer, and more ductile than their rolled counterparts. The goal of this research is to study the effect of column flange thickness associated with thick double Tee connections used in SMF. For this purpose, thick Tee flanges were used to make sure no significant deformation exists. The column flange thickness used in the experiment ranged from 15 mm to 40 mm (covers all possible failure modes with column sections ranging from HEA320 to HEM450 (W12x53 to W18x175)). In fact, the thin column (15mm) was designed according to the minimum design thickness for flexural yielding, the thick column (40mm) was designed for the connection to fail by bolt fracture and the intermediate column (25mm) was designed for potential mixed mode failure. The intent was to study the column flange behavior associated with thick double Tee connections. Thus, built-up column sections were used to be able to vary the column flange thickness easily to cover all possible failure modes. It should be noted that the sections used in the experiment behaved

similar to rolled ones where no distress was observed in the welds. One specimen was designed with continuity plates in the column to eliminate the *secondary* prying effect and to quantify the net *primary* prying forces for all seven specimens. Recalling that the Tee sections used in the experimental study were identical for all specimens, the *primary* prying forces were equal for all seven specimens.

Table 1 shows the geometrical parameters of the specimens used in the experiment. Note that  $t_{cf}$  and  $t_{tf}$  are the thickness of column and Tee flange, respectively. Also,  $g_{cf}$  and  $g_{tf}$  are the gage distance of the column and Tee flange, respectively. According to the American practice, the ratio  $g_{tf}/t_{tf}$ , representing the slenderness ratio of the Tee flange, defines whether the Tee flange is thick, medium, or thin [44]. In *Annex J* of the *Eurocode 3*, Tee flanges are classified according to a parameter  $\beta$  that represents the ratio of flexural resistance of the flange to the bolt axial resistance [45]. To cover all possible failure modes of column flange/bolt system, the Tee flange was designed to be classified as thick for all specimens ( $3 \leq g_{tf}/t_{tf} = 3.75 \leq 4$ ) ( $\beta > 2$ ) [5, 44] whereas the column flange was designed to be classified as thin ( $g_{cf}/t_{cf} = 10$ ) ( $\beta < 0.7$ ) (TM1 and TC1), medium ( $g_{cf}/t_{cf} = 6$ ) ( $0.7 < \beta < 2$ ) (TM2 and TC2), and thick ( $g_{cf}/t_{cf} = 3.75$ ) (TM3, TC3, and TM4) [44, 45].

The test setup and instrumentation used in the experiment are shown in Fig. 4 Two LVDTs (LVDT 1 and 2) were used to measure the column flange deformation and two LVDTs (LVDT 3 and 4) were used to measure the Tee flange displacement. Also, four load cells were attached to the exterior bolts (Load cell 1 and 2) and interior bolts (Load cell 3 and 4) to measure the bolt force variation throughout the test.

**Table 1. Test results**

Test ID	$t_{cr}$ (mm)	$g_{cr}/t_{cr}$	$t_{tr}$ (mm)	$g_{tr}/t_{tr}$	Testing procedure	Failure mode	Maximum load (kN)*	Column flange deformation (mm)**	Column flange deformation (%)	Tee flange deformation (mm)***	Tee flange deformation (%)	Total flange deformation (mm)****	Total Prying (%)	Primary Prying (%)	Secondary Prying (%)	Interior bolt force (kN)	Exterior bolt force (kN)	Energy dissipation ( $\times 10^3$ kN.mm)*****
TM1	15	10	40	3.75	Monotonic	Flange mechanism	580	26	96	1	4	27	56	0	56	184	120	14
TC1	15	10	40	3.75	Cyclic	Flange mechanism	512	35	90	4	10	39	68	0	68	190	127	22
TM2	25	6	40	3.75	Monotonic	Mixed mode	610	9	75	3	25	12	21	0	21	196	165	6
TC2	25	6	40	3.75	Cyclic	Mixed mode	694	38	97	1	3	39	21	0	21	198	163	27
TM3	40	3.75	40	3.75	Monotonic	Partial yielding and bolt fracture	859	1	100	0	0	1	5	0	5	203	201	1
TC3	40	3.75	40	3.75	Cyclic	Partial yielding and bolt fracture	834	2	100	0	0	2	3	0	3	201	200	1
TM4	40	3.75	40	3.75	Monotonic	Bolt fracture	995	1	100	0	0	1	0	0	0	149	150	2

\*Maximum tensile force experienced during the test (not the load at failure)

\*\*Maximum tensile deformation at failure in the column flange. Obtained by averaging displacements of LYDTs 1 and 2

\*\*\*Maximum tensile deformation at failure in the Tee flange. Obtained by averaging displacements of LYDTs 1 and 2

\*\*\*\*Summation of Tee and column flange deformation at failure

\*\*\*\*\*Total energy dissipated till full failure of connection

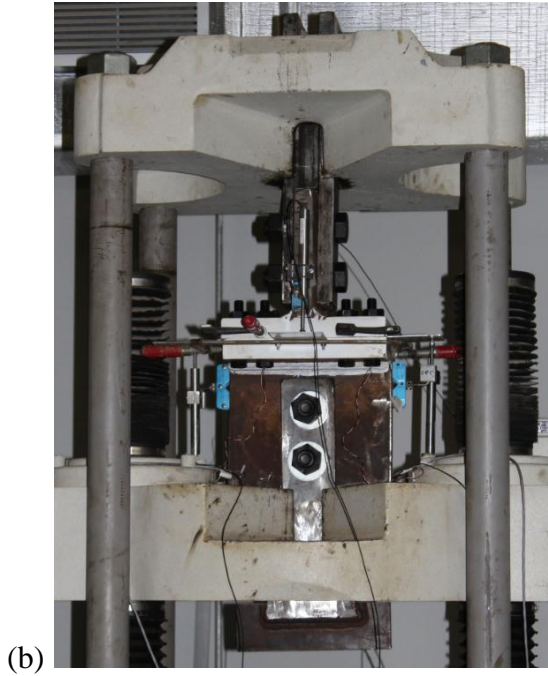
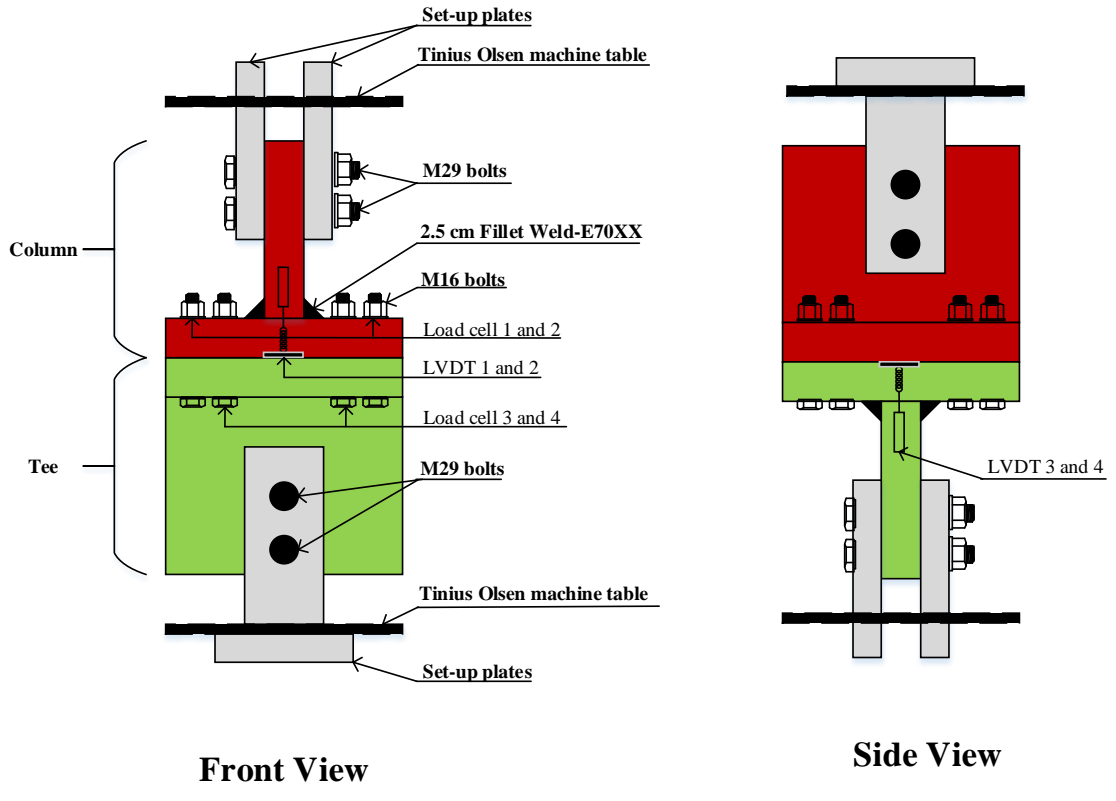


**Figure. 4.** (a) Test setup and instrumentation, (b) Experimental setup

Tension bolts in all specimens were preloaded, using direct torque control, according to the minimum pretension load specified by the *ANSI/AISC 360-16* [4]. The specimens were subjected to either a monotonically increasing load to failure (TM1, TM2, TM3, and TM4) or a cyclically variable load in tension (TC1, TC2, and TC3) similar to the *ANSI/AISC 341-16* seismic load history [3].

## ***2. Component test results***

The summary of the test results is presented in Table 1. Specimens TM1 and TC1 (having thin column flange thickness) failed due to column flange yielding mechanism followed by interior and exterior bolt fracture although this column flange thickness was designed according to the *ANSI/AISC 358-16* [2] for column flange flexural yielding failure mode. The load-total flange displacement curves and the failure mode of these specimens are shown in Figs. 5(a) and (b), respectively. It is noted that TC1 exhibited large energy dissipation and ductility capacities.

Specimens TM2 and TC2 (having medium column flange thickness) failed by mixed mode failure in the column flange/bolt system. This type of failure is characterized by plastic hinge formation at the K-zone followed by interior bolt fracture and followed later by exterior bolt fracture. The corresponding load-total flange displacement experimental curves and failure mode are shown in Figs. 5(c) and 6(a), respectively. Note that TM2 was expected to fail in mixed mode as previously mentioned; however, due to a defect in the set-up of this specific specimen, caused by manufacturing error, one interior bolt failed at an early stage.

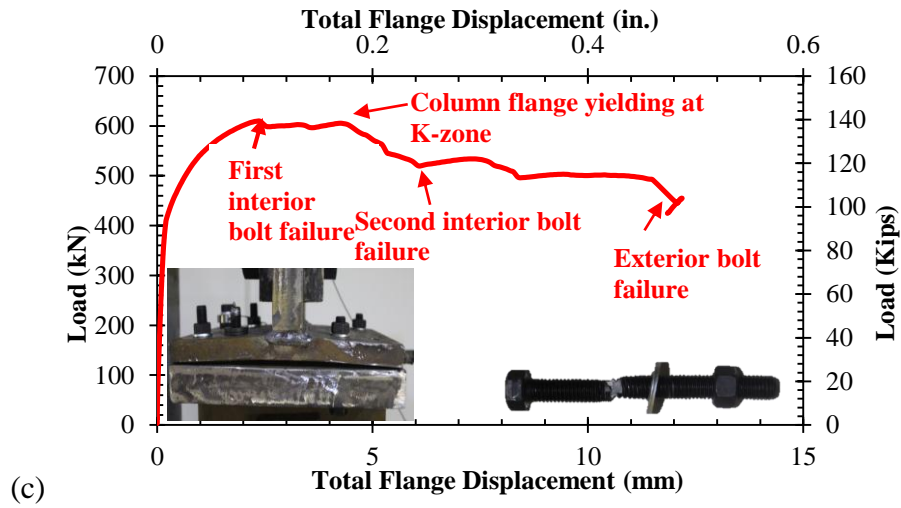
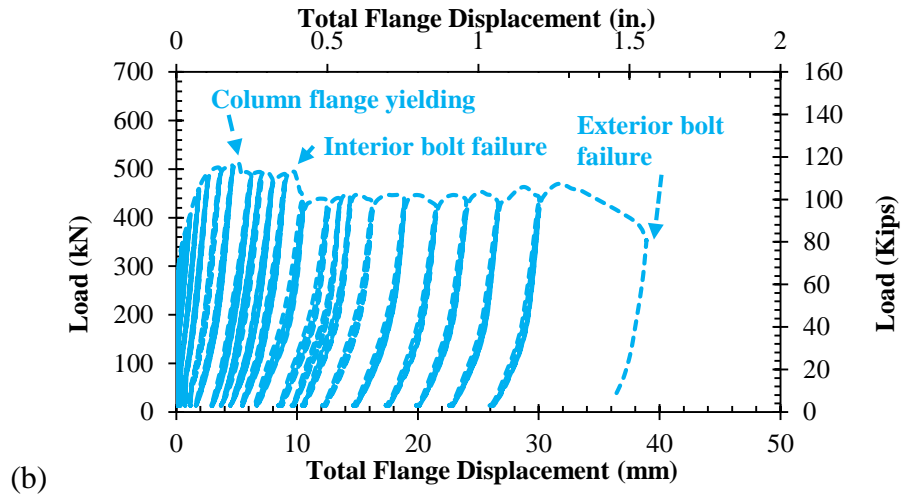
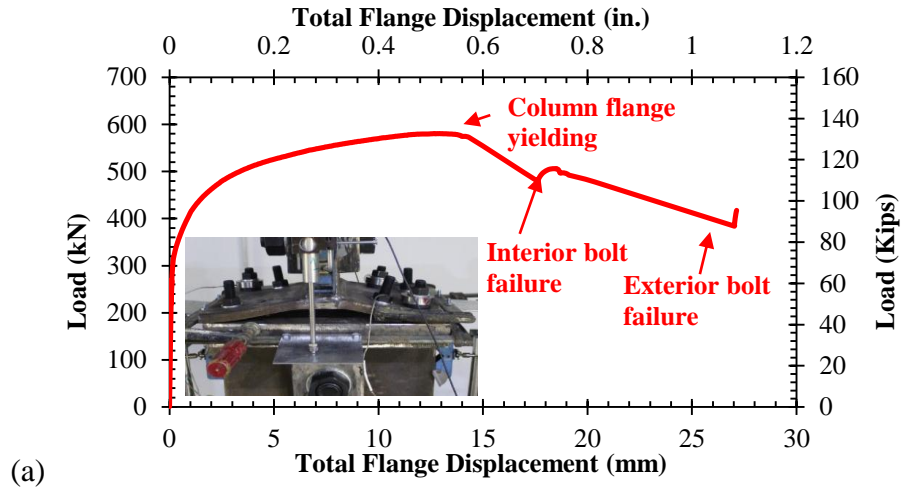


**Figure 5.** Load-Total flange displacement: (a) TM1, (b) TC1, (c) TM2

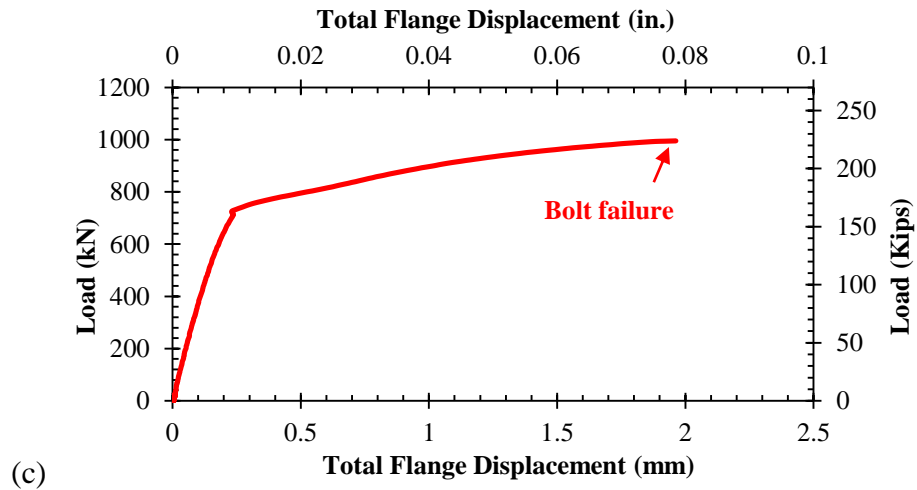
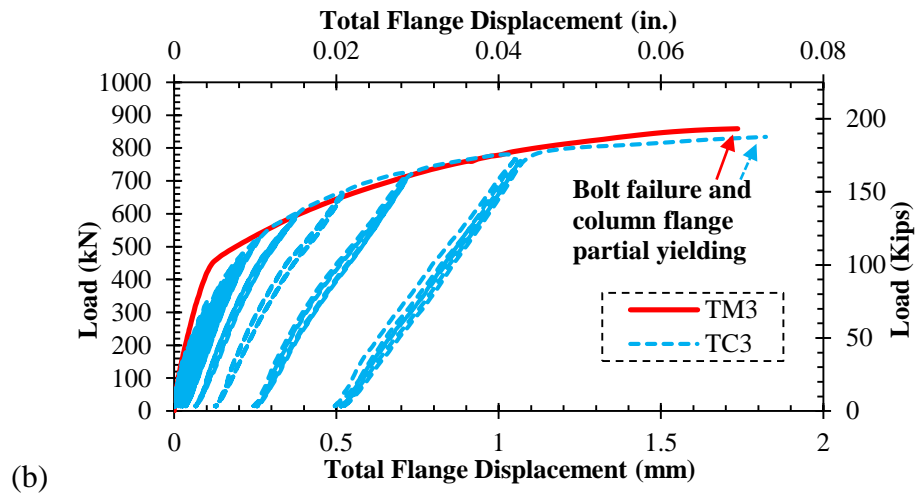
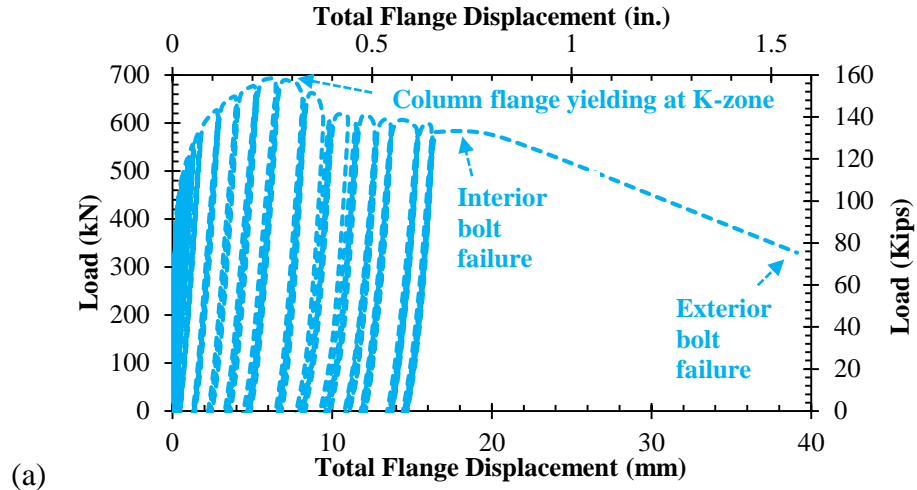


**Figure. 6.** Load-Total flange displacement: (a) TC2, (b) TM3 and TC3, (c) TM4

For all specimens associated with thin and medium thickness column flange (TM1, TC1, TM2, TC2), the Tee flange contributed to a maximum of 10 % of the total flange deformation. The major contributor to the overall deformation of the corresponding double Tee connection is the column flange (around 90 %).

Specimens associated with thick column flange and detailed without continuity plates failed by partial yielding of column flange at the K-zone followed by interior and exterior bolt fracture (TM3 and TC3). When supplying continuity plates (TM4), failure was due to fracture of all tension bolts. Figures 6(b) and (c) show the load-total flange displacement of these specimens, respectively. Results show that the use of thick column flange increased the stiffness and ultimate strength of the connection. Additional FE and analytical parametric studies, to further characterize the thick column flange detailed without continuity plates, are subject of future research.

Figure 7 shows a comparison of the monotonic load-total flange displacement response of all specimens. Results show that the initial stiffness and the maximum load increased with the column flange thickness whereas the plastic deformation capacity decreased.



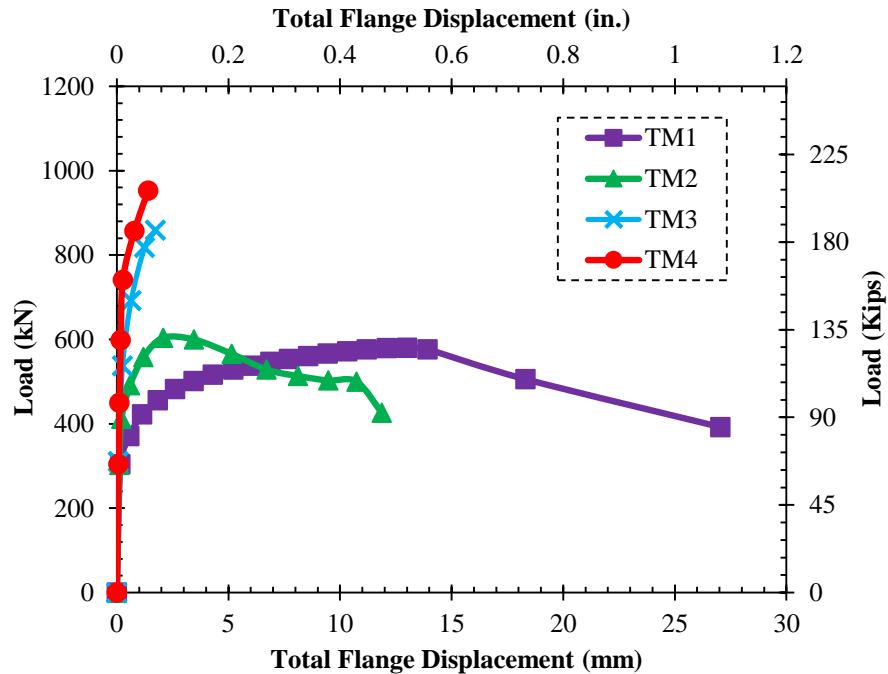


**Figure. 7.** Load-Total flange displacement: monotonic specimens

a. Interior and exterior bolt force

One objective of this experimental investigation is to determine the ratio of interior to exterior bolt force as a function of column flange thickness. Columns are *four-bolted* to double Tee connections as shown in Fig. 3. When loaded in tension, the interior and exterior tension bolts do not always carry equal loads [2]. If a thick or stiffened column flange is used, *secondary* prying forces are negligible, interior and exterior tension bolts resist equal loads (applied tensile force divided by total number of tension bolts). Whereas, if a medium or thin column flange thickness is used, significant *secondary* prying forces develop in the bolts, interior bolts are subjected to bending and resist larger tensile forces than exterior ones and are expected to fail first.

Table 1 shows the interior and exterior bolt force of all specimens at failure. Interior to exterior bolt force ratio for thick double Tee connections associated with thin column flange

(TM1 and TC1) is  $B_{int}/B_{ext} = 1.5$  and with medium thickness column flange (TM2 and TC2) is  $B_{int}/B_{ext} = 1.2$ . In the cases where thick double Tee connections are associated with thick column flange (TM3 and TC3) or stiffened column flange (TM4), the interior and exterior bolts carry the same load and fail simultaneously:  $B_{int}/B_{ext} = 1.0$ . In these cases *secondary* prying forces are negligible.

Figure 8 compares the interior bolt force variation for different column flange thicknesses. Note that in Fig. 8, B is the force of one interior bolt (kN) obtained from averaging load cells 3 and 4 and T is the applied tensile force per bolt (kN) obtained from dividing the total applied load by eight bolts. All bolts start with the same pretension load level. Bolts associated with thinner column flanges carry larger forces at earlier stages of the loading process than those associated with thicker column flanges. This is due to the *secondary* prying forces. Note that it is shown from Fig. 8 that the interior bolt force in specimens TM1, TM2, and TM3 reached a higher value than the interior bolt force in specimen TM4. This is due to the fact that load cells 3 and 4 in specimen TM4 (last specimen tested) yielded incorrect readings. However, the intent is to prove that *secondary* prying forces develop in tension bolts and increase as the column thickness decreases.

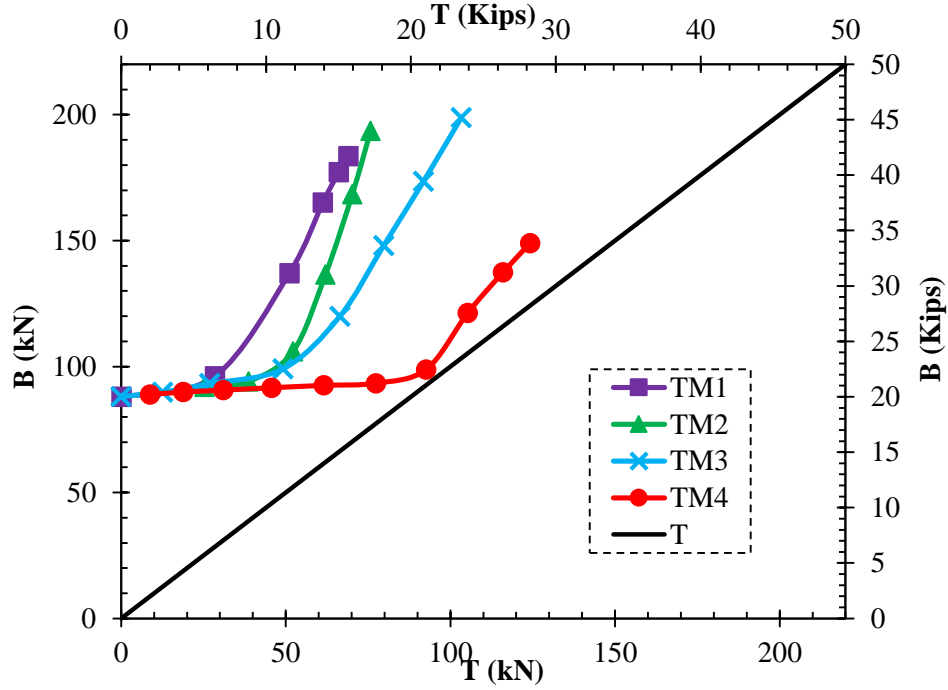


**Figure. 8.** Interior bolt force vs. applied load

Load cells were set to measure the bolt force variation of interior and exterior bolts throughout the loading process. Total prying is determined for every specimen as follows:

$$Q_{total} = \left( \frac{4B_{int} + 4B_{ext} - T}{T} \right) 100 \quad (1)$$

where  $Q_{total}$  is the total prying (%),  $B_{int}$  is the interior bolt force measured from the load cells at point of maximum tensile applied load (kN),  $B_{ext}$  is the exterior bolt force measured from the load cells at point of maximum tensile applied load (kN), and  $T$  is the maximum tensile applied load (kN).

The *primary* prying forces can be determined from specimen TM4. This specimen was designed to specifically eliminate *secondary* prying forces by stiffening the column flange. Using Eq. (1) to specimen TM4, resulted in negligible *primary* prying forces. Thus, *secondary* prying forces are equal to the total prying forces for all remaining specimens. Although the load

cells yielded incorrect readings for this specimen, as previously stated, very negligible deformation occurred in the Tee flange. This yields negligible primary prying forces. The results are shown in Table 1.

b. Energy dissipation

Another objective of this experimental research is to quantify the contribution of column flange ductility and energy dissipation capacity of thin column flange connected to thick double Tee connections without continuity plates. The total energy dissipation capacity of all specimens is calculated as follows [46]:

$$E_T = \sum_2^n (\Delta_i - \Delta_{i-1}) \left( \frac{P_i + P_{i-1}}{2} \right) \quad (2)$$

where  $E_T$  is the total cumulative dissipated energy till total failure of the connection (as per experiment),  $\Delta_i$  is the deformation at data point  $i$ ,  $P_i$  is the load at data point  $i$ , and  $n$  is the number of data points.

It can be seen from Table 1 that thinner column flanges exhibit higher energy dissipation capacity than thicker ones. This is due to the large plastic deformation of thin column flanges. It should be noted that the major energy dissipating mechanism is due to the column flange flexural deformation. And full scale testing of the connection assembly is needed for quantifying the energy dissipation capacity of column flanges detailed without continuity plates and its effect on the overall performance.

## B. Mechanical model

A mechanical model is developed to predict the force-deformation, bolt force variation, and energy dissipation of thick double Tee moment connections subjected to monotonic loading. The model uses geometrical and mechanical properties consistent with previous mechanical models that are based on incremental analysis. A previously developed mechanical model for prediction of built-up thick double Tee connections including *secondary* prying effects was developed by Hantouche and Abboud [8] as mentioned earlier. Although the model is comprehensive and accounts not only for axial and bending deformations, but also for shear deformations, it covers only the range of double Tee connections whereby column flange failure occurs in a mixed mode (full plastification near the K-zone followed by interior bolt fracture). For this reason, a proposed mechanical model is developed to cover all four failure modes of columns in thick double Tee connections that were encountered in the experiment. Yielding mechanisms that govern the behavior of thick double Tee connections are accounted for in the model. These include interior and exterior tension bolts elongation and bending of column flange. Also, the proposed model includes the effect of column stem in the connection response. It is important to note that the stiffness due to the Tee is not included in the formulation since no significant deformation is encountered in the Tee (rigid) as shown in the experimental results (Table 1). It should be noted that modeling a *four-bolted* Tee is complex because all mechanisms interact with one another and hence a simplified model cannot be provided to predict the behavior of such connections.

Figure 9(a) shows the column/tension bolt system geometry used in the mechanical model. For the system shown, the following geometric properties are defined:

$$a = \frac{g_{cf} - t_{cs}}{2} - \frac{2}{3}w - \frac{d_b}{2} \quad (3)$$

$$c = e + \frac{d_b}{2} \quad (4)$$

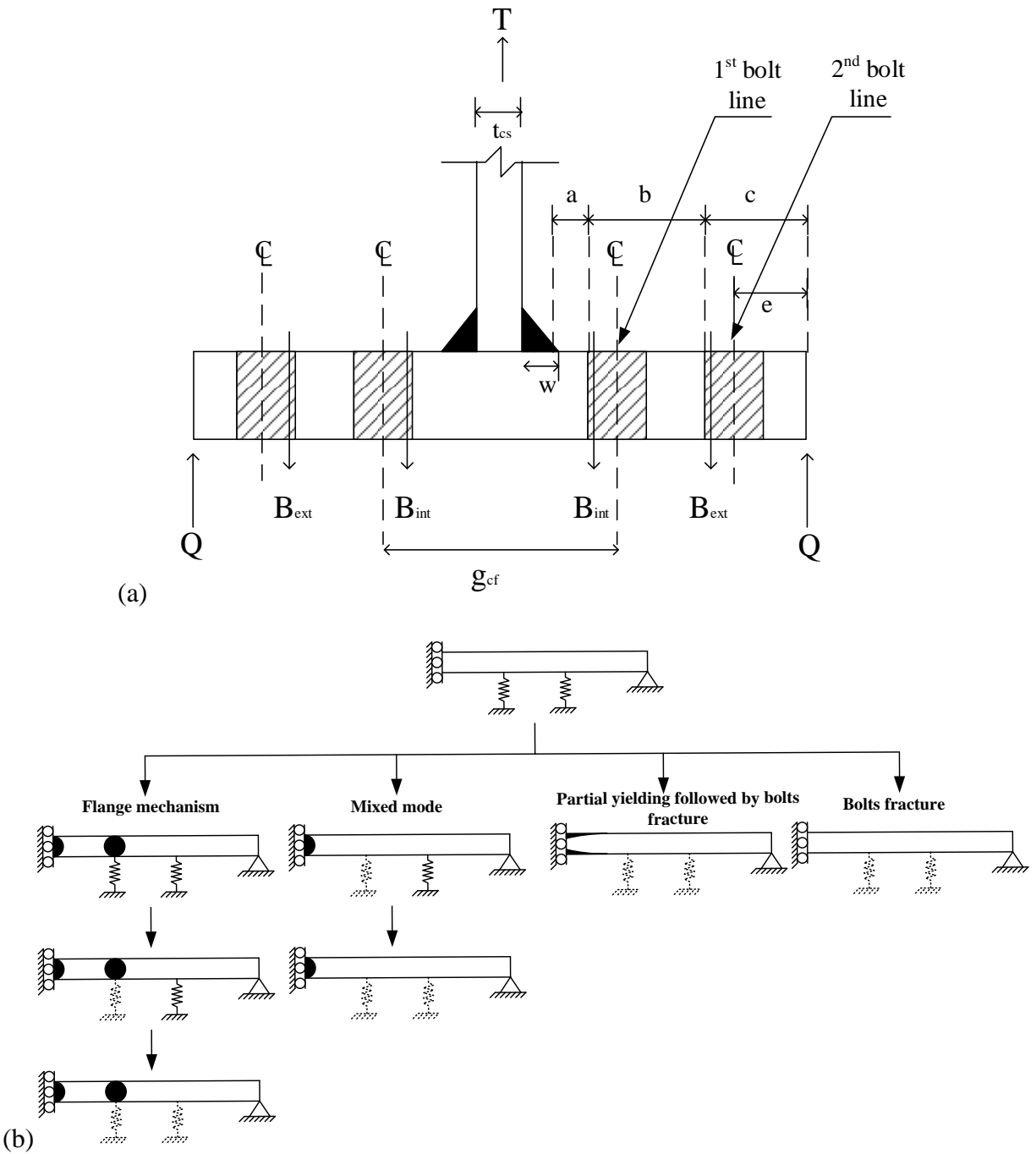


**Figure 9.** (a) Column flange geometry, (b) Decision tree for half of the column flange

where  $a$  is the length of the column flange measured from the inside edge of the interior bolt to the location of occurrence of the plastic hinge at the K-zone of the column flange,  $g_{cf}$  is the column flange gage distance,  $t_{cs}$  is the column stem thickness,  $w$  is the fillet weld size (the plastic hinge is located at a distance equal to  $2/3w$  away from the stem face of built-up Tees as shown in Hantouche et al. [44]),  $c$  is the length of the column flange measured from the inside edge of the exterior bolt line to the outside edge of the column flange,  $d_b$  is the bolt diameter,  $e$  is the edge distance, and  $b$  is the gage distance between the tension bolts. Note that the interior and exterior bolt lines are shifted a distance of  $d_b/2$  from the bolt centerline due to the stress distribution caused by the bending of the flange and bolt as per [46],  $T$  is the applied tensile force,  $B_{int}$  is the interior bolt force;  $B_{int} = K_{int} \delta_{int}$ , and  $B_{ext}$  is the exterior bolt force;  $B_{ext} = K_{ext} \delta_{ext}$ , where  $\delta_{int}$  and  $\delta_{ext}$  are the respective vertical displacements at the interior and exterior bolt lines, and  $K_{int}$  and  $K_{ext}$  are the respective interior and exterior bolt stiffness.

The proposed model is composed of a beam representation of half column flange as mentioned earlier (Fig. 9(b)). To include the effect of column stem, the beam moment of inertia is adjusted as follows:

$$I = I_{cf} + I_{cs} \quad (5)$$

where  $I$  is the total moment of inertia contributing from column flange and column stem,  $I_{cf}$  is the moment of inertia of column flange, and  $I_{cs}$  is the moment of inertia of column stem.

The total moment of inertia can be calculated as follows:

$$I = \left(\frac{1}{12} t_{cf}^3 p\right) L_{cf} + \left(\frac{1}{12} \left(t_{cf} + \frac{2}{3} w\right)^3 p\right) L_{cs} \quad (6)$$

where  $p$  is the tributary width of the column flange tributary per tension bolt ( $p = 4W/n_{tb}$ ,  $W$  is the width of column flange and  $n_{tb}$  is the tension bolts number),  $t_{cf}$  is the column flange thickness,  $L_{cf}$  and  $L_{cs}$  are dimensionless ratios representing the contribution of column flange and stem, respectively ( $L_{cf} = (a+b+c)/(a+b+c+2/3w+t_{cs}/2)$ , and  $L_{cs} = (2/3w+t_{cs}/2)/(a+b+c+2/3w+t_{cs}/2)$ ). Note that the effective length of column stem is taken as  $2/3w+t_{cs}/2$  and the effective thickness of column stem is taken as  $2/3w+t_{cf}$ .

The following series of equations, developed using the direct stiffness method, represent the change in the vertical displacement at the interior bolt line,  $\Delta\delta_{int}$ , the change in the vertical displacement at the exterior bolt line,  $\Delta\delta_{ext}$ , and the change in the vertical displacement near the column stem face,  $\Delta\delta_C$ .

$$\Delta\delta_{int} = \frac{\Delta T[\gamma_1(1+K_{ext}\gamma_5) - \gamma_4(K_{ext}\gamma_3)]}{[(1+K_{int}\gamma_2)(1+K_{ext}\gamma_5) + (K_{int}\gamma_3)(K_{ext}\gamma_3)]} \quad (7)$$

$$\Delta\delta_{ext} = \frac{\Delta T\gamma_4 - \Delta\delta_{int}K_{int}\gamma_3}{1+K_{ext}\gamma_5} \quad (8)$$

$$\Delta\delta_C = \Delta T\gamma_6 - \Delta B_{int}\gamma_1 - \Delta B_{ext}\gamma_4 \quad (9)$$

$$\gamma_1 = (3a^2b + 3a^2c + 6ab^2 + 12abc + 6ac^2 + 2b^3 + 6b^2c + 6bc^2 + 2c^3) / (6EI) \quad (10)$$

$$\gamma_2 = (b^3 + 3b^2c + 3ab^2 + 3bc^2 + 6abc + c^3 + 3ac^2) / (3EI) \quad (11)$$

$$\gamma_3 = (3b^2c + 6bc^2 + 6abc + 2c^3 + 6ac^2) / (6EI) \quad (12)$$

$$\gamma_4 = (3a^2c + 6abc + 6ac^2 + 3b^2c + 6bc^2 + 2c^3) / (6EI) \quad (13)$$

$$\gamma_5 = (3ac^2 + 3bc^2 + c^3) / (3EI) \quad (14)$$

$$\gamma_6 = (a^3 + 3a^2b + 3a^2c + 3ab^2 + 6abc + 3ac^2 + b^3 + 3b^2c + 3bc^2 + c^3) / (3EI) \quad (15)$$



where  $\Delta T$  is the change in the applied load,  $\gamma_1, \gamma_2, \gamma_3, \gamma_4, \gamma_5$ , and  $\gamma_6$  are constants used in the calculation of the vertical displacements.

The proposed mechanical model is to be applied in an incremental computer automated iterative solution. An engineer would start by applying an incremental vertical tensile force,  $\Delta T$ . Then, the engineer would calculate  $\Delta\delta_{int}, \Delta\delta_{ext}, \Delta B_{int}$  and  $\Delta B_{ext}$  corresponding to the current load step. The incremental vertical displacement of the column,  $\Delta\delta_C$ , is then determined and a new incremental load,  $\Delta T$ , is applied. Several checks need to be made to determine which limit states and failure modes will be reached. The possible limit states are: (1) full plastification at the K-zone, (2) partial plastification at the K-zone, (3) full plastification at the interior bolt line, (4) failure of the interior bolt, and (5) failure of the exterior bolt. Thus, both the force-deformation curve ( $T$  vs.  $\delta_C$ ), and the bolt force variation curve ( $B_{int}$  vs.  $T$  and  $B_{ext}$  vs.  $T$ ) can be developed for the thick double Tee connection, where  $T, \delta_C, B_{int}$ , and  $B_{ext}$  are the corresponding cumulative forces and displacement.

### ***1. Bolt mechanical model***

The bolt mechanical model proposed by Hantouche and Abboud [8] is used to model the tension bolt throughout the loading history of the double Tee connection. Note that, at every loading step, the cumulative bolt forces,  $B_{int}$  and  $B_{ext}$ , are to be compared with the pretension, yield, ultimate, and fracture forces generated from the bolt mechanical model. Whenever one of the bolt limit states is reached, the stiffness of the interior and exterior bolts,  $K_{int}$  and  $K_{ext}$  respectively, should be adjusted accordingly.

## 2. Failure modes

The proposed model is able to predict four failure modes for the thick double Tee connections: bolt fracture, partial yielding of column flange at the K-zone followed by bolt fracture, mixed mode failure in the column flange, and column flange mechanism. Figure 9(b) shows the four failure modes. Note that the dashed spring indicates bolt fracture. The behavioral characteristics of every failure mode are explained in this section.

### a. Bolt fracture

This failure mode is characterized by pure fracture of all tension bolts and no yielding in the column flange:  $B_{int} = B_{ext} = B_{fracture}$ , where  $B_{fracture}$  is the bolt fracture load as defined in the bolt mechanical model [8].

### b. Column flange partial yielding followed by bolt fracture

This mechanism is characterized by partial yielding in the column flange at the K-zone followed by fracture of all tension bolts:  $B_{int} = B_{ext} = B_{fracture}$  and  $M_{stem} = M_{pp} < M_{pl}$ , where  $M_{pp}$  is the partial plastic moment of column flange; ongoing FE and mechanical investigations are being performed to determine the exact value of  $M_{pp}$  at failure,  $M_{pl}$  is the plastic moment of column flange ( $M_{pl} = (1/4) p t_{cf}^3 F_y$ , where  $F_y$  is the expected yield strength of the column), and  $M_{stem}$  is the moment at the column stem face:

$$M_{stem} = \frac{T - B_{int}(b+c) - B_{ext}(c)}{a+b+c} \quad (16)$$

c. Mixed mode

This failure mode is characterized by plastic hinge formation in the column flange at the K-zone followed by interior bolt fracture:  $M_{stem} = M_{pl}$ ,  $B_{int} = B_{fracture}$ , and  $B_{ext} < B_{fracture}$ .

d. Flange mechanism

This failure mode is characterized by two plastic hinges formation in the column flange at the K-zone and at the interior bolt line and no bolt fracture:  $M_{stem} = M_{pl}(1 + \delta)$  (where  $\delta = 1 - d_h/p$  [46] and  $d_h$  is the bolt hole diameter) and  $B_{int} < B_{fracture}$  and  $B_{ext} < B_{int}$ .

### 3. *Model performance*

The performance of the proposed mechanical model is assessed by comparing its prediction capability with the experimental results reported in this research. The results (Figs. 10 and 11) show that the proposed model predicts with high accuracy both the force-deformation and the bolt force variation responses of built-up thick double Tee connections till first component failure (component yielding). Note that Figs. 11 (a) and (b) represent the force of one interior ( $B_{int}$ ) and exterior ( $B_{ext}$ ) bolt, respectively, versus the total applied load per bolt ( $T$ ). Future research work will be focused on the response of thick double Tee connections after first component failure using both FE fracture and mechanical modeling.

The mechanical model was validated against column sections used in the experiment which were built-up for reasons mentioned earlier. However, rolled column sections are frequently used in moment connections. For this purpose, an additional double Tee moment connection, using rolled column section, was designed and tested in the FE software *ABAQUS* and validated against the proposed mechanical model to prove that the used built-up column sections behave as rolled ones. The designed connection had the same geometry and

configuration as the tested double Tee connections with the only difference of using an HEB400 (W16x100) rolled column section.

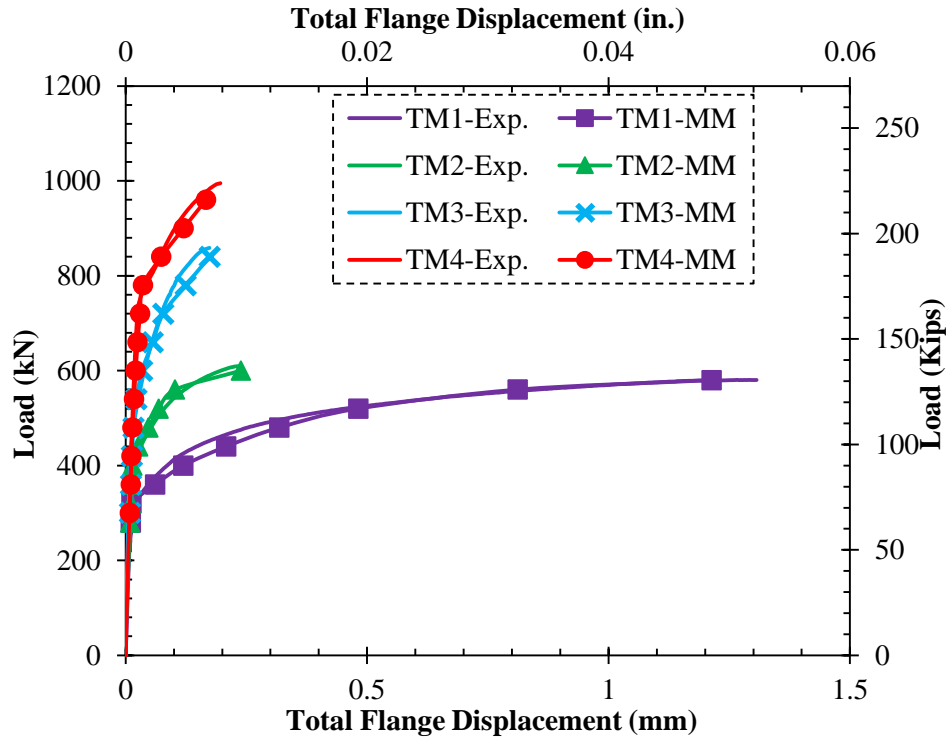
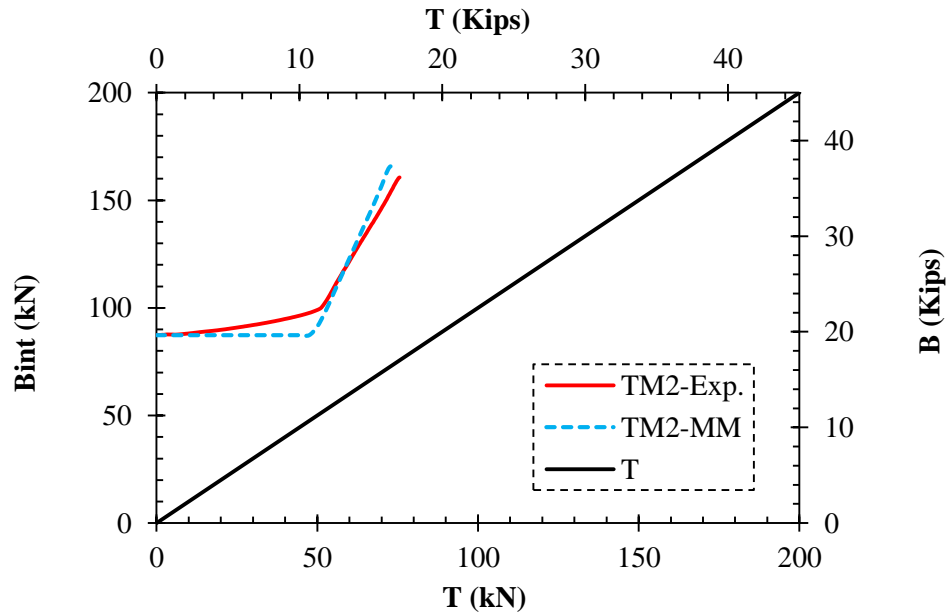


**Figure. 10.** Load-Total flange displacement: Mechanical model (MM) vs. Experiment (Exp.)



(a)

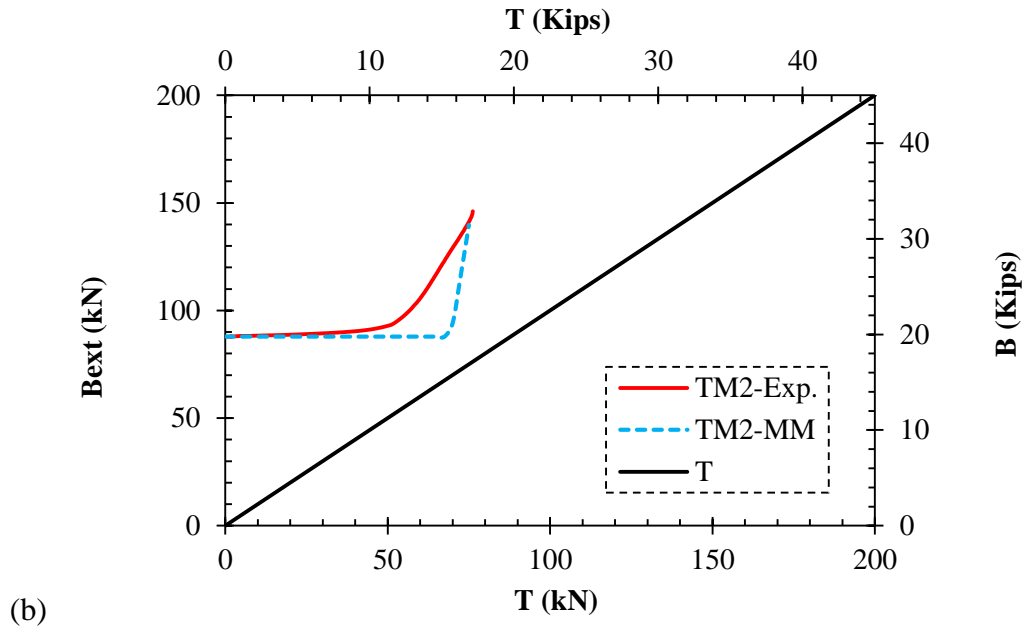


**Figure. 11.** Bolt force-Load of TM2: Mechanical model (MM) vs. Experiment (Exp.): (a) Interior bolt, (b) Exterior bolt

## C. FE modeling

### 1. Geometric and force boundary conditions

The specimen was loaded in two steps. In the first step, tension bolts were subjected to a pretension force of 88 kN. The load was modeled by applying a pressure on the nuts of the bolts equivalent to the minimum required pretension force. In the second step, a displacement controlled monotonic load was applied at the tip of the Tee stem. During all steps of the analysis, the column stem was fixed against any translation and rotation.

### 2. Material Properties

A bilinear stress-strain material model was used for all steel materials. The mechanical properties of the Tee and column were S355 for steel base material. It is noted that according to the *AISC* seismic design provisions [3], the stress-strain behavior for A572-50 (S355) base

material can be increased by an amount of 10%; so,  $R_y F_{yt}$  (390 MPa), the expected yield stress and  $\epsilon_{py} = 0$ , the plastic strain at yield, and  $R_t F_{ut}$  (561 MPa), the expected tensile strength and  $\epsilon_{pu} = 0.4$ , the plastic strain at ultimate, with  $R_y = 1.1$  and  $R_t = 1.1$ , were used in the model. Tension bolts were grade 8.8 ( $F_y = 640$  MPa  $\epsilon_{py} = 0$  and  $F_u = 800$  MPa,  $\epsilon_{pu} = 0.04$ ).

### ***3. Model discretization***

Discretization of all the components of the connection model in *ABAQUS* was performed using *C3D8-R* (eight-node brick elements with reduced integration). At regions where failure was expected to occur (at the proximity of the connection), and at regions where stress was likely to concentrate (around bolt holes) a finer mesh and a mapped mesh were adopted in order to advance the accuracy of interpolations. Surface-to-surface contact with a finite sliding coefficient was used to reproduce contact surfaces between the bolt shank, the Tee, and the column. This finite sliding was used to represent a friction coefficient of 0.25. The finite sliding allowed separation, sliding, and rotation of the contact surfaces.

#### **a. Analytical modeling**

The proposed mechanical model was applied to predict the force-deformation of the designed connection. The model is applicable as shown in Fig. 12. The only modification made to the proposed model is to replace the “ $2/3 w$ ” term in Eqs. (3) and (6) by “ $0.8k$ ”, where  $k$  is the fillet radius of the rolled section [46].

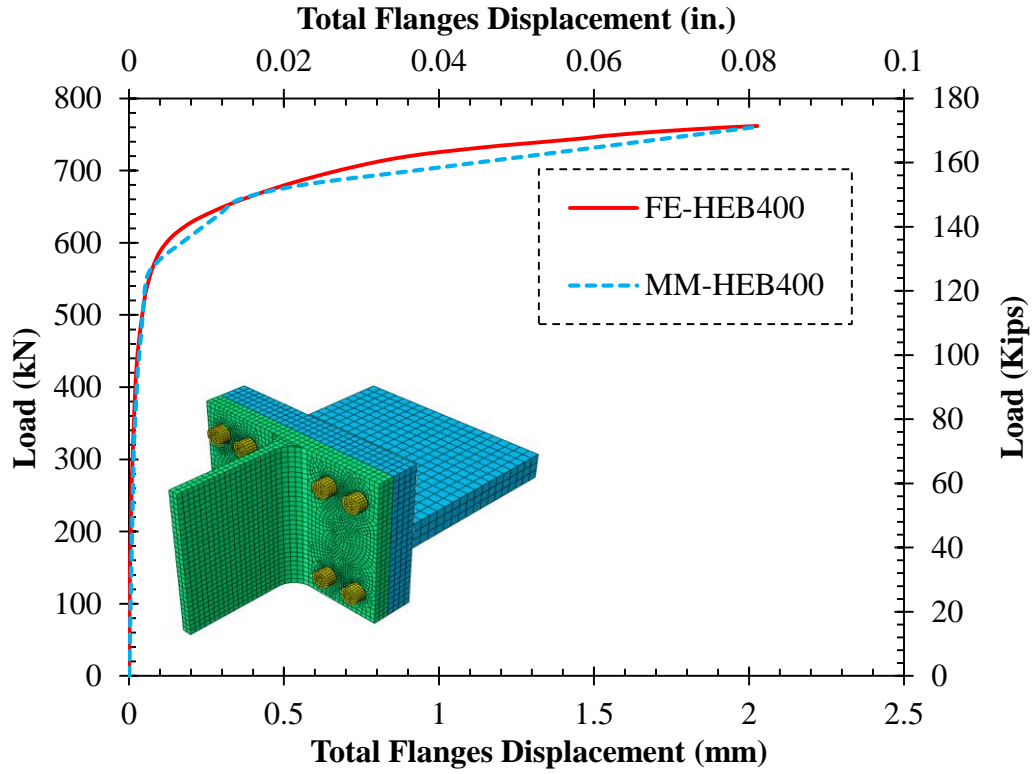


**Figure. 12.** Load-Total flange displacement of rolled section: Mechanical model (MM) vs. FE

b. Energy dissipation

The prediction of the energy dissipation capacity is important as it enables the designers to predict the overall ductility. The following equation is used to predict the double Tee connection energy dissipation capacity:

$$E_{TS} = \sum_2^n (\Delta\delta_{ci} - \Delta\delta_{ci-1}) \left( \frac{\Delta T_i + \Delta T_{i-1}}{2} \right) \quad (17)$$

where  $E_{TS}$  is the total cumulative dissipated energy till first component failure,  $\Delta\delta_{ci}$  is the deformation of the column at load step  $i$ , and  $\Delta T_i$  is the load applied at load step  $i$ . Note that this is obtained from Eq.(2) by replacing  $\Delta_i$  by  $\Delta\delta_{ci}$  and  $P_i$  by  $\Delta T_i$  at every load step  $i$ .

The performance of the energy dissipation model was validated by comparing the model predictions with the energy dissipation capacity values predicted from the experimental results. The model accurately predicts the energy dissipation capacity of double Tee connections till first component failure. Table 2 shows the model predictions against the experimental results.

**Table. 2.** Energy dissipation till first component failure

Test ID	Total energy dissipation till 1 <sup>st</sup> component yielding ( $\times 10^3$ kN.mm)		Error (%)
	Experiment	Mechanical Model	
TM1	6.8	6.2	9.4
TM2	1.2	1.3	2.9
TM3	1.2	1.3	9.0
TM4	1.6	1.6	1.0

#### D. Conclusions

In designing moment connections, all failure modes should be accounted for including those encountered in column flange due to the *secondary* prying effect. An experimental investigation was performed to study the effect of column flange on the response of thick double Tee connections detailed with and without continuity plates. Experimental results showed that four different failure modes can be associated with column flange/bolt system depending on the thickness of the flange. Also, results showed that increasing the column flange thickness decreases the flexural deformation and the *secondary* prying forces and increases the strength of thick double Tee moment connections. Also from experimental results it was concluded that interior and exterior bolts carry different load values when thin column flange is used due to the *secondary* prying effect. A proposed mechanical model was developed to predict the load-



deformation, interior and exterior bolt force variation, energy dissipation, and four failure modes of thick double Tee connections. The proposed mechanical model showed excellent agreement with experimental results. The results show that the column flange contributes significantly to the overall ductility of the connection. This study highlights the need to design for the additional load induced in the tension bolts due to *secondary* prying effect specifically when continuity plates are omitted. Also, this study highlights the need to include the characterization of *four-bolted* Tees in current design guidelines. It also highlights the possibility of detailing thick double Tee connections with thin and medium column flanges without continuity plates while satisfying the ductility and the strength requirements for seismic applications. Removing continuity plates reduces the fabrication cost, and omits the need to weld in regions of low toughness. In fact, the column flange thickness is controlled by a lower bound (flexural yielding of the column flange) and an upper bound (thick column flange or thin column flange associated with continuity plates). In this research, it was shown that for column flange thickness between the lower and upper bounds, the failure mode is either mixed mode failure in the column flange or partial yielding at the K-zone followed by bolt fracture. Thus this research provides a dataset for developing new guidelines in designing double Tee moment connections in which the requirement to provide continuity plates can be relaxed. It should be noted that, full scale tests should be the subject of future research work to investigate the effect of continuity plates removal and column flange thickness on the overall seismic behavior of double Tee moment connection assemblies and to check if the connection under study can meet the prequalification requirements for use in all MRFs. Strength design equations for thin column flanges detailed without continuity plates should be developed and incorporated in current design practices in

case a full scale testing proves that it is adequate to remove continuity plates (keeping the strong-column weak-beam premise).

## CHAPTER IV

### PRYING EFFECT IN UNSTIFFENED EXTENDED ENDPLATE CONNECTION WITH CIRCULAR BOLTS CONFIGURATION

Component tests were conducted on eight-bolt unstiffened extended endplates with circular bolts configuration subjected to monotonic and cyclic loadings. The strength and prying forces of the proposed connection were evaluated and the different failure modes were identified. Also, FE models were developed and validated against the experimental results. More importantly, FE parametric studies were performed in which the column flange thickness was varied for different beam sections, endplate thicknesses, and tension bolt diameters. The data collected from the experimental and FE studies lead to the development of a strength model to predict the strength and prying forces of the proposed connection covering the failure modes encountered in the experiment. Finally, a design procedure and an example were presented.

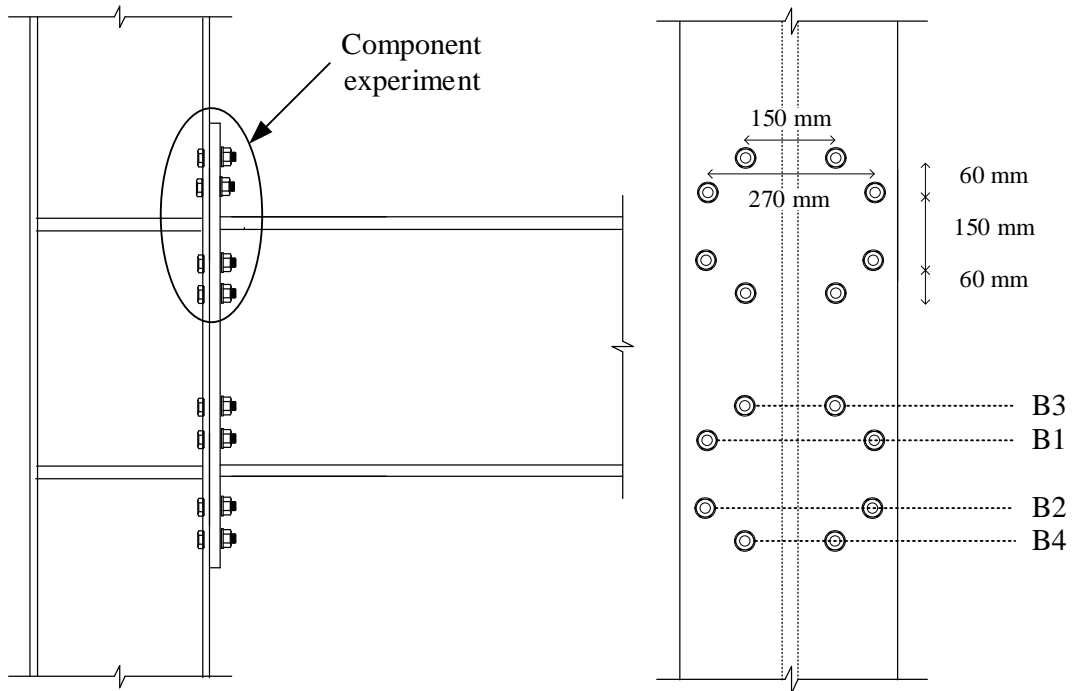
#### **A. Experimental program**

##### *1. Component tests*

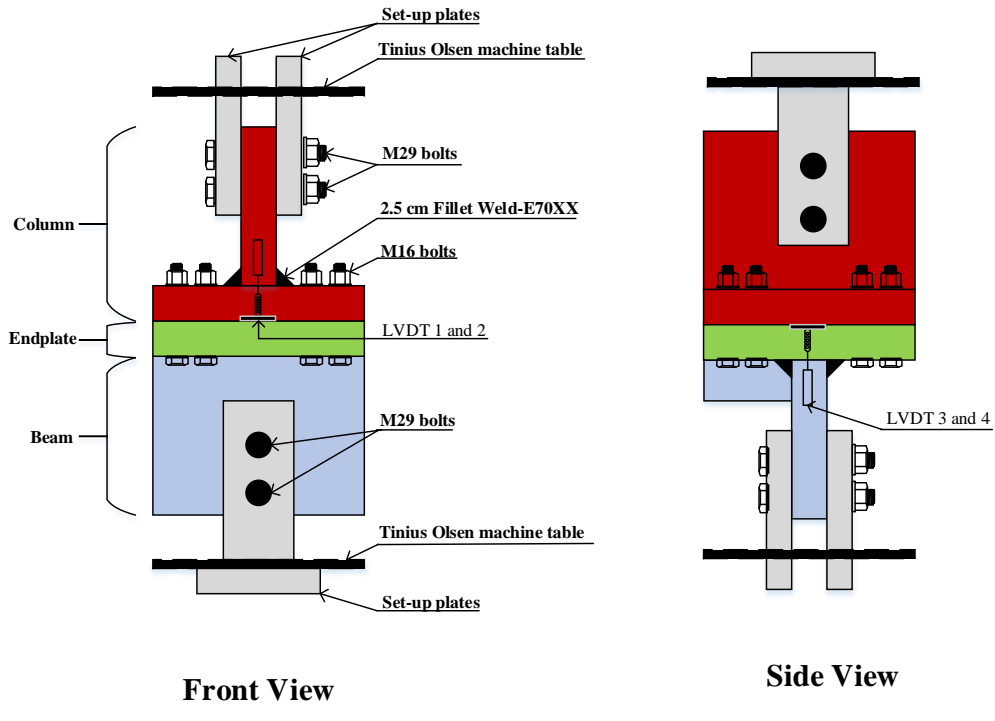
The scope of this experimental program is to study the effect of omission of stiffeners, the distribution of tension bolts in a circular pattern, and the column flange thickness on the strength and prying forces of the eight-bolt extended endplate connection. The experimental tests were limited to the component level.

Figure 13(a) shows the side and front views of the designed connection. The circular bolt pattern was designed as per Hantouche and Mouannes [19] recommendations. Figure 13(b) shows the experimental setup of the tested specimens. As shown in Fig. 13(b), a Tee section (S355 steel (A572-50)), representing half the column, was connected using eight M16 tension

bolts (grade 8.8 (A325)) to the endplate which was in turn welded (using *fillet welds* (E70XX)), to a Tee section representing half the beam. Figure 14 shows a test specimen. Two LVDTs were attached to the column flange to record its deformation and two LVDTs were attached to the endplate to record its deformation. Also, four load cells were attached to the four tension bolts (B1 to B4 in Fig. 13(a)) to measure the bolt-force variation and prying forces throughout the tests. Load cells were only attached to specimens M2 and M5 as they represent the extreme cases (thick column flange - expected lowest prying forces, and thin column flange – expected highest prying forces).



(a)



**Figure. 13.** (a) Typical eight-bolt unstiffened extended endplate connection (b) Experimental setup

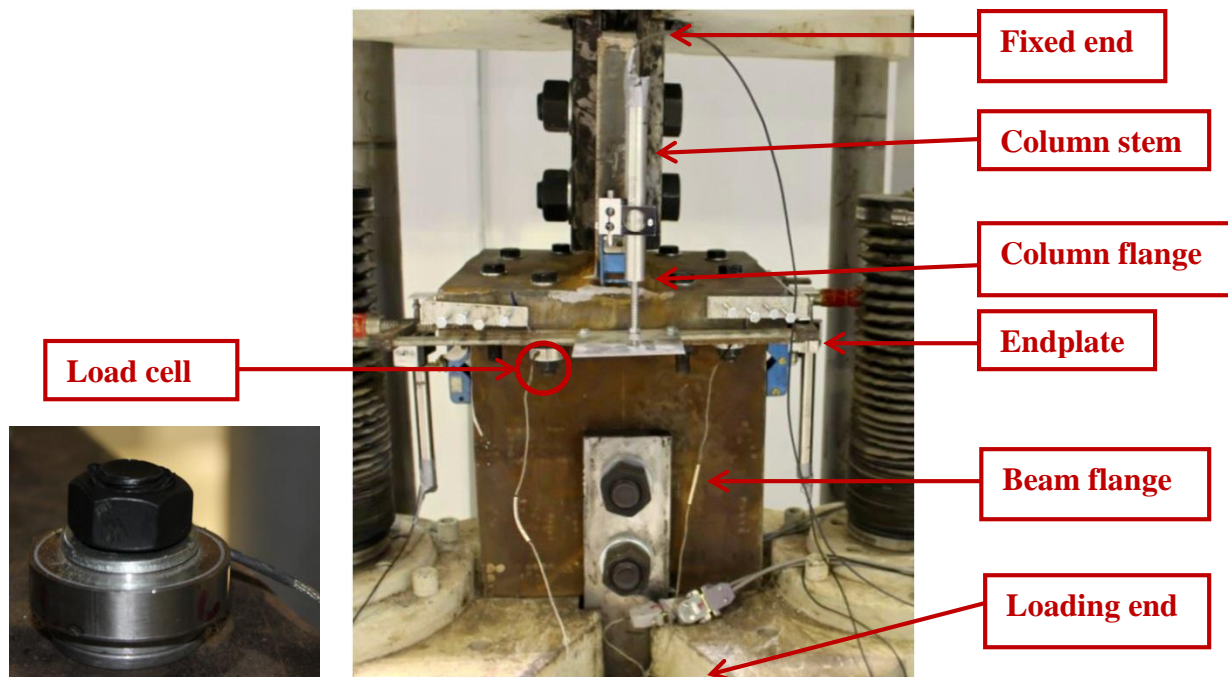


**Figure. 14.** Test specimen

Table 3 shows the geometric parameters of the tested specimens. The endplate thickness and bolt diameter were held constant while the column flange thickness was varied to study its effect on the behavioral characteristics of the connection. The beam section was chosen based on the capacity of the Tinius-Olsen machine of 2000 kN. The endplate was designed as per the *ANSI/AISC 358-16* [2] for the rectangular bolt configuration and including beam flange stiffeners. The stiffeners were removed and the bolts were arranged in a circular pattern as per Hantouche and Mouannes [19] to study the effect of these changes on the behavior of extended endplates and prying forces. The thick column flange was chosen to ensure a rigid response, while the medium column flange was chosen to match the endplate thickness, and the thin column flange was designed to eliminate the flexural yielding of the column as per *ANSI/AISC 358-16* [2]. That is, the thin column flange is the minimum required column flange thickness to eliminate flexural yielding. The beam and column sections used were built-up sections. However, they behaved similar to rolled sections and no distress was observed in the welds after testing.

Tension bolts in all specimens were pre-tensioned, using direct torque control, according to the minimum pretension load specified by the *ANSI/AISC 360-16* [4] and *Eurocode* [47]. The specimens were subjected to either a monotonically increasing load to failure (loading rate of 4mm/sec) or a cyclically variable load in tension similar to the *ATC24* [48] seismic load history.

**Table 3.** Test parameters and results

Test ID	$t_{cf}$ (mm)	$t_p$ (mm)	Beam section	Testing procedure	Failure mode	Maximum load (kN) <sup>a</sup>	Column flange deformation (mm) <sup>b</sup>	Endplate deformation (mm) <sup>c</sup>	Total deformation (mm) <sup>d</sup>	B at ultimate (kN)	Total Prying (%)	Primary Prying (%)	Secondary Prying (%)
M1				Monotonic		719	0	17	17	NA <sup>e</sup>	NA	NA	NA
M2	40			Monotonic	Endplate yield mechanism with B1&B2 fracture	669	0	16	16	B <sub>1</sub> =B <sub>2</sub> =200 B <sub>3</sub> =B <sub>4</sub> =180	9	9	0
C1				Cyclic		696	0	20	20	NA	NA	NA	NA
M3	16		W410x39 (W16x26)	Monotonic	Column flange & Endplate yield mechanism with B4 fracture	573	41	1	42	NA	NA	NA	NA
C2				Cyclic		603	44	1	45	NA	NA	NA	NA
M4				Monotonic		512	44	2	46	NA	NA	NA	NA
M5	13			Monotonic	Column flange yield mechanism with B4 fracture	501	37	2	39	B <sub>1</sub> =B <sub>4</sub> =200 B <sub>2</sub> =180 B <sub>3</sub> =160	22	9	13
C3				Cyclic		508	45	2	47	NA	NA	NA	NA

<sup>a</sup> Maximum tensile force experienced during the test (not the load at failure)

<sup>b</sup> Maximum tensile deformation at failure in the column flange. Obtained by averaging displacements of LVDTs 1 and 2

<sup>c</sup> Maximum tensile deformation at failure in the endplate. Obtained by averaging displacements of LVDTs 3 and 4

<sup>d</sup> Summation of endplate and column flange deformation at failure

<sup>e</sup> Not Applicable

## ***2.Component results***

### **a. Failure modes**

Three failure modes were encountered in this series of component tests. Specimens M1, M2, and C1 (having thick column flange thickness) failed due to flexural mechanism and bolt fracture in the endplate/bolt system. This type of failure is characterized by B1 and B2 (Fig. 13(a)) fracture with simultaneous yielding of the endplate at the k-zone and at the bolt line. The failure of the endplate proves that the use of circular bolts distribution requires thicker endplates. This was previously shown by Morrison et al. [49] using FE analysis. Thus, new design equation is needed for the flexural yielding of the endplate with circular bolt pattern.

Specimens M3 and C2 (having medium column flange thickness) failed by flexural mechanism in the column flange/endplate system and bolt fracture. This type of failure is characterized by simultaneous plastic hinge formation at the k-zone and at the bolt line of both the column flange and the endplate with simultaneous fracture of bolt B4. Bolt B4 is the closest bolt to the beam web as shown in Fig. 13(a). Large tensile forces were induced in this bolt due to the separation of the endplate and column flange.

Specimens M4, M5, and C3 (associated with thin column flange) failed due to flexural mechanism and bolt fracture in the column flange/bolt system. This type of failure is characterized by B4 fracture with simultaneous yielding of the column flange at the k-zone and at the bolt line.

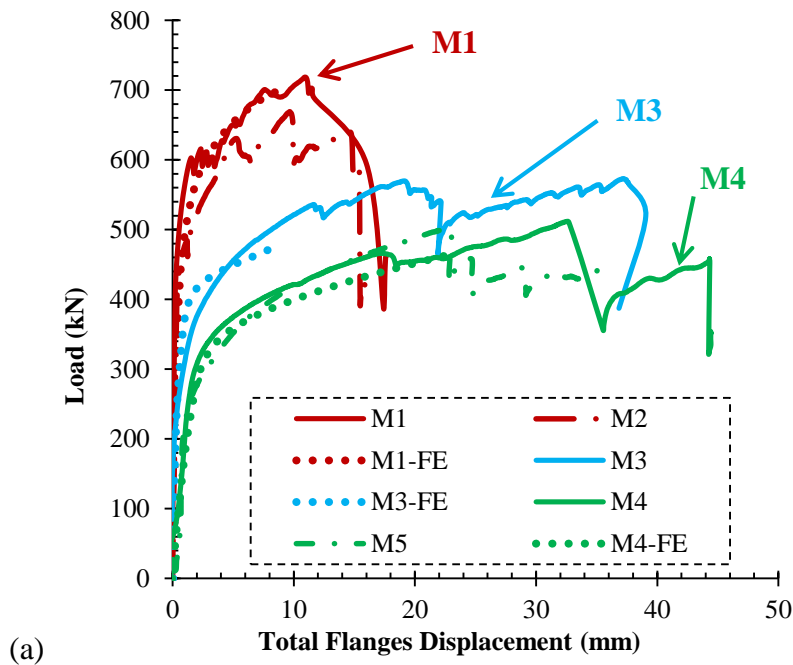
### **b. Load-displacement**

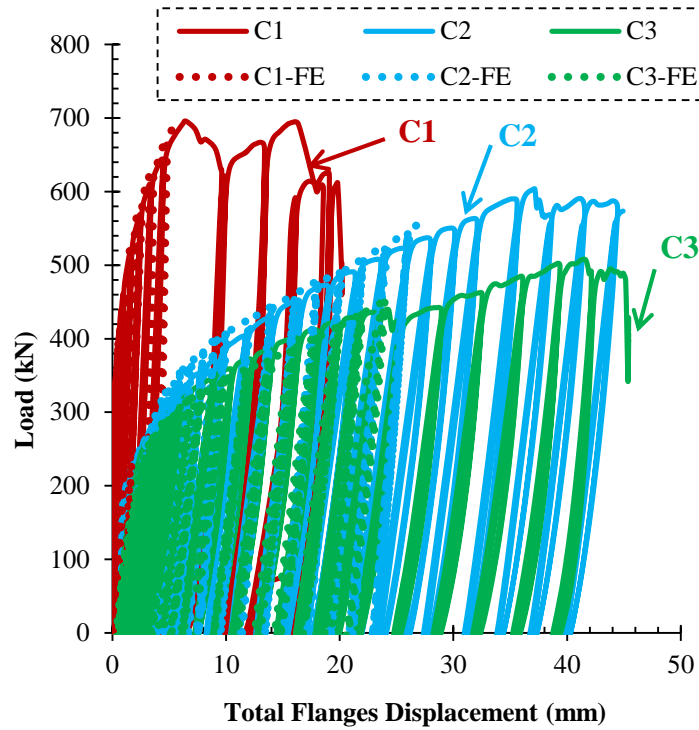
The load-total displacement curves of all monotonic tests are shown in Fig. 15(a). The total displacement is the summation of the column flange and endplate deformations, obtained from the LVDTs. The separate column flange and endplate deformations are summarized in



Table 3. Specimens M1 and M2 show negligible deformation of the column flange. Subsequently, it is considered rigid in these specimens and no secondary prying forces (caused by column flange deformation) exist. Also, the results show that the initial stiffness and the maximum load increase with the column flange thickness whereas the plastic deformation decreases.

Figure 15(b) shows the load-total displacement curves of the cyclic tests. The large inelastic cyclic deformations developed in specimens C2 and C3, as opposed to C1, show that the flexible column flange leads to large energy dissipation capacity.





**Figure. 15.** Load-Total displacement: Experiment vs. FE (a) Monotonic tests, (b) Cyclic tests

c. Bolt force

The bolt force distribution of specimens M2 and M5 is shown in Figs. 16(a) and (b), respectively. The force in one bolt (B in kN) obtained from the load cells is plotted against the tensile force per bolt (T in kN) obtained from dividing the total applied load by eight bolts.

The results show that all bolt rows are active in transferring the load even the far bolts B3 and B4. This proves the efficiency of the circular bolts configuration in improving the distribution of the tension force among all eight bolts.

Also, it is clearly shown from Figs 16(a) and (b), respectively, that the stiffening effect of the beam flange and web, results in high prying forces in the nearest bolts (B1 and B2 – nearest to beam flange – for M2 and B4 – nearest to beam web – for M5). This is due to the large

deformation of the connected plates in these regions and the stiffening effect of the beam flange and web.

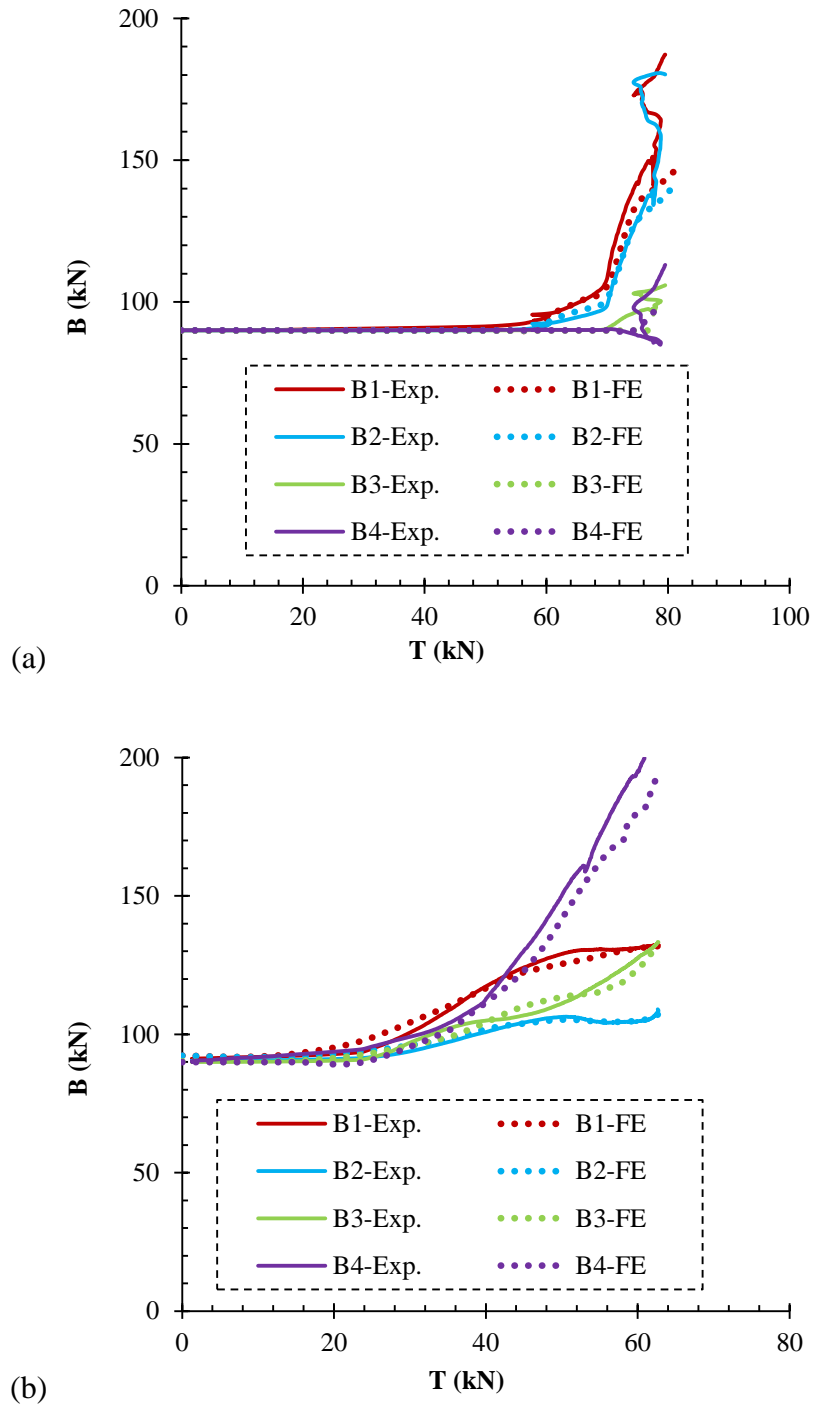


**Figure. 16.** Bolt-force distribution- Experiment (exp.) vs. FE: (a) M2 (b) M5

Analysis of the bolt force at ultimate load (Table 3 *column 11*) indicates that in specimens M2 and M5, four of the bolts are 100% effective, while the other four are 80% to 90% effective. That is, between 7.4 and 7.6 out of 8 bolts are effective in carrying the load in the connection having a circular bolt configuration. Recall that only 6.8 bolts are effective for the rectangular bolts configuration [50], the circular bolts configuration enhances the bolt-force distribution. That is, more bolts are effective in carrying the load. Requiring the same bolts diameter as the rectangular configuration, the circular bolts configuration has higher capacity due to the increased effectiveness of the bolts.

Finally, the total prying forces in specimens M2 and M5 are calculated as follows:

$$Q_{\text{total}}(\%) = \left( \frac{2(B_1 + B_2 + B_3 + B_4) - T_{\text{max}}}{T_{\text{max}}} \right) 100 \quad (18)$$

where:  $Q_{\text{total}}(\%)$ : total prying percentage;  $B_1, B_2, B_3, B_4$ : bolts forces measured from load cells at maximum tensile applied load;  $T_{\text{max}}$ : maximum tensile applied load.

The primary prying forces are determined from specimen M2. The column flange deformation for specimen M2 is negligible. No secondary prying forces are induced in this specimen and the total prying forces are equal to the primary prying forces. For specimen M5, the column flange is flexible and undergoes significant deformation (as shown in Table 3), thus secondary prying forces caused by the column flange deformation exist. The primary prying forces are deducted from the total prying forces to obtain the secondary prying forces. The results are shown in Table 3.

## B. FE validation

FE models were developed in *ABAQUS* to reproduce the load-deformation and bolt-force variation of the experimental program for validation purposes.

### 1. Description of the connection model

The eight component specimens were reproduced in *ABAQUS*. The specimens were loaded in two steps. In the first step, the tension bolts were subjected to a pretension force of 90 kN. The load was modeled by applying a bolt-force equivalent to the minimum required pretension force. In the second step, a displacement controlled monotonic load (M1, M2, M3, M4, and M5) or cyclic load (C1, C2, and C3) was applied at the tip of the beam flange. During all steps of the analysis, the column web was fixed against any translation and rotation.

A bilinear stress-strain material model was used for all steel materials. The mechanical properties of the endplate, column, and beam were S355 steel base material. It is noted that according to the *OPUS* [51] report, the stress-strain behavior for S355 base material can be increased by an amount of 25%. So,  $R_y F_{yt}$  (440 MPa with  $\epsilon_{py}=0$ ), the expected yield stress and plastic strain, and  $R_t F_{ut}$  (590 MPa with  $\epsilon_{pu}=0.4$ ), the expected tensile strength and plastic strain, with  $R_y = 1.25$  and  $R_t = 1.25$ , were used in the model. Tension bolts were M16 (grade 8.8) ( $F_y = 640$  MPa,  $\epsilon_{py}=0$  and  $F_u = 800$  MPa,  $\epsilon_{pu}=0.1$ ) and welds were E70XX ( $F_y = 460$  MPa,  $\epsilon_{py}=0$  and  $F_u = 485$  MPa,  $\epsilon_{pu}=0.01$ ). For the specimens loaded monotonically, an isotropic plastic hardening model was specified for all steel materials. For the specimens loaded cyclically, a kinematic plastic hardening model was specified to account for the *Bauschinger* effect.

Discretization of all the components of the connection model in *ABAQUS* was performed using *C3D8-R*. Surface-to-surface contact with a finite sliding coefficient was used to

reproduce the contact surfaces. This finite sliding was used to represent a friction coefficient of 0.25 as per a sensitivity analysis performed by Daryan and Yahyai [52].

## 2. Comparison of FE predictions with experiments

The failure criterion used in *ABAQUS* was the von Mises. Thus, the FE results were reported till first component full yielding. That is, the FE results reach the nonlinear range whenever any component of the connection starts yielding; however, the models were terminated once any component is fully yielded (i.e. bolt yielding across the diameter, endplate or column flange yielding across the thickness...). The load-deformation curves of the monotonic (Fig. 15(a)) and cyclic (Fig. 15(b)) responses as well as the bolt-force variation curves of specimens M2 (Fig. 16(a)) and M5 (Fig. 16(b)) show that the FE models predict with acceptable accuracy the experimental results. Furthermore, Fig. 17 shows a comparison between the experimental and the FE failure of the column flange. The developed FE models predict the response of the connection till first component failure with high accuracy.

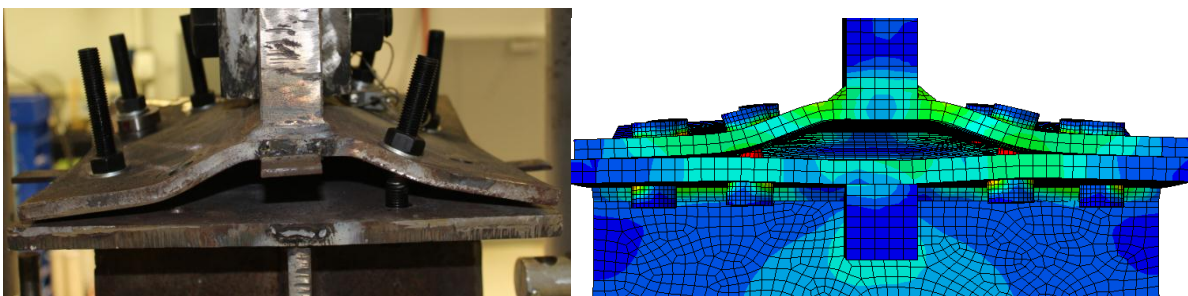


**Figure. 17.** Comparison of failure in experiment vs. FE: column flange mechanism

### C. FE parametric study

The goal is to increase the available data in order to develop a reliable strength model and a design procedure for the eight-bolt extended endplate connection with circular bolts configuration. For this purpose, FE models were designed and developed in *ABAQUS* and used to conduct a parametric study. The column flange thickness was varied for various beam sections ranging from medium (W18) beam section to deep (W24) beam section.

#### 1. Description of the connection model

A total of 9 component connections were designed as per the *ANSI/AISC 358-16* [2] recommendations and Hantouche and Mouannes [19] circular bolts configuration was adopted. Table 4 shows the geometric and material properties of all the specimens.

**Table. 4.** Parametric study tests matrix

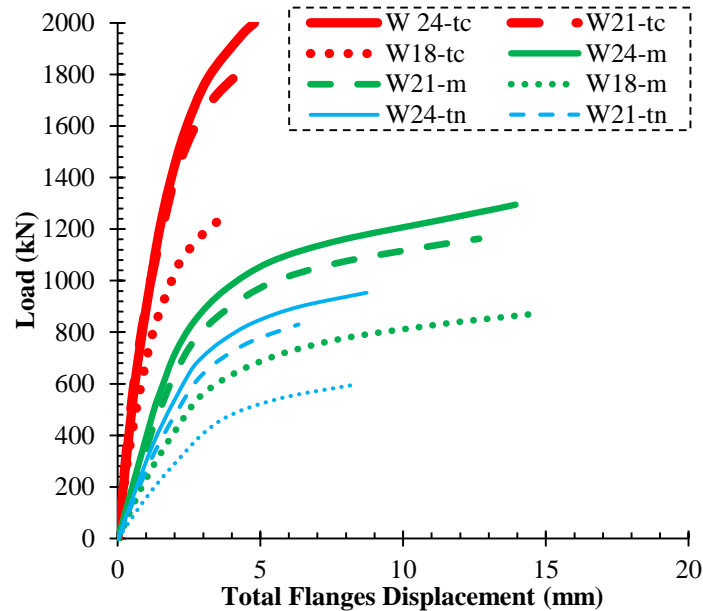
Test ID	Beam section	Column section	$t_f$ (mm)	Bolt size	$t_p$ (mm)	$g_1$ (mm)	$g_2$ (mm)
W18-tc	W460x82 (W18x55)	W360x382 (W14x257)	48	M24	19	170	340
W18-m			19				
W18-tn			15				
W21-tc	W530x92 (W21x62)		48	M27	22	165	330
W21-m			22				
W21-tn			18				
W24-tc	W610x113 (W24x76)		48	M30	22	160	320
W24-m			22				
W24-tn			10				

Material properties of all steel components and boundary conditions of the connection were similar to the ones used in the validation presented in the previous section. The bolts were subjected to the minimum pretension load specific for every bolt diameter in the first step of the

analysis. A displacement controlled monotonic load was applied in the second step of the analysis. Discretization of all the components was performed using *C3D8-R* and a friction coefficient of 0.25 was used.

## 2. Results

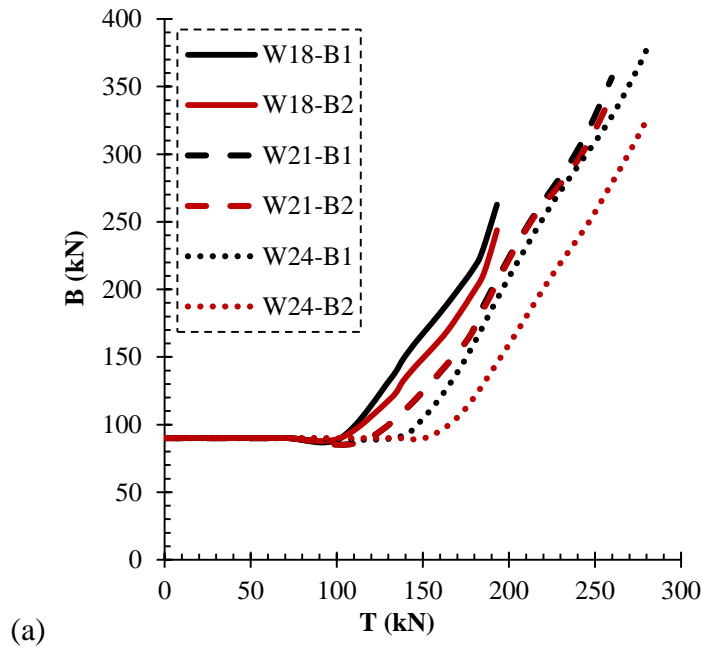
Figure 18 shows the load-deformation curves of all nine tested specimens. The results of the parametric study are consistent with the experimental results in the following: first, specimens with thick column flange have the largest strength capacity while specimens with thin column flange have the largest ductility. Second, the FE results showed the same failure modes as the experiment: endplate flexural mechanism and B1 and B2 fracture for thick column flange specimens. Flexural mechanism in column flange and endplate and B4 fracture for medium thickness column flange specimens. And, flexural mechanism in column flange and B4 fracture for thin column flange specimens.



**Figure. 18.** Load-Total displacement of FE parametric study



Figures 19(a) and 19(b) show the bolt-force variation of the specimens associated with the thick and thin column flanges, respectively. The distribution of tensile force among all eight tension bolts in the FE parametric study is similar to the experimental one. Analysis of Figs. 19(a) and 19(b) shows that between 7.4 and 7.6 bolts are effective in carrying the load. For the specimens with thick column flange (Fig. 19(a)), B1 and B2 carry almost equal loads till failure while B3 and B4 become effective at later stages of the loading process. For the specimens with thin column flange (Fig. 19(b)), all bolts carry the applied load from early stages of the loading process with B4 carrying the largest load.



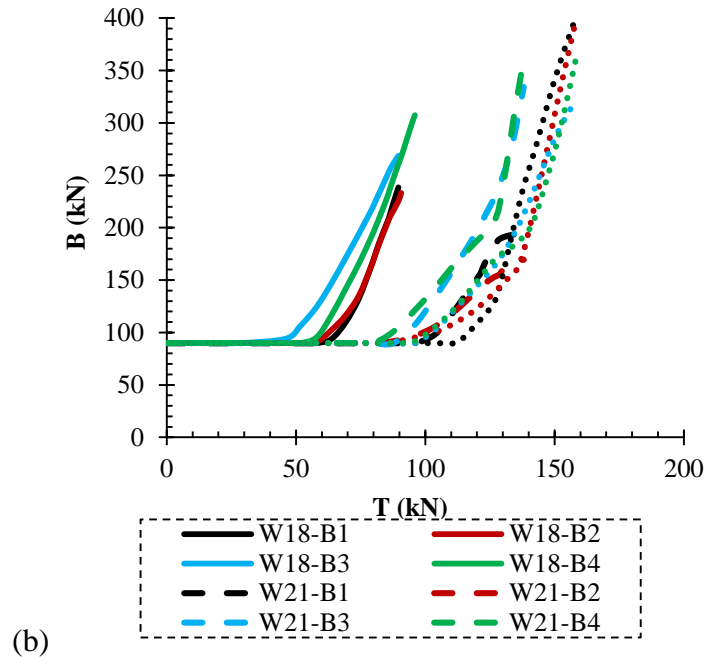


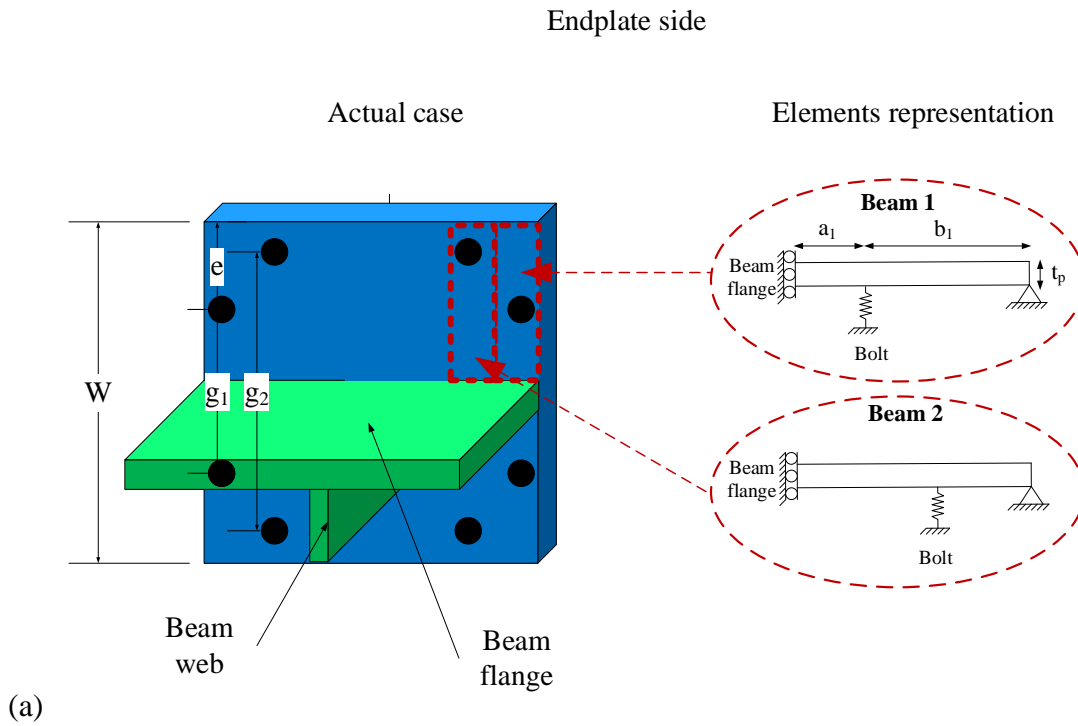
**Figure. 19.** Bolt-force distribution in FE parametric study: (a) for thick column flange specimens, (b) for thin column flange specimens

#### D. Strength model

The data set collected from the experimental and FE results are used to develop a strength model to predict the capacity of the circular eight-bolt unstiffened extended endplate connection for the three failure modes encountered in this research. The strength model also predicts the total prying forces in the connection to account for the additional load in the design of tension bolts, endplate thickness, and column flange thickness.

To develop the strength model, the behavior of representing elements approach is adopted. That is, beam-like elements are identified in the endplate and column flange to determine the factors affecting the strength of the connection, the failure modes, and finally developing equations that predict the strength of the connection based on its material and

geometric characteristics. Figure 20 shows the beam elements identified in the endplate and column flange. As it can be deduced from Fig. 20, the bolts associated with beams 1 and 1' are subjected to higher prying action due to the stiffening effect of the beam flange for the endplate (Fig. 20(a)) and to the stiffening effect of the beam web for the column flange (Fig. 20(b)). That is, beams 1 and 1' govern the strength of the endplate and column flange respectively.



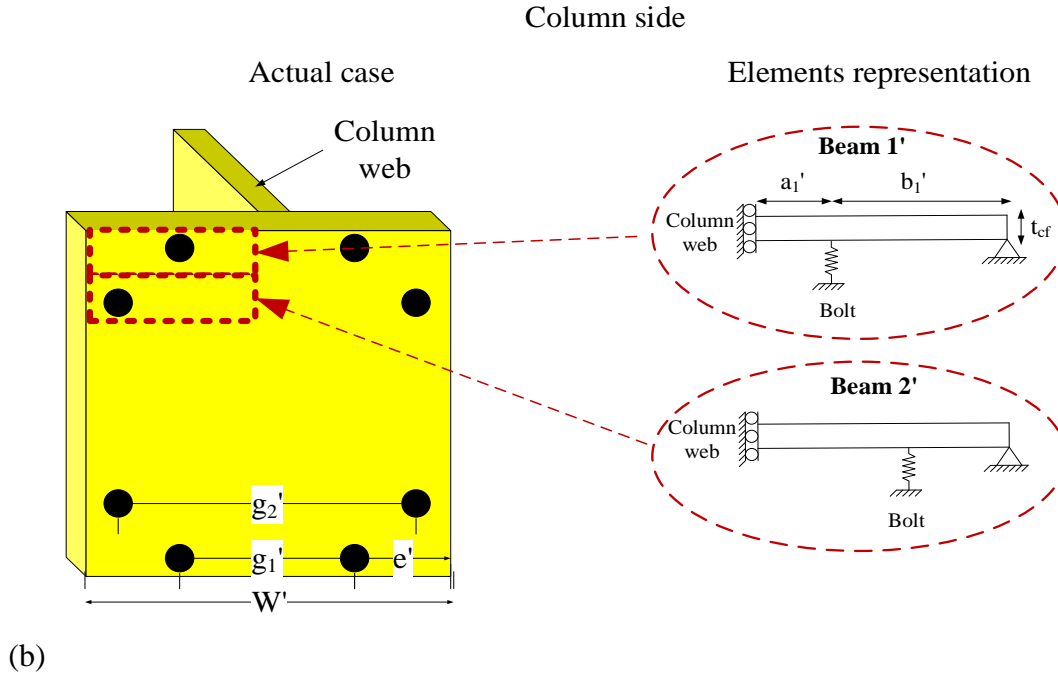


**Figure. 20.** Elements representation: (a) Endplate, (b) Column

**1. F1: Endplate flexural mechanism and B1 and B2 fracture**

This failure mode is encountered when the column flange is thicker than the endplate.

The total connection strength is calculated as follows:

$$T = 4T_{/beam1} + 4T_{/bolt} \quad (19)$$

where:  $T_{/beam1} = \frac{M_{pl}(1+\delta)}{a_1 + b_1}$ ;  $T_{/bolt} = B_{ultimate}$ ;  $M_{pl} = (1/4)pt_p^3F_y$ ;  $p = 4W/n_{tb}$ ;

$$\delta = 1 - d_h / p; a_1 = \frac{g_1 - t_{bf}}{2} - \frac{2}{3}w - \frac{d_b}{2}; b_1 = e + d_b / 2$$

where: T: total connection strength;  $T_{/beam1}$ : strength of beam 1;  $T_{/bolt}$ : strength per bolt;  $M_{pl}$ : plastic moment capacity of endplate;  $a_1$ : length of endplate measured from inside edge of bolt to location of occurrence of plastic hinge at k-zone of endplate;  $b_1$ : length of

endplate measured from inside edge of bolt line to outside edge of endplate;  $B_{ultimate}$  : bolt ultimate strength;  $p$  : tributary width of endplate per tension bolt;  $t_p$  : thickness of endplate;  $F_y$  : base material yield strength;  $W$  : width of endplate;  $n_{tb}$  : tension bolts number;  $d_h$  : bolt hole diameter;  $g_1$  : gage distance of endplate;  $t_{bf}$  : thickness of beam flange;  $w$  : fillet weld size;  $d_b$  : bolt diameter;  $e$  : edge distance of endplate.

Note that the interior and exterior bolt lines are shifted a distance of  $d_b/2$  from the bolt centerline due to the stress distribution caused by the bending of the flange and bolt. Also note that the plastic hinge is located at a distance  $(2/3)w$  away from the stem face of built-up Tees [44]. In the case of a rolled section the  $(2/3)w$  is replaced by  $0.8k$ , where  $k$  is the fillet radius of rolled section.

## 2. F2: Column flange/endplate flexural mechanism and B4 fracture

This failure mode is encountered when the column flange and endplate have equal thicknesses. The total connection strength is calculated as follows:

$$T = 4T_{/beam1} + 4T_{/beam1'} + 2T_{/bolt} \quad (20)$$

$$\text{where: } T_{/beam1'} = \frac{M_{pl}'(1+\delta')}{a_1'+b_1'}; \quad M_{pl}' = (1/4)p't_{cf}^3 F_y; \quad p' = 4W'/n_{tb}; \quad \delta' = 1 - d_h/p';$$

$$a_1' = \frac{g_1' - t_{cs}}{2} - \frac{2}{3}w - \frac{d_b}{2}; \quad b_1' = e' + d_b/2$$

where:  $T_{/beam1'}$  : strength of beam 1';  $M_{pl}'$  : plastic moment capacity of column flange;  $a_1'$  : length of column flange measured from inside edge of bolt to location of occurrence of plastic hinge at k-zone of column flange;  $b_1'$  : length of column flange measured from inside

edge of bolt line to outside edge of column flange;  $p'$ : width of column flange tributary per tension bolt;  $t_{cf}$ : thickness of column flange;  $W'$ : width of column flange;  $g_1'$ : gage distance of column flange;  $t_{cs}$ : thickness of column web;  $e'$ : edge distance of column flange.

### ***3. F3: Column flange flexural mechanism and B4 fracture***

This failure mode is encountered when the column flange is thinner than the endplate.

The total connection strength is calculated as follows:

$$T = 4T_{/beam1'} + 2T_{/bolt} \quad (21)$$

### ***4. Total prying forces***

The total prying forces developed in the connection are calculated as follows:

$$Q_{total} = B_T - T_s \quad (22)$$

where:  $Q_{total}$ : total prying forces;  $B_T$ : total bolt-force; - summation of all eight bolts forces;  $T_s$ : smallest of the strengths equations.

The experimental and FE results were used to determine the corresponding bolts forces to compute  $B_T$ . For F1 failure mode: bolts B1 and B2 forces are equal to  $B_{ultimate}$  while bolts B3 and B4 forces are equal to  $B_{pretension}$ , where  $B_{pretension}$ : bolt pretension force. For F2 failure mode: bolt B4 force is equal to  $B_{ultimate}$  while bolts B1, B2, and B3 forces are also equal to  $B_{pretension}$ . For F3 failure mode: B4 force is equal to  $B_{ultimate}$  while bolts B1, B2, and B3 forces are equal to  $0.8 B_{ultimate}$ . Note that, the strength model predicts the connection strength till first component failure only. Thus, the bolts forces obtained in this section are lower than the bolts forces encountered at the end of the experimental program.

The strength model results are compared to the experimental and FE results in Table 5. It is shown from the results that the strength model is able to predict the strength and total prying forces of the isolated connection with less than 10 % error.

**Table. 5.** Strength model results

Test ID	Load at failure (kN)			Total prying force (kN)		
	<i>ABAQUS</i> / Experiment	Strength model	Error (%)	<i>ABAQUS</i> / Experiment	Strength model	Error (%)
M1, M2, C1 (average)	695	672	5	63	66	5
M3 and C2 (average)	588	553	6	-	83	-
M4, M5, C3 (average)	507	505	0	112	115	3
W18-tc	1106	1100	1	100	105	5
W18-m	869	845	3	131	142	8
W18-tn	595	596	0	131	136	4
W21-tc	1734	1702	2	155	151	3
W21-m	1162	1188	2	180	172	4
W21-tn	830	822	1	185	191	3
W24-tc	1906	1932	1	181	173	4
W24-m	1294	1283	1	190	182	4
W24-tn	953	957	0	204	211	3

### E. Design procedure and example

The distribution of tension bolts and the column flange thickness check for flexural yielding, specific to the circular bolts distribution, is done as per the recommendations of Hantouche and Mouannes [19]. Second, the strength of the connection is checked using Eqs. 19, 20, and 21. Third, the additional tensile forces induced in tension bolts are calculated using Eq. 22. Fourth, the diameter of tension bolts and endplate thickness are modified by taking into account the additional load due to prying forces. Fifth, the column flange thickness is checked again adding the effect of the prying forces.

Note that only the differences from the design guidelines of the *ANSI/AISC 358-16 Chapter 6* [2] are stated in this example. Also note that all nomenclature used in this example is defined as per *ANSI/AISC 358-16* [2] and thus is not repeated here.

A W14x257 (A992) column is connected to a W18x55 (A992) beam using a PL 15x35x<sup>3</sup>/<sub>4</sub> (A992) and <sup>7</sup>/<sub>8</sub> in. diameter bolts (A490). The strength of the connection is checked against the equations developed in this research. The results are presented in Table 6.

**Table 6.** Design example: summary of results

Flexural yielding of endplate and B1 & B2 fracture	Flexural yielding of endplate and column flange and B4 fracture	Flexural yielding of column flange and B4 fracture
$d_e = 50\text{mm}$ , $p_b = 90\text{mm}$ , $p_{fi} = p_{f0} = 50\text{mm}$ , $s = 125\text{mm}$ , $h_1 = 305\text{mm}$ , $h_2 = 393\text{mm}$ , $h_3 = 511\text{mm}$ , $h_4 = 600\text{mm}$		
$g_1 = g_1' = 162\text{mm}$ , $g_2 = g_2' = 324\text{mm}$		
$p = p' = 191\text{mm}$ , $\delta = \delta' = 0.875$		
$a_1 = 41\text{mm}$ , $b_1 = 121 > 1.25a_1 = 51 \rightarrow b_1 = 51\text{mm}$		
$a_1' = 5\text{mm}$ , $b_1' = 121 > 1.25a_1' = 6 \rightarrow b_1' = 6\text{mm}$		
$M_{pl} = 4920\text{kN.mm}$ , $M_{pl}' = 78700\text{kN.mm}$		
$T_{/beam1} = 100\text{kN}$ , $T_{/bolt} = 272\text{kN}$ , $T_{/beam1}' = 15400\text{kN}$		
$T_1 = 1490\text{kN}$	$T_2 = 62400\text{kN}$	$T_3 = 62000\text{kN}$
$Q = B_T - T_1 = 472\text{kN}$		



The results show that  $T_1$  governs the design and the connection is expected to fail in flexural mechanism of endplate and  $B_1$  and  $B_2$  fracture. After computing the additional prying forces and incorporating them in  $M_f$ , the required bolt diameter can be calculated as follows:

$$d_b = \sqrt{\left(\frac{M_f}{2(h_1 + h_2 + h_3 + h_4)}\right) \frac{4}{\pi \phi_{nt} F_{nt}}} = 7/8 \text{ in.} \rightarrow \text{(the same bolt diameter is needed)} \quad (23)$$

The endplate thickness is checked for flexural yielding for the critical yield line shown in Fig. 21. The required endplate thickness is:

$$t_p \geq \sqrt{\frac{M_f}{Y_p F_y}} = 0.8 \text{ use: } t_p = 7/8 \text{ in.} \rightarrow \text{(thicker endplate is needed)} \quad (24)$$

Note that  $Y_p$  is derived using the virtual work method:

$$Y_p = b_p \left( \left( \frac{1}{p_{fi}} \right) h_2 + \left( \frac{1}{p_{fi}} \right) h_3 + \left( \frac{1}{s} \right) h_4 \right) + \frac{2}{g_1} \left( s + \frac{b_p}{4} - \frac{e}{2} \right) h_4 + \frac{2}{g_2} \left( p_{fi} + \frac{b_p}{2} - e \right) h_3 \quad (25)$$

Finally, the column flange thickness is checked for flexural yielding adding the effect of the prying forces:

$$t_{cf} \geq \sqrt{\frac{F_u + Q}{\left[ 2 \left( \frac{b_{cf}}{2s} \right) + 2(1 + 2p_b) \frac{1}{g_2} + 4(p_b + s) \frac{1}{g_1} \right] F_y}} = 1.02 \rightarrow t_{cf} = 1.89 \geq 1.02 \text{ in.} \quad (26)$$

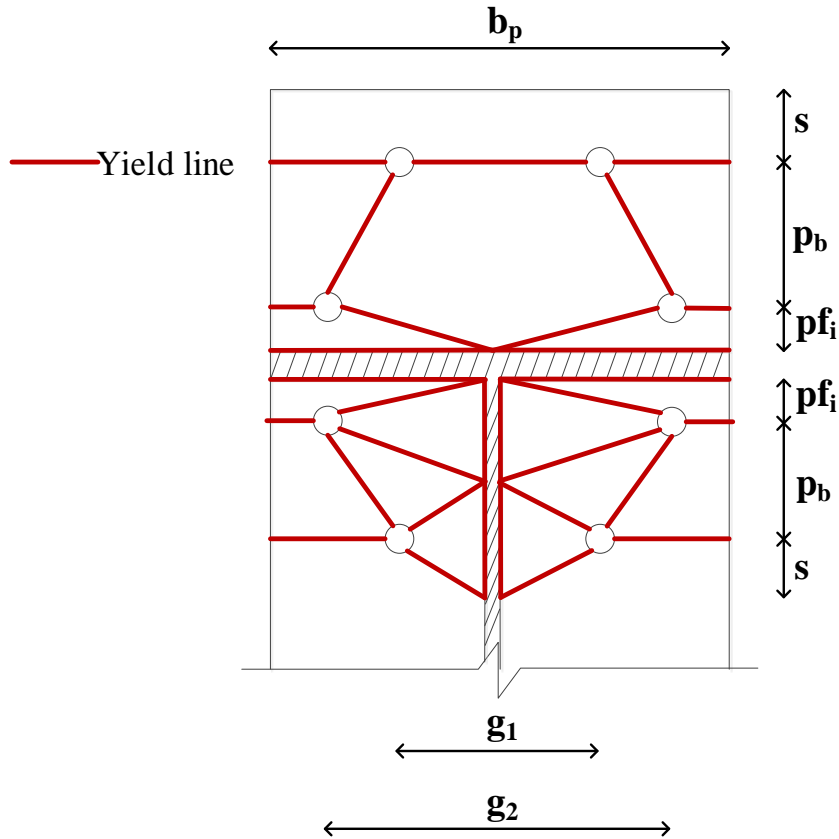


**Figure. 21.** Endplate yield line mechanism

## F. Conclusions

The goal of this research is to investigate, through experimental and analytical studies the eight-bolt unstiffened extended endplate connection with circular bolts configuration for use in seismic applications. An experimental investigation was conducted to study the effect of the circular bolts pattern on the force-displacement, bolt-force distribution, prying forces and overall performance of the connection. Different column flange thicknesses were studied and the respective failure modes were characterized. The results of this study showed that the circular bolts distribution guarantees a minimum of 7.4 bolts, out of the 8 bolts present in the connection, effective in carrying the load. Thus, the performance of the bolts is enhanced from 85 % (rectangular bolts pattern) to larger than 90 % (circular bolts pattern). Thus, the design capacity

of the extended endplate associated with circular bolts configuration is higher than the one associated with rectangular bolts configuration. Additionally, the experimental investigation was validated using FE analysis and an FE parametric study was performed to cover deeper beam sections. Then, a strength model was developed to predict the strength and total prying forces of the isolated connection. It should be noted that the strength model is applicable for the circular bolts pattern proposed by Hantouche and Mouannes [19] only. Finally, a design procedure and an example were presented in order to determine the required bolt diameter and endplate and column flange thicknesses accounting for the additional prying forces.

In summary, previous and current research have shown that omitting stiffeners and distributing tension bolts in a circular pattern, in the eight-bolt extended endplate connection, improve the connection seismic performance and reduce the fabrication although a thicker endplate is required. The research performed in this chapter is part of broader experimental and analytical studies on detailing and designing extended endplates with circular bolts configuration for use in IMF and SMF which satisfy prequalification requirements.

## CHAPTER V

# METHODOLOGY AND APPLICATION OF DUCTILE FRACTURE MODELING ON BOLTED STEEL CONNECTIONS

### A. Introduction

Despite all the research conducted so far on the ductile fracture of steel material under combined loading effect for any steel grade and loading conditions, the researchers have yet to agree on a unified model, a calibration process, and the values of the calibrated parameters. Furthermore, the application of the developed fracture models to steel connections has been very limited. To counteract these limitations, this chapter employs the *SMCS* and the *Hooputra* ductile fracture criterion in *ABAQUS* in order to reproduce the experimental results of steel moment connections subjected to monotonic and cyclic loadings. Double Tee and extended endplate connections are chosen since they can be considered two of the most commonly used prequalified bolted moment connections for seismic applications. A detailed methodology is first presented to guide researchers and designers to model the ductile fracture of steel material in *ABAQUS*. Then, the calibration of steel base (A992, A572-50, A36, S355, S275, ST44) and bolt (A490, A325, Grade 8.8, Grade 10.9) material grades is presented. Following, the experimental results, available in the literature, of both moment connections are validated against the proposed fracture model in *ABAQUS*.

## B. Methodology of FE fracture modeling in *ABAQUS*

In this section, a step-by-step approach to model the fracture of steel structures under different loading scenarios and for different steel grade, using the FE ductile fracture models available in *ABAQUS*, is presented.

The existing ductile fracture models include the combined effect of tensile and shear loadings in one model. However, the difficulties associated with applying these models via user-defined subroutines in *ABAQUS*, make it very complex for designers. For this reason, this research uses the built-in ductile damage models available in *ABAQUS*. These models are easy to apply and require as input several material characteristics that will be generated in this research for a wide range of steel grades.

### 1. Ductile damage

The ductile damage of steel due to tensile loading can be modeled by the *SMCS* model defined known as “ductile damage” in *ABAQUS*. The following equation is defined:

$$\varepsilon_p^f = \alpha \exp^{-\beta\eta} \quad (27)$$

$$\text{where } \eta = \frac{-\bar{\sigma}}{\sigma_m} ; \sigma_m = \sqrt{\frac{(\sigma_1 - \sigma_2)^2 + (\sigma_1 - \sigma_3)^2 + (\sigma_2 - \sigma_3)^2}{2}} ; \bar{\sigma} = \frac{\sigma_1 + \sigma_2 + \sigma_3}{2}$$

Where  $\alpha$  is the toughness parameter indicating the material opposition to macro-voids formation,  $\beta$  is the material specific parameter related to modeling the process of void growth,  $\varepsilon_p^f$  is the equivalent plastic strain at failure initiation,  $\eta$  is the stress triaxiality,  $\bar{\sigma}$  is the hydrostatic or mean stresses,  $\sigma_m$  is the von Mises stresses, and  $\sigma_1, \sigma_2, \sigma_3$  are the principle stresses.

The model parameters,  $\alpha$  and  $\beta$ , are specific for every material and need to be calibrated in order to identify the equivalent plastic strain at fracture for various values of stress triaxiality. Also, *ABAQUS* requires the user to input the strain rate. Fracture in a material due to tensile loading will initiate when the specimen's plastic strain vs. stress triaxiality curve meets the material-specific curve.

## 2. Shear damage

The ductile fracture of steel due to shear loading can be modeled by the *Hooputra* model defined as “shear damage” in *ABAQUS*. The following equations are defined:

$$\theta = \frac{1 - k_s \eta}{\phi} \quad (28)$$

$$\varepsilon_{p-s}^f = \frac{\varepsilon_s^+ \sinh[f(\theta - \theta^-)] + \varepsilon_s^- \sinh[f(\theta^+ - \theta)]}{\sinh[f(\theta^+ - \theta^-)]} \quad (29)$$

Where  $\theta$  is the shear stress parameter,  $k_s$  is the material parameter in shear fracture,  $\phi$  is the ratio of maximum shear stress to von Mises stress,  $\varepsilon_{p-s}^f$  is the equivalent plastic strain at failure initiation due to shear stresses,  $f$  is the material parameter in shear fracture,  $\varepsilon_s^+$  is the equivalent plastic strain in equibiaxial tension at shear fracture,  $\varepsilon_s^-$  is the equivalent plastic strain in equibiaxial compression at shear fracture,  $\theta^+$  is the shear stress parameter for equibiaxial tension ( $\theta^+ = 2 - 4k_s$ ), and  $\theta^-$  is the shear stress parameter for equibiaxial compression ( $\theta^- = 2 + 4k_s$ ).

Applying the *Hooputra* model requires the user to calibrate several material parameters. The parameters  $\varepsilon_s^+$  and  $\varepsilon_s^-$  can be directly obtained from an equibiaxial tension test (i.e. Erichsen test), a one direction (extrusion direction) test with different stress triaxiality, and/or a three point

bending test [26]. However, due to the lack of testing apparatus and material needed to perform these tests and due to the lack of experimental data, in the literature, needed for the calibration process of the steel material, in this research, some parameters are obtained from the literature and others are calibrated using FE analysis of coupon tests. In this research, some parameters are obtained from the literature and others are calibrated using FE analysis of coupon tests. Also, *ABAQUS* requires the user to input the strain rate. Fracture in a material due to shear loading initiates when the specimen's plastic strain versus the shear stress parameter curve meets the material specific curve.

### **3. Material Definition**

The aforementioned ductile fracture models are included in the material definition in *ABAQUS*. Three components of the material definition are to be specified by the user as shown in Fig. 22:

- 1) The undamaged behavior: the elastic (modulus of elasticity and poisson's ratio) and the plastic (true stress-strain curve in the plastic range) characteristics of the material up to point A.
- 2) The damage initiation point, A, at which the strength of the material starts degrading. This damage initiation point is the most critical between the plastic strain versus the stress triaxiality included in the "Ductile Damage" criterion and the plastic strain vs. shear stress parameter included in the "Shear Damage" criterion.
- 3) The "damage evolution" between points A and B; which defines the material behavior and strength degradation after fracture initiation till total failure.

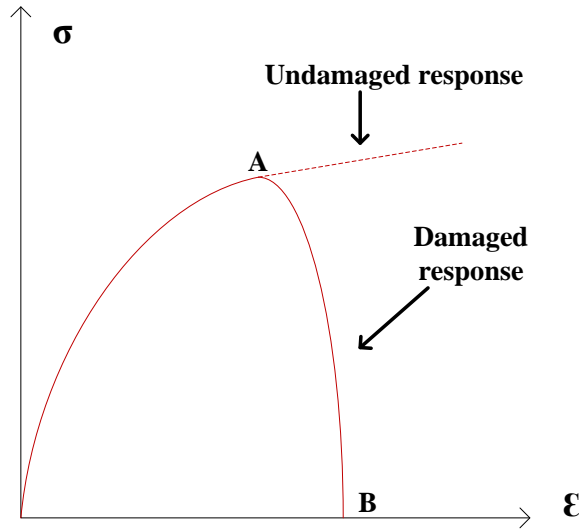


**Figure. 22.** Material Components [53]

#### ***4. Damage Evolution***

Crack formation is not only dependent on the dominating fracture model but also on the damage evolution law represented by the damage variable,  $D$ . Where  $D$  is the damage evolution variable.  $D$  is defined as an index that describes the process of damage evolution starting from the first macro-crack formation where  $D = 0$ , till the full fracture surface formation where  $D = 1$ . The damage evolution law can be specified in *ABAQUS* as fracture energy per unit area or plastic displacement as the point of full failure [53]. Where the fracture energy criterion is used, the user needs to input  $G_f$  which represents the area under the stress-plastic displacement curve that can be either linear or exponential. Whereas in case the plastic displacement criterion is used, the user needs to specify  $u_f^{pl}$ , which is the plastic displacement at which full fracture occurs.  $u_f^{pl}$  is related to the plastic strain at fracture,  $\varepsilon_f^{pl}$ , as follows:  $u_f^{pl} = l^* \varepsilon_f^{pl}$ . The characteristic length,  $l^*$ , is determined through fractographic studies based on microstructural measurements such as grain



size and dimple diameter. In this research, a characteristic length ( $l^*$ ) of 0.2 mm was used as recommended by Wang et al. [32]. Whenever the damage variable,  $D$ , reaches the value of one (full fracture), the plastic displacement reaches the value of  $u_f^{pl}$ . The damage evolution in between is specified by  $D$  versus the plastic displacement curve which can be defined as linear, exponential or tabular data.

## 5. Methodology

The following steps are required in order to model the ductile fracture of steel material in *ABAQUS*:

- 1) Use the *Explicit ABAQUS* solver.
- 2) In the material definition enter, in addition to the elastic, plastic and density characteristics, the following:
  - a. “Ductile Damage”: the tabulated values of the strain at fracture, stress triaxiality, and strain rate. As per, Johnson and Cook [25], the effect of strain rate on ductile fracture of steel is minimal and thus it is taken as  $0.001s^{-1}$ .
  - b. “Shear Damage”:  $k_s$  and the tabulated values of strain at fracture, shear stress parameter, and strain rate (also taken as  $0.001s^{-1}$  in this research).
  - c. For both models, the sub-option of “damage evolution” should be specified as displacement or fracture energy.
- 3) Activate the *STATUS*, *DAMAGET* (*Tensile damage*), and *DAMAGESHR* (*Shear damage*) field outputs for the fracture to be visualized.
- 4) Assign amplitudes to all loading conditions to secure a quasi-static application of the loads rather than dynamic.

- 5) Use an explicit mesh and activate the “delete” option so that elements that reach their fracture capacity are removed.

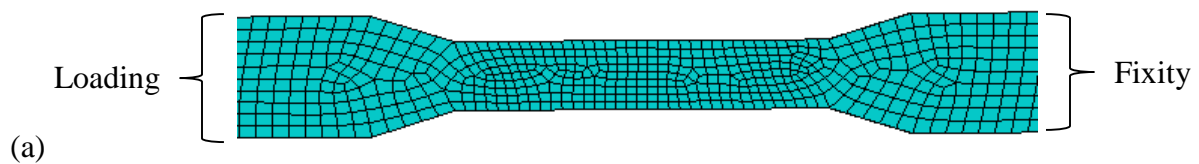
## **D. Material calibration**

### ***1. SMCS***

As previously mentioned in the literature review, researchers have proposed different methods for calibrating the *SMCS* fracture model in order to determine  $\alpha$  and  $\beta$  for any required material. Rice and Tracey [23] derived analytically the value of  $\beta$  to be 1.5. Also, Myers et al. [31] showed that, despite being material dependent, the difference between the analytical value of  $\beta$  and the calibrated values is statistically insignificant and a value of 1.5 is adequate for all steel material. Hence, in this research,  $\beta$  is taken as 1.5.

As for the toughness parameter  $\alpha$ , the process of material calibration consists of reproducing the experimental results of two coupon tests (regular and notched coupons), for the required steel material, using the true stress-strain characteristics of the material. It is important to have a diverse variety of experiments describing different stress states so as to calibrate the model reliably. That is, the geometry of the two coupons has to be different (regular/notched, varying notch geometry or radius). The experimental results are first reproduced using an assumed value of  $\alpha$ . The generated stress-strain curve is compared to the experimental one. The value of equivalent plastic strain and the corresponding stress triaxiality at the center of the coupon at the necking point (location and instance of fracture initiation, respectively) are compared with the corresponding ones generated by the assumed value of  $\alpha$ . The toughness parameter is varied until convergence of experimental and generated results.

Using the explicit solver FE analysis program *ABAQUS*, two coupons for several steel grades are simulated in *ABAQUS* using the methodology presented in section 2.5 and including material nonlinearity. Only “Ductile Damage” is activated and no “Shear Damage” is specified since the coupons are subjected to tensile loading only. The weighted average method recommended by Ling [54] is used to simulate the true stress-strain curve of all steel material input. The engineering stress-strain characteristics used are obtained from the experimental results of coupon tests used in the calibration process. Besides material nonlinearity, geometric nonlinearity is considered in all analyses. The initial analysis includes fracture simulation with an assumed toughness parameter of 2. Three-dimensional *C3D8R* solid brick elements are used. For the boundary and loading conditions, one end of the notched bar is fixed against rotation and displacement in all directions. The other end is released for displacement in the axial direction. Displacement is applied at the released end (Fig. 23 (a)). To obtain the fracture toughness parameter, first the stress-strain curves of the simulated coupon tests are plotted against the experimental ones. Divergence between the two starts at the necking point due to the assumed value of  $\alpha$ . Second, the stress triaxiality versus strain at fracture history at the center of the coupon is plotted against the material specific curve generated using the assumed value of  $\alpha$ , using Eq. 27. A process of trial and error is used to calibrate  $\alpha$  for both stress-strain and stress triaxiality-strain at fracture responses for both coupons.



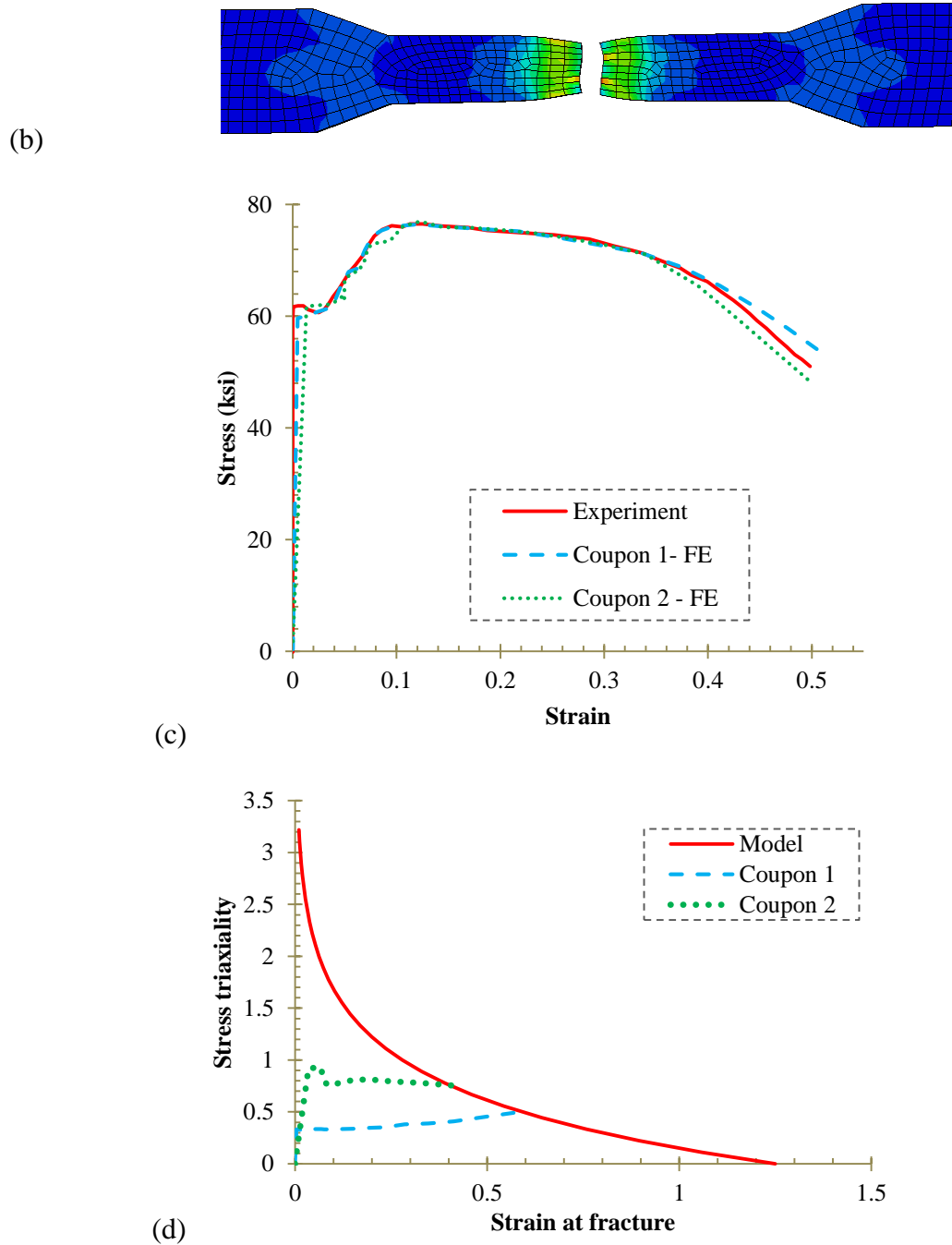


**Figure. 23.** A992: (a) Coupon 1 - mesh, (b) Coupon 1 - deformed shape, (c) stress vs. strain, (d) stress-triaxiality vs. strain at fracture

The results of the calibration (fracture, stress-strain, and stress triaxiality-strain at fracture) of A992 are shown in Fig. 23. All remaining steel material is calibrated using the same approach as the A992 (Check appendix A). The calibrated values of  $\alpha$  are presented in Table 7.

**Table. 7.** Calibration of steel material

Material	Coupon 1	Coupon 2	$\alpha$	$\epsilon_s^+$	$\epsilon_s^-$
A992	Hu [58]	Kiran and Khandelwal [33]	1.25	-0.855	0.929
A572-50 or S355	Ribeiro et al. [59]	Ribeiro et al. [59]	1.65	0.555	6.94
ST44	Versaillet [60]	Brnic et al. [61]	0.9	0.447	-1.487
A36 or S275	Versaillet [60]	Versaillet [60]	0.9	1.767	0.638
A490 or Grade 10.9	Moore et al. [62]	Christopher [63]	2.0	0.347	0.278
A325 or Grade 8.8	Moore et al. [62]	Moore et al. [62]	0.6	1.205	0.189

## 2. Hooputra

*Hooputra* [55] developed the shear fracture model for aluminum alloys. The material parameter in shear fracture,  $f$ , was determined to be 4.04 for quasi-static tests and 2.05 for dynamic tests for all metals. In this study,  $f$  is assumed to be 4.04. Moreover, Adewole and Teh [56] determined  $k_s$  to be 0.1 for steel material. Subsequently,  $\theta^+ = 1.6$  and  $\theta^- = 2.4$ .

For the calibration of  $\epsilon_s^+$  and  $\epsilon_s^-$ , the coupons used for tension calibration are used also to calibrate the shear fracture parameters [57]. At the boundaries of the notched region, fracture

is caused by shear stresses, thus, the shear stress parameter,  $\theta$ , is calculated from the stress results at the boundaries of the fractured area. Also, the equivalent plastic strain at shear fracture  $\varepsilon_{p-s}^f$  is obtained from the FE output results at the boundaries of the notch. Then,  $\varepsilon_s^+$  and  $\varepsilon_s^-$  are obtained by solving the system of two equations two unknowns using Eq. 29 for the two coupons. The results of the shear fracture parameters calibration are also presented in Table 7.

### **C. Validation**

As previously mentioned the main focus of this research is on predicting fracture in double Tee and extended endplate moment connections. That is, the FE fracture models are developed in *ABAQUS* using the methodology described earlier and the calibrations results presented in Table 7. The FE results are then compared with the experimental results available in the literature to validate the proposed model. For this purpose, several experimental results on double Tees and extended endplates are compiled in Table 8 and used for comparison with the proposed FE ductile fracture model.

#### ***1. Geometric, force boundary, and material properties***

All twenty-five specimens are reproduced in *ABAQUS*. The specimens are loaded in two steps. In the first step, where applicable, bolts are pretensioned by applying a pressure equivalent to the minimum required pretension force. In the second step, a displacement controlled monotonic load or cyclic load is applied according to the corresponding testing features. During all steps of the analysis, the corresponding boundary conditions are set. The complete true stress-true strain curve is used for all steel material with isotropic hardening for monotonically loaded specimens and kinematic hardening for cyclically loaded specimens. Both

tension and shear fracture models are specified for all steel material regardless of the expected failure mode. Thus, the failure envelopes are automatically tested at every load increment and the governing one defines the failure pattern.

**Table 8.** Experiments details

Authors	Test ID	Ultimate load			Displacement at fracture		
		Experiment	FE	Error (%)	Experiment	FE	Error (%)
El Kalash and Hantouche [64]	TM1	580 kN	564 kN	2.8	27 mm	28 mm	3.7
	TC1	512 kN	520 kN	1.6	39 mm	39 mm	0
	TM2	610 kN	626 kN	2.6	13 mm	14 mm	7.7
	TC2	793 kN	778 kN	1.9	39 mm	40 mm	2.6
	TM3	859 kN	842 kN	2	2 mm	2 mm	0
	TC3	834 kN	846 kN	1.4	2 mm	2 mm	0
	TM4	995 kN	985 kN	1	2 mm	2 mm	0
El Kalash and Hantouche [65]	M1	512 kN	511 kN	0.2	17 mm	18 mm	5.9
	C1	508 kN	504 kN	0.8	21 mm	23 mm	9.5
	M3	573 kN	558 kN	2.6	41 mm	43 mm	4.9
	C2	653 kN	623 kN	4.6	44 mm	47 mm	6.8
	M4	719 kN	745 kN	3.6	44 mm	45 mm	2.3
	C3	696 kN	750 kN	7.8	49 mm	50 mm	2.0
Coelho et al. [66]	WT1 g	182 kN	176 kN	3.3	21 mm	20 mm	4.7
	WT61 b	215 kN	214 kN	0.5	8 mm	8 mm	0
Piluso and Rizzano [67]	A1	306 kN	305 kN	0.3	36 mm	37 mm	2.8
	B1	253 kN	245 kN	3.1	60 mm	62 mm	3.3
	C1	200 kN	208 kN	4	83 mm	81 mm	2.4
	D1	312 kN	306 kN	1.9	19 mm	21 mm	4.7
Kiamanesh [68]	Circular	99 kips	97 kips	2.0	0.2 in.	0.2 in.	0
Massimo et al. [69]	Test 1	156 kN	159 kN	1.9	27 mm	26 mm	3.7
	Test 2	241 kN	232 kN	3.7	15 mm	15 mm	0
	Test 3	353 kN	362 kN	2.5	3 mm	3 mm	0
Sun et al. [70]	T1-test3	581 kN	582 kN	0.2	12 mm	12 mm	0
	T2-test3	490 kN	479 kN	2.2	21 mm	21 mm	0

## 2. Model discretization

Discretization of all the components of the connections models in *ABAQUS* is performed using explicit *C3D8-R*. At regions where failure is expected to occur and at regions where stress is likely to concentrate (around bolt holes) a finer and a mapped mesh are adopted in order to advance the accuracy of interpolations. Surface-to-surface contact with a finite sliding



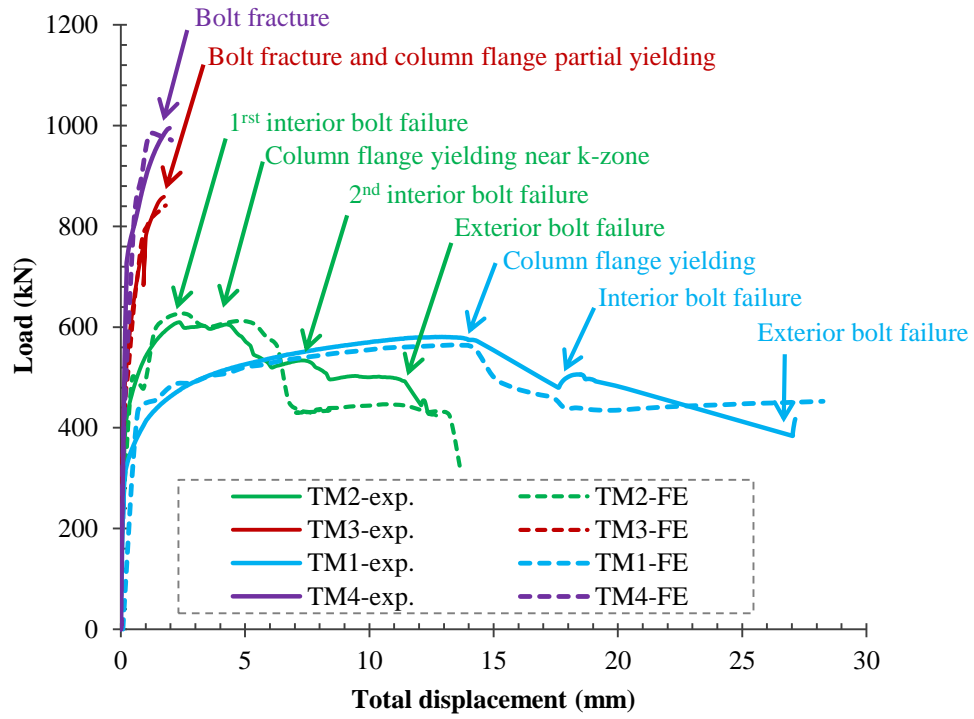
coefficient is used to reproduce contact surfaces between all components of the specimens. This finite sliding is used to represent a friction coefficient of 0.25. The finite sliding allowed separation, sliding, and rotation of the contact surfaces. A general contact interaction is specified to overcome the excessive distortion issues faced in the explicit fracture modeling.

### ***3. Comparison of FE predictions with experiments***

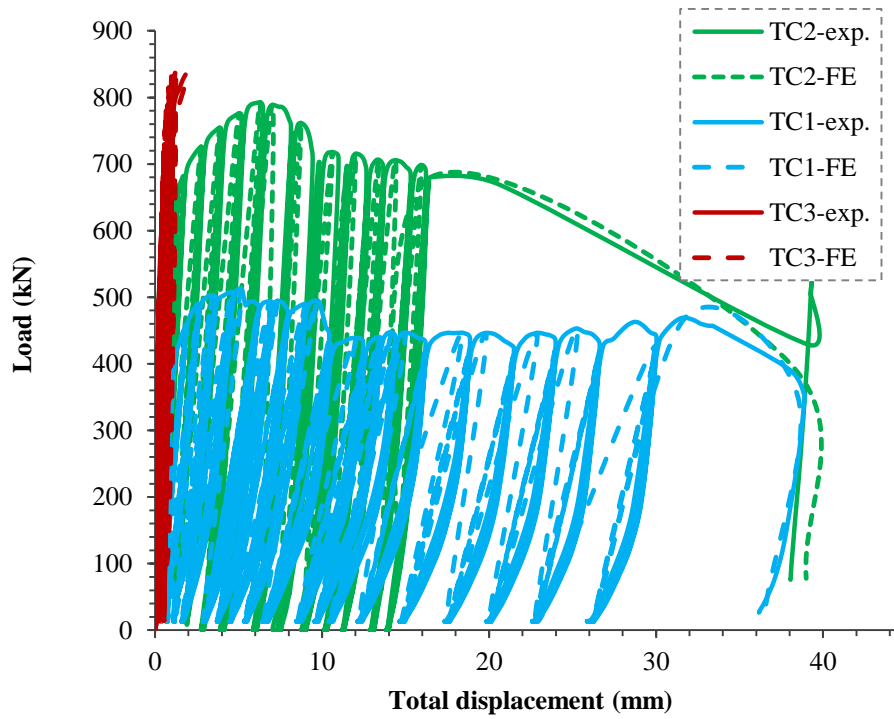
The capability of the FE fracture model to predict the fracture response of double Tees and extended endplates subjected to monotonic and cyclic loadings is validated against the experimental results obtained from the literature. Following is the detailed analysis of the results.

#### ***a. El Kalash and Hantouche [64]***

Seven component tests on column flange/thick Tee connected back-to-back were tested under monotonic and cyclic loadings. Figure 24 shows a comparison between the experimental and FE fracture results of the load-displacement curves. The results show that the FE fracture model predicts with high accuracy the experimental results. Figure 24 and Table 8 show that the proposed FE fracture model is able to predict the ultimate load with a percentage error less than 3. Similarly, comparing the displacement at fracture, the percentage error varies from zero to 8. Also, Figure 24(a) shows the various limit states encountered for every specimen. All limit states were met in the developed FE fracture models as well. Figure 24(b) shows that the FE fracture model is able to predict accurately the cyclic response of the double Tee connections. The results show that the proposed model is able to predict both loading and unloading stages, pre-yielding and post-yielding, till full fracture with high accuracy.



(a)



(b)

**Figure. 24.** El Kalash and Hantouche [64] –Load-displacement: Exp. vs. FE: (a) Monotonic, (b) Cyclic

Four failure modes were encountered in the column flange and bolts. Specimen TM1 failed by flange mechanism in the column. This can be shown from the FE fracture models results (Fig. 25(a)) where plastic hinges are formed at the k-zone and interior bolt line in the column flange. Specimen TM2 failed in mixed mode. It is clearly shown from Fig. 25(b) that plastic hinge mechanism forms at the k-zone of the column flange and fracture of the interior bolts occur simultaneously. As for specimen TM3 (Fig. 25(c)), it failed by partial yielding at the k-zone of the column flange with simultaneous bolts fracture. Finally, specimen TM4, failed by bolts fracture as can be seen in Fig. 25(d). Note that the failure modes of specimens TC1, TC2, and TC3 are the same as the failure modes of specimens TM1, TM2, and TM3, respectively.

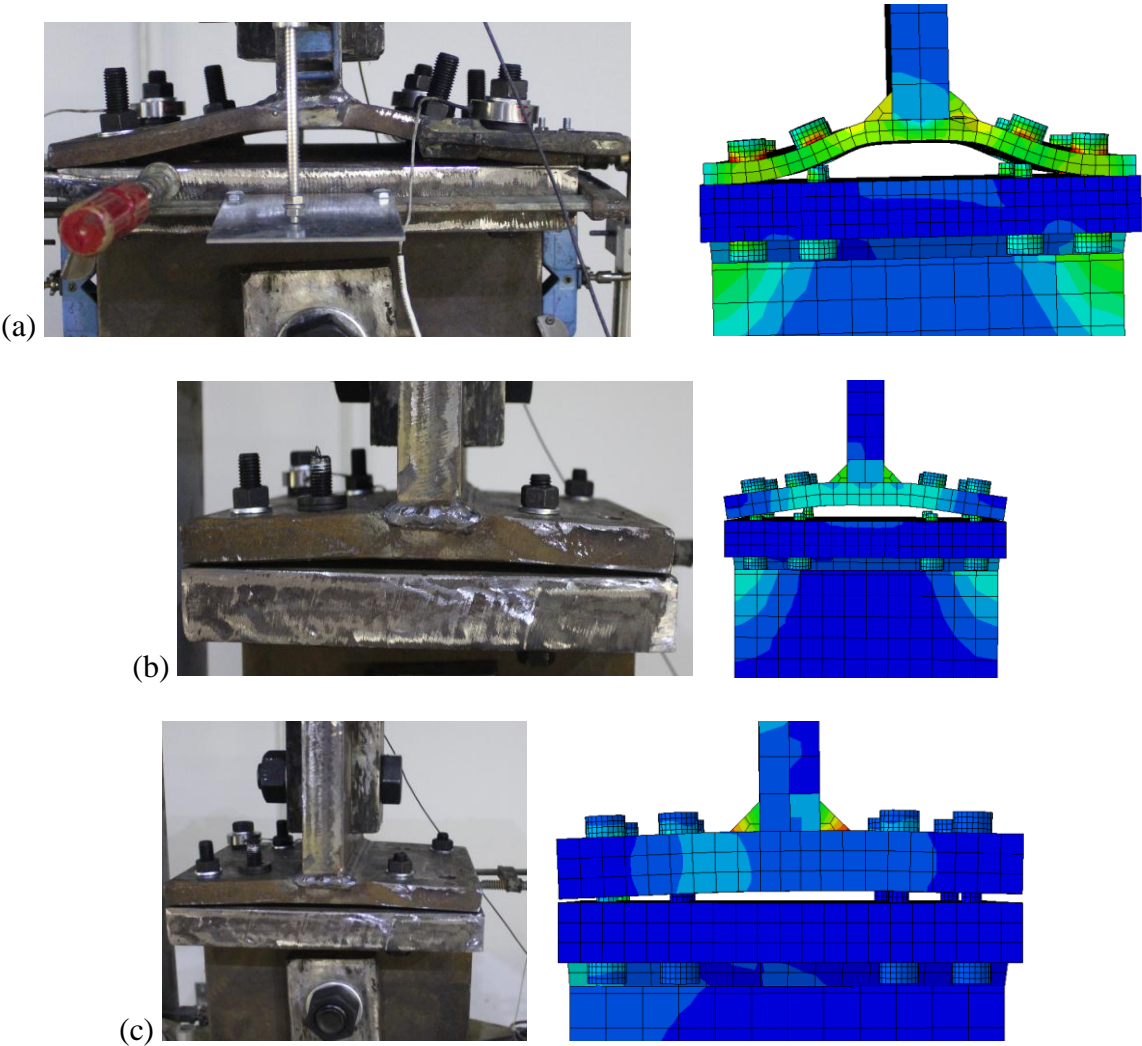




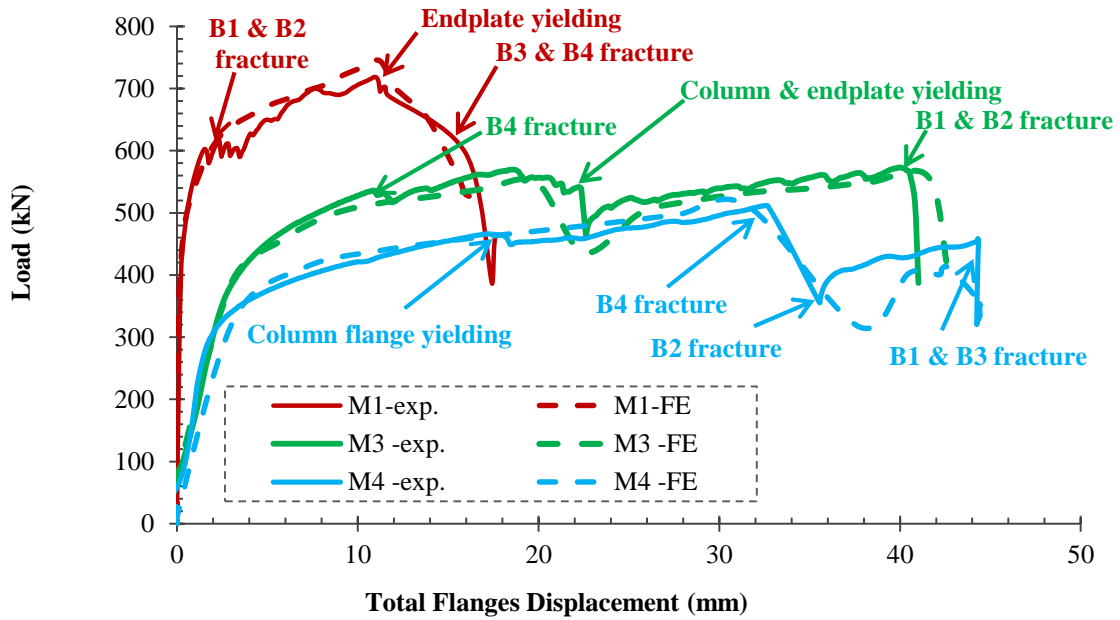
**Figure. 25.** El Kalash and Hantouche [64] – Failure mode: Exp. vs. FE: (a) TM1, (b) TM2, (c) TM3, (d) TM4

The results of specimens TM1 and TM2 show that the displacement at fracture is greatly larger than the displacement at ultimate load. That is, for these ductile specimens (flexible column flange), the displacement at ultimate load for specimen TM1 is 14mm while at fracture the displacement is 27mm this means that 93% increase in the displacement occurred between ultimate and fracture. Similarly, a 500% increase in the displacement of specimen TM2 occurred between the ultimate load and the load causing fracture. This proves that, modeling the fracture of steel connections is essential, especially for seismic applications where large inelastic deformations are expected.

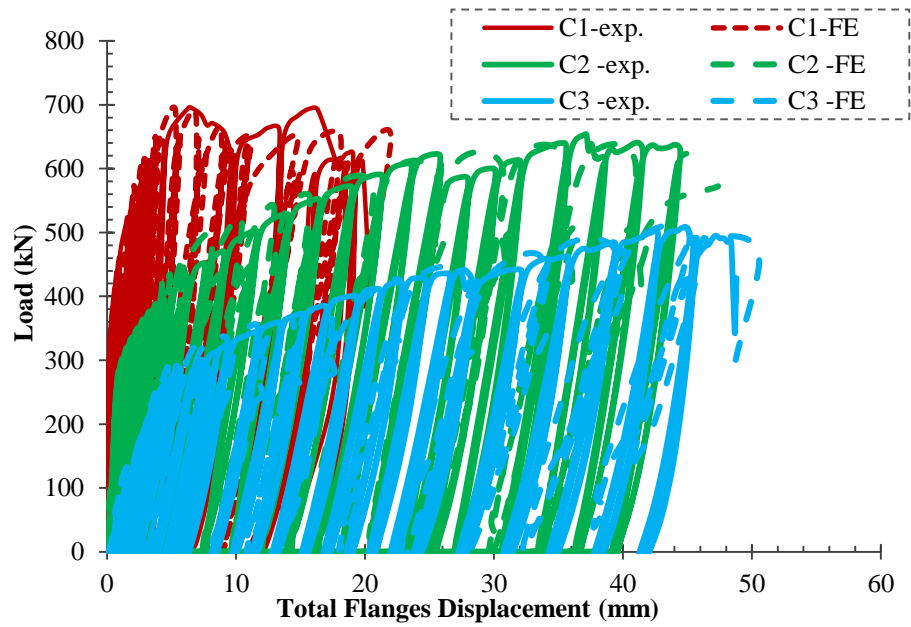
b. El Kalash and Hantouche [65]

Eight component tests on eight-bolt unstiffened extended endplate connections with circular bolts configuration subjected to monotonic and cyclic loadings were performed. Figure 26 shows the comparison of load-displacement responses of the experimental versus the FE fracture results. It is evident from Fig. 26 and Table 8 that the fracture model is able to predict the load-displacement response of the tested specimens with excellent accuracy and with percentage error less than 10. Figure 26(a) shows the different limit states that every specimen went through till failure. All the encountered limit states occurred in the FE fracture simulations as well. Also, Fig. 26(b) shows the load-displacement response of the specimens tested under

cyclic loading. The results show that the FE fracture model predicts well the cyclic response of extended endplates including the loading and unloading curves.



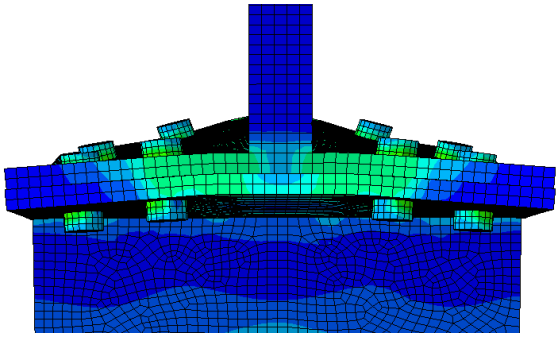
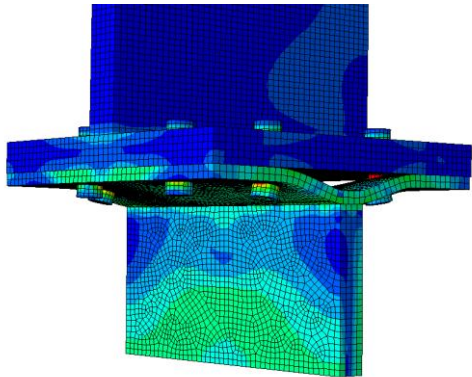
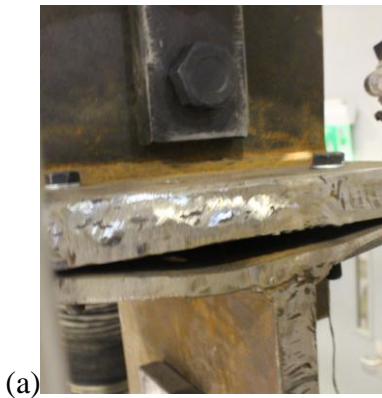
(a)



(b)

**Figure. 26.** El Kalash and Hantouche [65] – Load-displacement: Exp. vs. FE: (a) Monotonic, (b) Cyclic

Three failure modes were encountered in the column flange, endplate, and tension bolts. Figure 26 shows a comparison between the experimental and FE fracture results of the three encountered failure modes in specimens M1, M3, and M4. As shown in Fig. 27(a), M1 failed by endplate yielding and fracture of two bolts. While M2 failed by endplate and column flange yield mechanism with one bolt fracture (Fig. 27(b) for the column and Fig. 27(c) for the endplate). Finally, specimen M4 failed by column flange yield mechanism and one bolt fracture. Note that the failure modes of specimens C1, C2, and C3 are the same as the failure modes of specimens M1, M2, and M3, respectively.



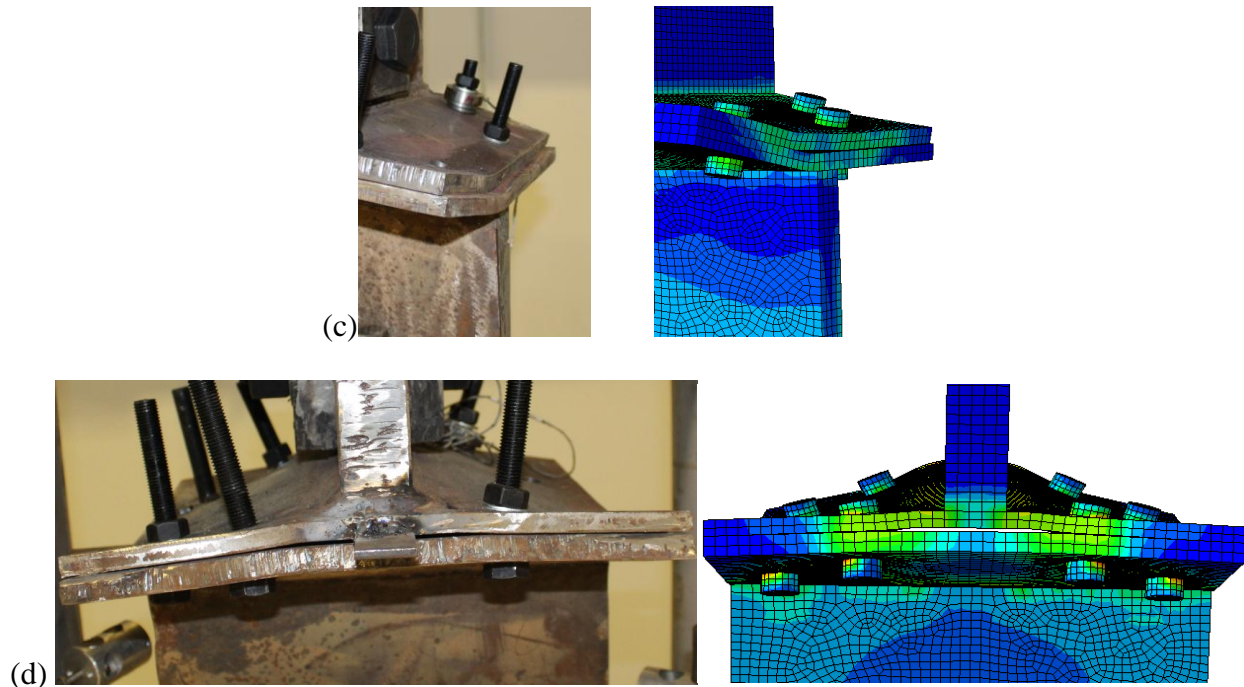
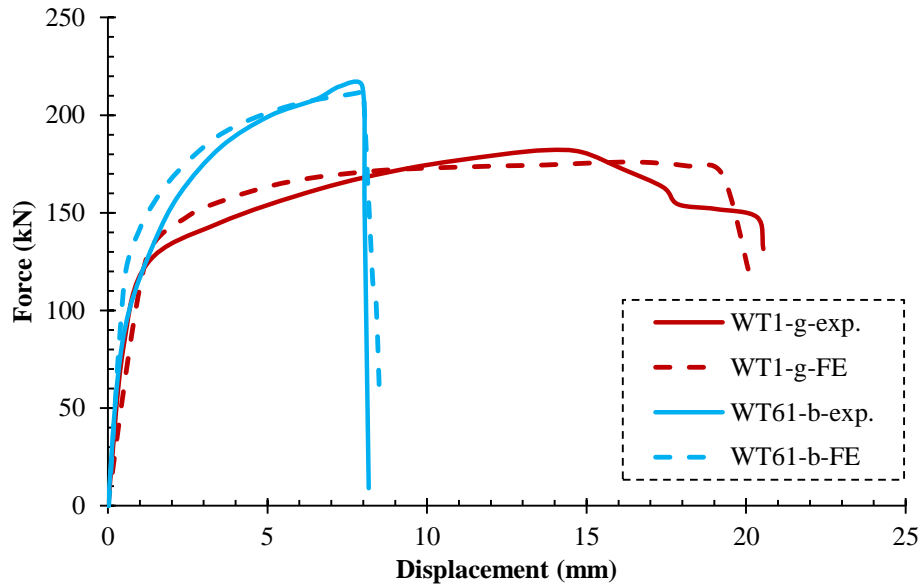


**Figure. 27.** El Kalash and Hantouche [65] – Failure mode: Exp. vs. FE: (a) M1, (b) M3-Column side, (c) M3-Endplate side, (d) M4

An increase of 55%, 110%, and 38% in the displacement of specimens M1, M2, and M3 occurred from the ultimate load to the fracture load. Large plastic displacement capacity was induced post the ultimate point till full failure.

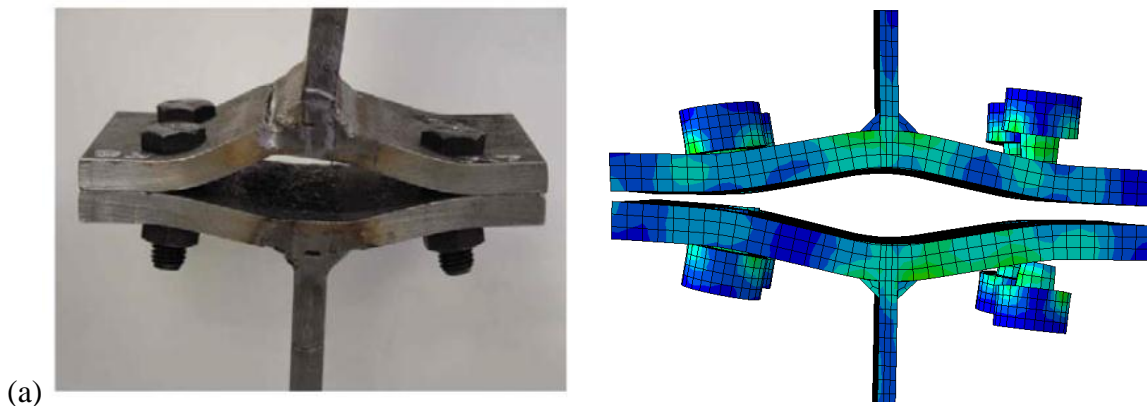
c. Coelho et al. [66]

Thirty-two component tests on welded double Tees connected back-to-back were tested under monotonic loading. Figure 28 shows the load-displacement response of two specimens that were modeled in *ABAQUS* for validation purposes. It is clearly shown from Fig. 28 and Table 8 that the FE fracture model is able to predict with excellent accuracy (less than 5% error) both the ultimate load and displacement at fracture.



**Figure. 28.** Coelho et al. [66] – Load-displacement: Exp. vs. FE

Figure 29 shows a comparison of the experimental and FE failure modes. Both specimens failed in bending and bolt fracture. This is clearly shown in the FE results of the specimens at fracture (Fig. 29). Specimen WT1g experienced cracking in the plate material at the heat affected zone as well. However, this was not predicted by the FE fracture model since the weld material was modeled with tie constraints attaching it to the base material rather than the actual welding process that involves heating the base material and possibly causing residual stresses to the material at the heat affected zone well before loading the specimen.





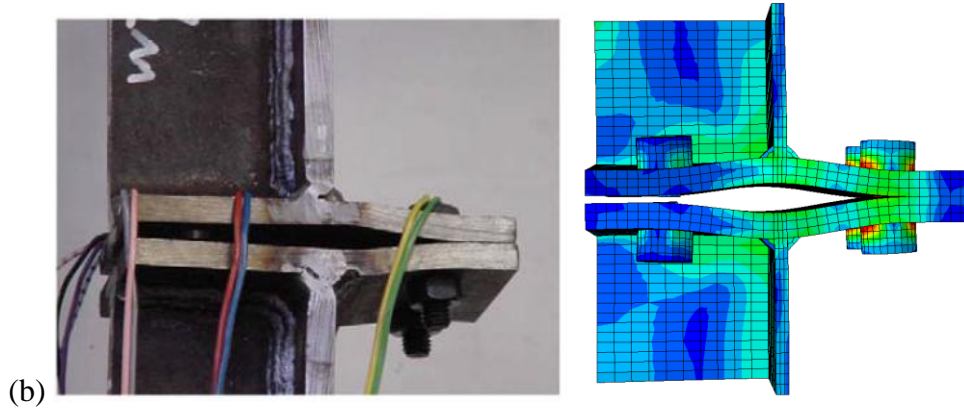


**Figure. 29.** Coelho et al. [66] – Failure mode: Exp. vs. FE: (a) WT1g, (b) WT61b

Specimen WT61b, associated with a stiffener plate, failed in a brittle manner due to the stiffening effect of the attached plate that caused the fracture of the bolts. That is, no noticeable plastic deformation beyond the point of ultimate occurred in this specimen. While for specimen WT1g, no stiffener plate was attached and the specimen failed in a ductile manner with plate bending and finally bolts fracture. An increase of 40% in the plastic deformation occurred between the ultimate and the fracture point. This proves again the importance of the FE fracture model in predicting the post-ultimate plastic deformation of double Tee specimens designed to fail by plate bending (ductile failure) for applications that require large inelastic deformation.

d. Piluso and Rizzano [67]

Twenty-eight component tests on hot rolled and built-up double Tees connected back-to-back were tested under cyclic and monotonic displacement controlled loadings. Four specimens with varying geometry and beam sections were validated using FE fracture analysis. Figure 30 shows the load-displacement comparison of the experimental and FE results. The FE fracture model predicts with high accuracy the response, till full fracture, of built-up and hot rolled double Tee connections. This is shown in Table 8 where the percent error between

experimental and FE fracture results is less than 5% for both the ultimate load and the displacement at fracture.

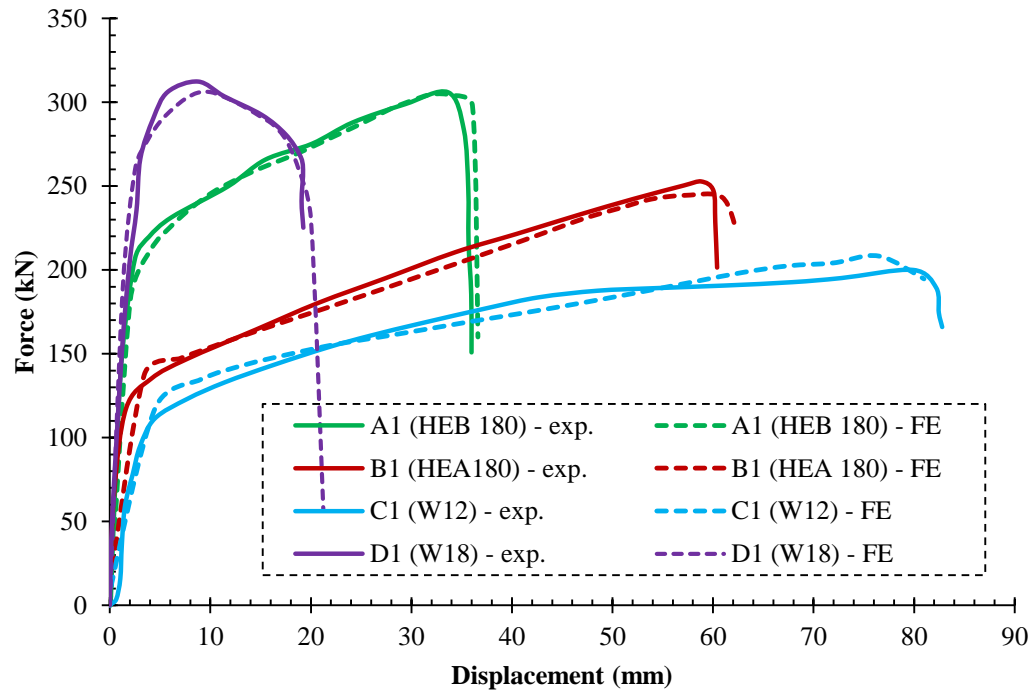


**Figure. 30.** Piluso and Rizzano [67] – Load-displacement: Exp. vs. FE

Figure 31 shows the failure modes encountered in the FE fracture simulations. Specimen A1 failed by mixed mode. This is evident in the plastic hinge formed at the k-zone of the Tee section and the fracture of bolts (Fig. 31(a)). Specimens B1 and C1 failed by flange mechanism. Figures 31(b) and 10(c) show the plastic hinge formation at the k-zone and at the bolt line in the Tee section. Finally, specimen D1 failed by bolt fracture (Fig. 31(d)).

Specimens A1, B1, and C1 failed in a ductile manner due to the plastic hinge formation. This is shown by the relatively large plastic deformation exhibited by the specimens, especially B1 and C1 (Fig. 31). While specimen D1 failed in a brittle manner (bolt fracture) and this is shown by the small plastic deformation exhibited by specimen D1 (Fig. 31).

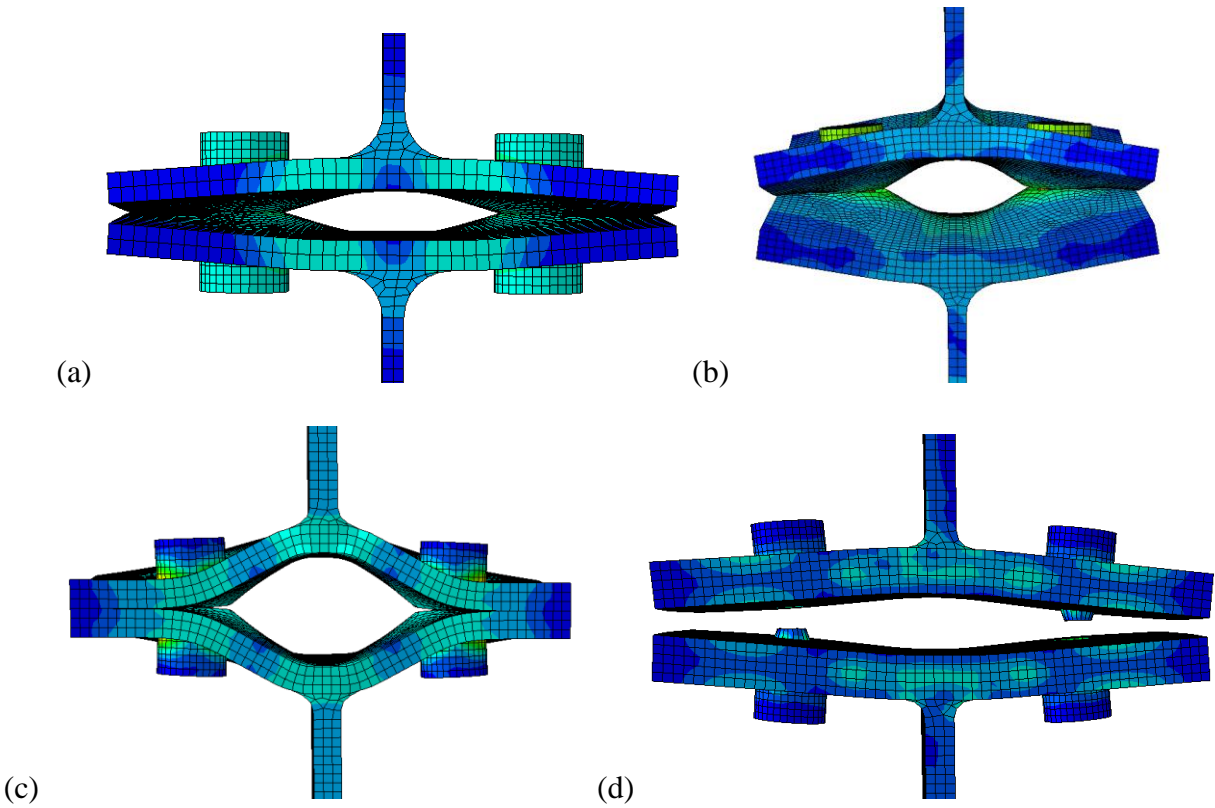


**Figure. 31.** Piluso and Rizzano [67] – Failure mode: Exp. vs. FE: (a) A1, (b) B1, (c) C1, (d) D1

e. Kiamaresh [68]

Three component tests on hot rolled double Tees connected back-to-back were tested under monotonic loading. The double Tee connection with circular bolt configuration was validated using FE fracture modeling. The load-displacement response is shown in Fig. 32. Comparison of experimental and FE fracture results show an excellent capability of the fracture model to predict both the ultimate load and plastic deformation at fracture (see Table 8).

Figure 33 shows the comparison of the failure mode between the experimental test and the FE simulation. The specimen failed by flange mechanism. This is shown by the two plastic hinge formation: at the k-zone and at the interior bolt line. This is also shown in the 100% increase in the plastic deformation between the ultimate load point and the fracture point.

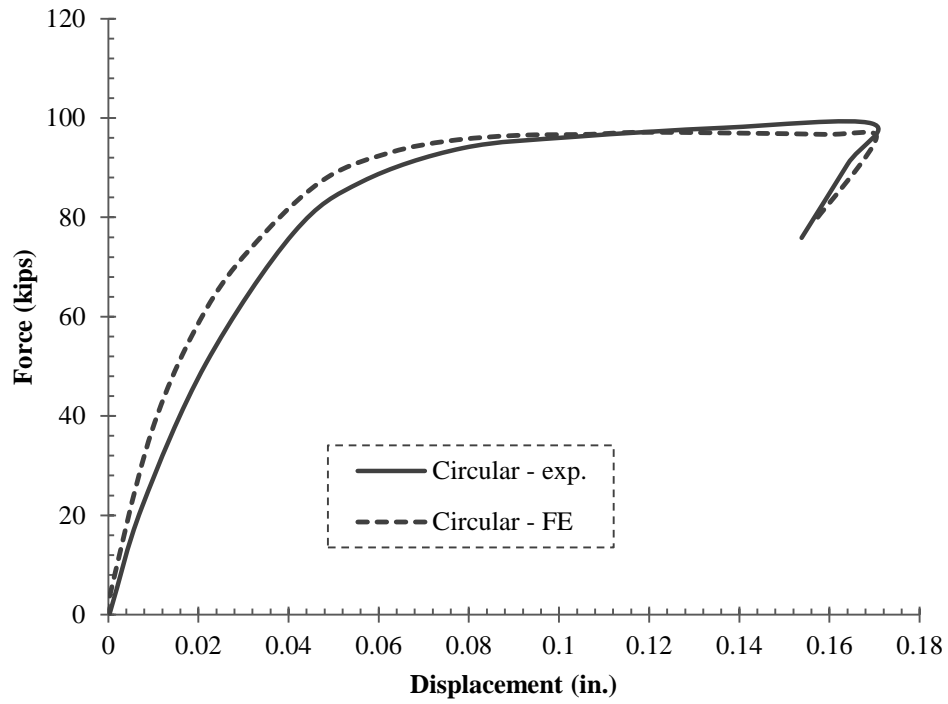


**Figure. 32.** Kiamanesh [68] – Load-displacement: Exp. vs. FE

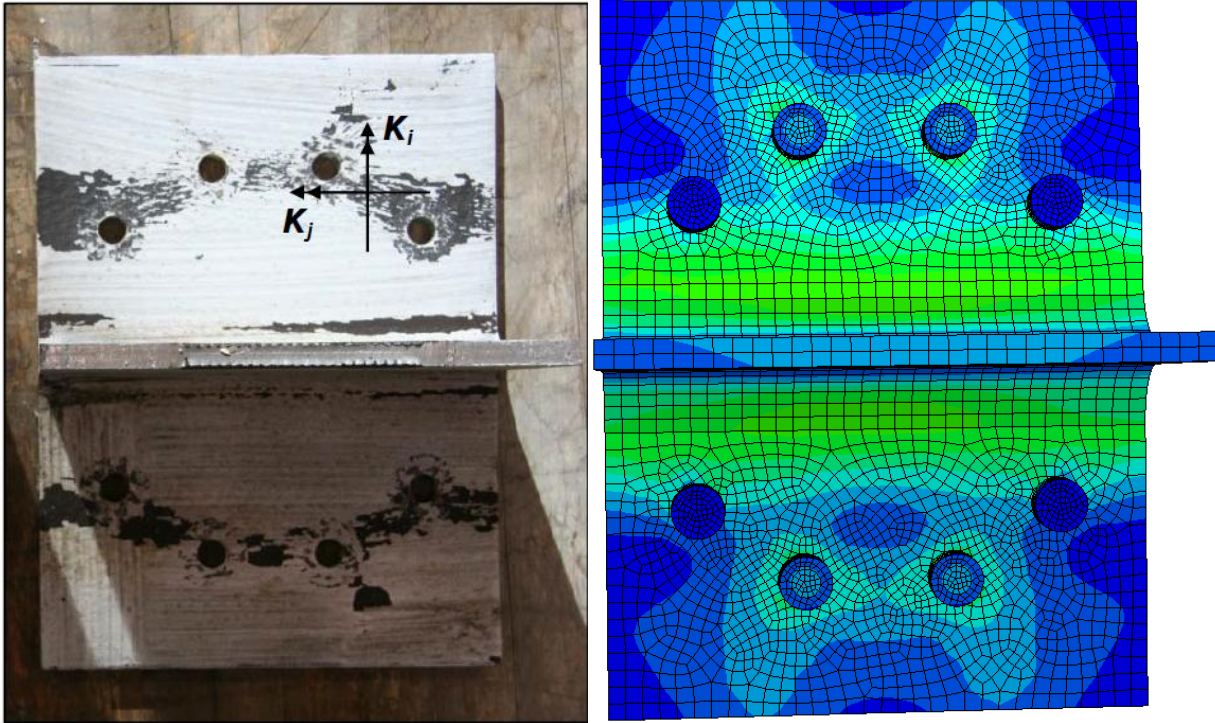


**Figure. 33.** Kiamanesh [68] – Failure mode: Exp. vs. FE

f. Massimo et al. [13]

Three built-up Tee sections were tested under monotonic loading to study the failure modes of equivalent Tee sections. Figure 34 shows the load-displacement curve of experimental versus FE fracture results. Comparison of the ultimate load and displacement at fracture shows that the fracture model was able to predict the response of the built-up Tees with excellent accuracy and with percent error less than 5 (Table 8).

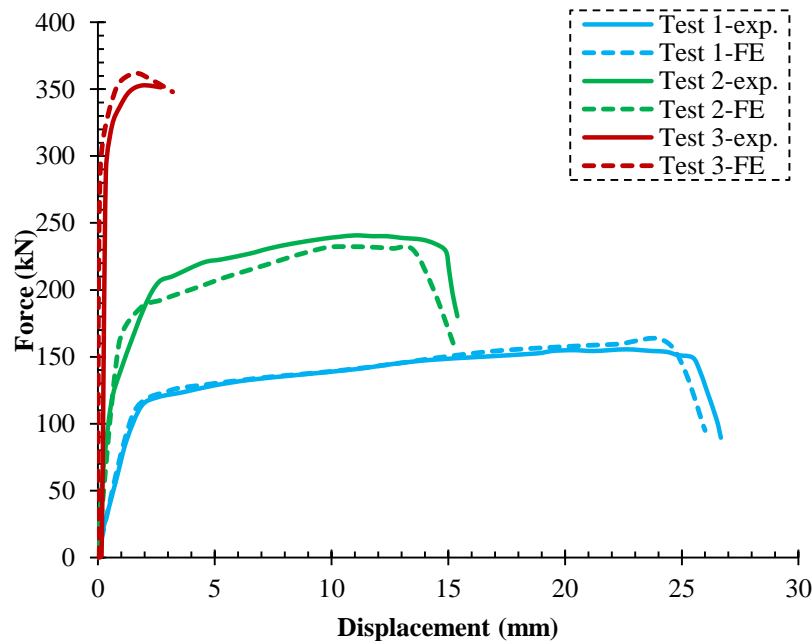


**Figure. 34.** Massimo et al. [13] – Load-displacement: Exp. vs. FE

The typical three failure modes were encountered: flange mechanism (Test 1), mixed mode (Test 2), and bolts fracture (Test 3). Comparison of the three typical failure modes between the experimental tests and the FE simulations is shown in Fig. 35. The fracture results are in excellent agreement with the experimental results.

Finally, it is shown from Fig. 34 that for Tests 1 and 2 the plastic deformation at fracture is larger than the deformation at ultimate. That is, Test 1 failed by flange mechanism, hence it exhibited the largest plastic deformation (100% increase in the plastic deformation) and

Test 2 failed by mixed mode, hence it showed a 50% increase in the plastic deformation. While Test 3 failed in a brittle manner (bolts fracture) and no plastic deformation was induced.

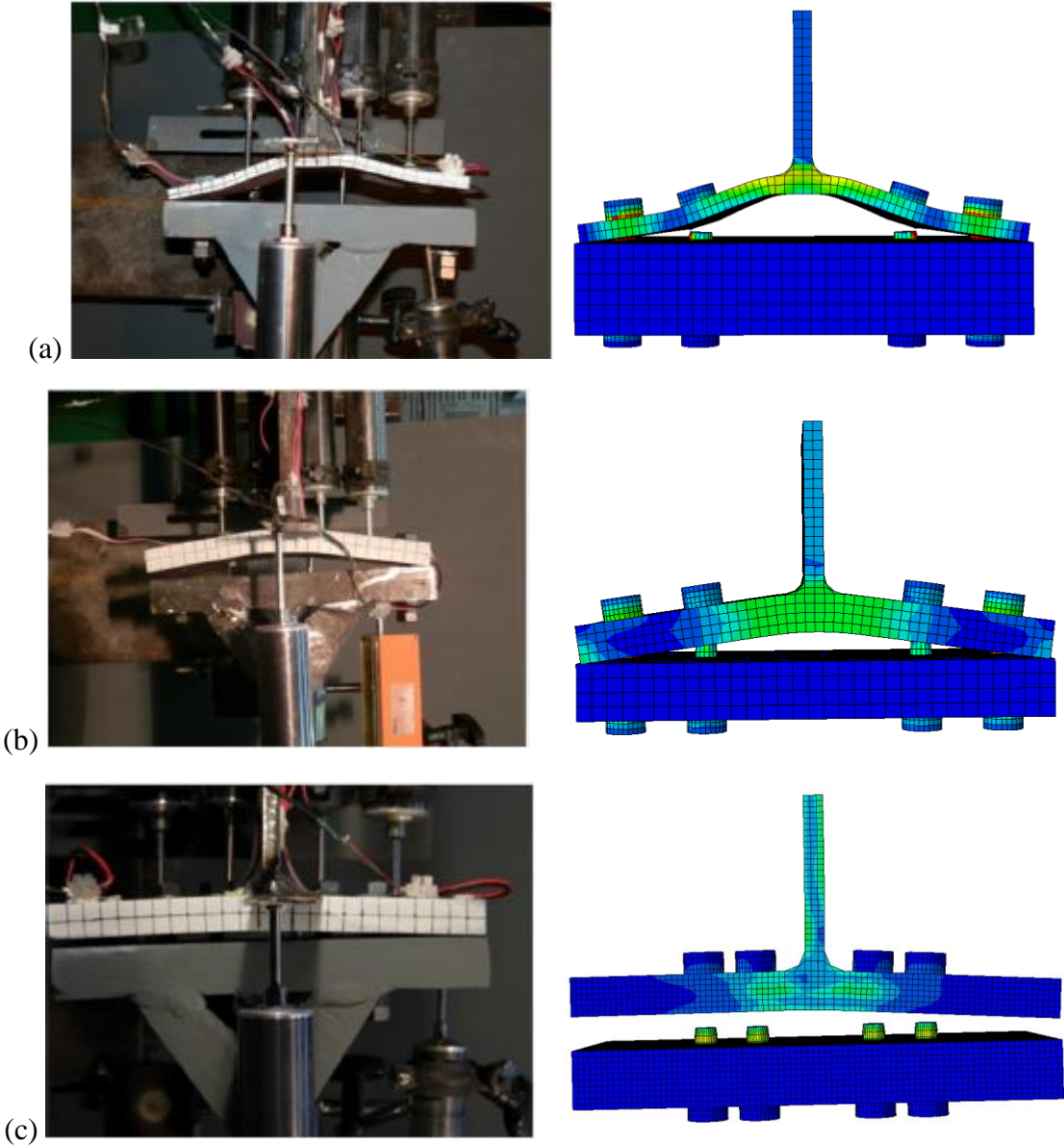


**Figure. 35.** Massimo et al. [13] – Failure mode: Exp. vs. FE: (a) Test 1, (b) Test 2, (c) Test 3

g. Sun et al. [70]

Six component tests on built-up Tees connected back-to-back were tested under monotonic loading. Two specimens were validated in *ABAQUS* using FE fracture analysis. Figure 36 shows the load-displacement responses of the two validated tests. Comparison of experimental and FE results show the excellent accuracy of the FE fracture model in predicting the ultimate load and displacement at fracture with less than 5% error (Table 8).

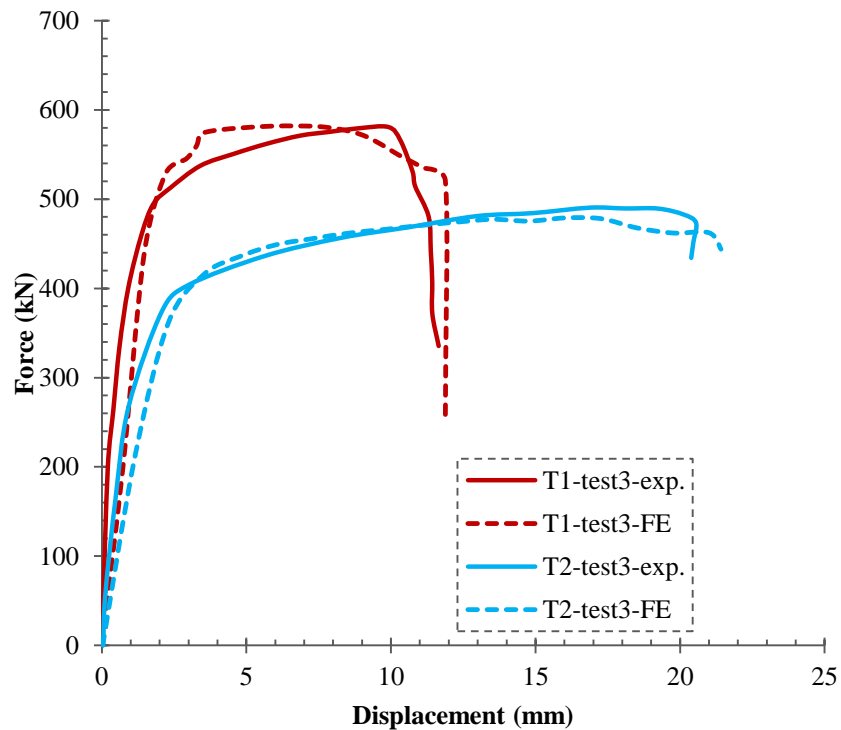


**Figure. 36.** Sun et al. [70] – Load-displacement: Exp. vs. FE

Figure 37 shows the failed experimental tests versus the FE fracture models. Both specimens failed by flange mechanism. This is clearly shown by the plastic hinge formation at the k-zone of the Tee flange and at the bolt line in both the experimental and FE tests.

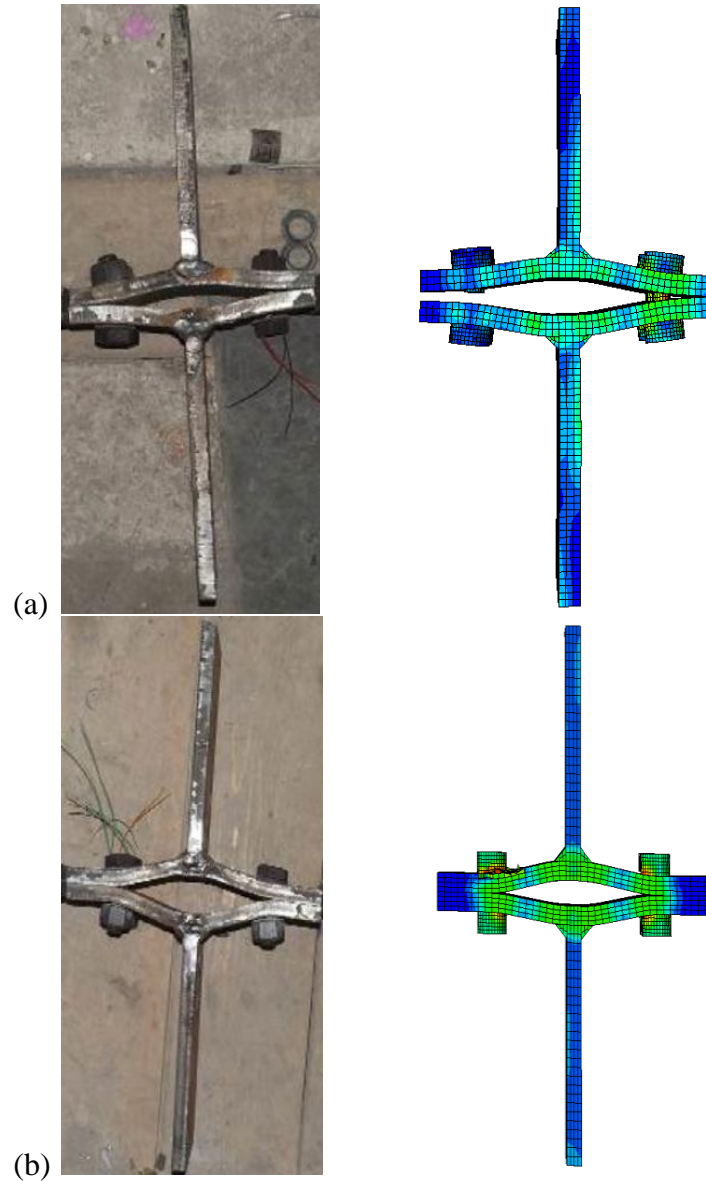


**Figure. 37.** Sun et al. [41] – Failure mode: Exp. vs. FE: (a) T1-test 3 (b) T2-test 3

The proposed FE fracture model was able to predict with excellent accuracy (less than 10% error) the ultimate load, the plastic deformation at fracture, and the failure modes and limit states of all the tested specimens. The validated tests included M12, M16, and M20 bolts using grade 8.8, grade 10.9, and A325 bolt material. Also, the validated tests included S355, ST44, and A572-50 base material. In addition, all possible failure modes and limit states of double Tees and



extended endplates were validated using the proposed FE fracture model with great accuracy for both monotonic and cyclic loading conditions.

The following two limitations bind the applicability of the developed fracture model: (1) failure of welds cannot be predicted by this model because calibration of weld material was not performed, (2) monotonic and cyclic tests at ambient temperature only can be simulated using the proposed fracture model and no elevated temperature models can be simulated because the calibration of steel material was performed at ambient temperature only.

#### **D. Conclusions**

The ductile damage of steel bolted moment connections was modeled using FE fracture analysis. Two built-in ductile damage models in *ABAQUS* (*SMCS* and *Hooputra* models) were used and a step-by-step methodology was developed. The methodology allows *ABAQUS* users to apply both damage models for any steel structure subjected to any loading condition (shear and/or tension and monotonic or cyclic). Different base and bolt steel material grades were calibrated for use in both damage models and the generated parameters are available for application. Also, the developed fracture model was validated against experimental tests of double Tee and extended endplate connections available in the literature. Comparison of load-displacement curves and failure modes proved the capability of the developed model to predict the ductile fracture of steel material over a wide range of material grades, loading conditions, and geometric characteristics. The proposed fracture model was able to predict with less than 10% error the ultimate load, the displacement at fracture, the full load-displacement response, and all limit states and failure modes encountered in the experiments. Furthermore, analysis of the deformation at ultimate versus deformation at fracture proved that, for flexible Tees and endplates, a large inelastic deformation is induced after the ultimate point till full fracture. That

is, predicting the response of steel connections till full fracture is of great interest for seismic applications where large inelastic deformation is needed. This research is part of an ongoing research that aims at fully understanding and modeling the ductile fracture of steel material. Future research work will include the fracture modeling of steel material at elevated temperatures.

## CHAPTER VI

### FE FRACTURE MODELING APPLICATION: ALTERNATE BLOCK SHEAR IN BEAMS

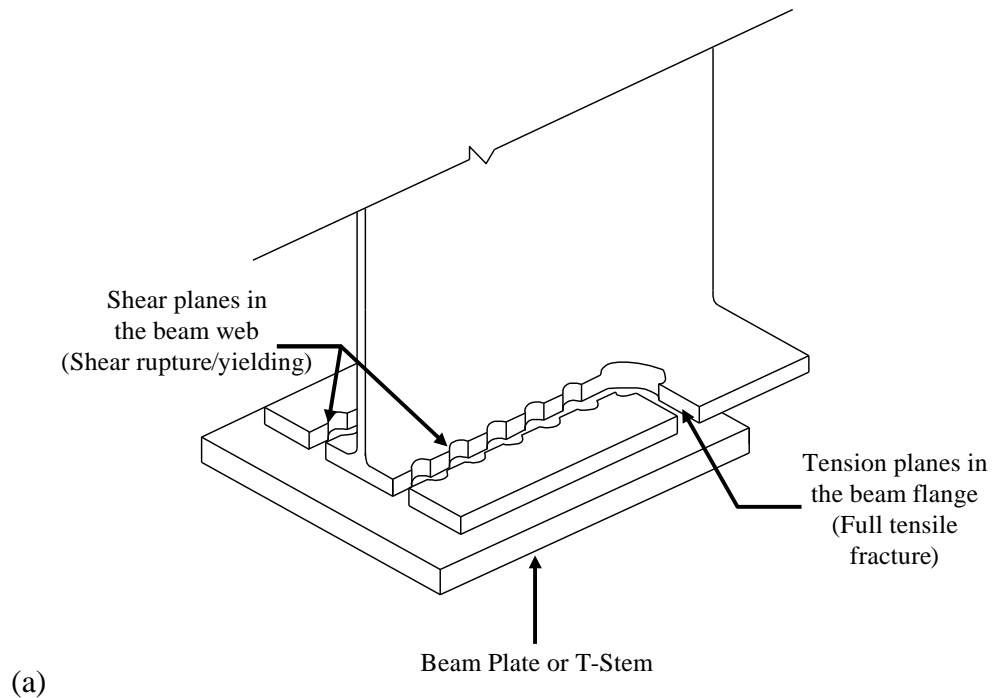
Steel connections are commonly designed by considering a range of potential failure modes, assessing the capacity for each mode, and taking the lowest mode as the governing for the connection. All other potential failure modes are then compared to the lowest mode and arranged from the lowest to the highest to obtain the sequence of potential failures.

Typical failure modes of beams in steel connections include plastic hinging (gross section yielding), net section fracture (NSF), block shear, and bolt tear-out and bearing. However, there are potential failure modes that might occur besides the aforementioned ones. The atypical failure mode in Tees connected through their flange was reported in the literature and termed as alternate block shear (ABS). This failure mode is similar to the traditional block shear failure mode which is recognized as a limit state in beams of moment connections as per the *ANSI/AISC 358-16* [2]. The failure mechanism of block shear combines a tensile fracture in one plane and shear failure (yielding or rupture) in the transverse plane. The ABS is defined as a combination of full tensile fracture in the beam flange followed by an alternate shear failure path propagating in the beam web toward the edge. Figure 38 shows the block shear and ABS failures in a beam section connected to a flange plate. The block shear failure is considered a ductile failure mode and is available in the *ANSI/AISC 360-16* specifications [4], unlike the ABS failure which is not recognized as a limit state.

ABS might be a potential failure mode of beams in bolted connections subjected to pure tensile forces. However, current design codes do not include the ABS failure mode check.

Considering the general case of I beam sections, block shear failure consists of two shear planes in the beam flange (Fig. 38(a)) while ABS failure consists of one shear plane in the beam web (Fig. 38(b)). Knowing that the beam web thickness is usually smaller than the beam flange thickness, ABS failure might have a lower capacity than the block shear failure. Therefore, it is essential to investigate experimentally and analytically the ABS failure in steel beams. Also, it is important to include ABS failure check in the available design codes to ensure a safe design.

All existing FE analyses, found in the literature, model the behavior of steel connections until first component yielding. However, FE fracture modeling is required for the analytical investigation to model the response after first component yielding. In fact, ductile fracture of steel starts from inherent flaws, present in the material, that grow into micro voids due to strain and stress demands. In this research, the ductile fracture due to both tension and shear stresses in the ABS failure mode is modeled.



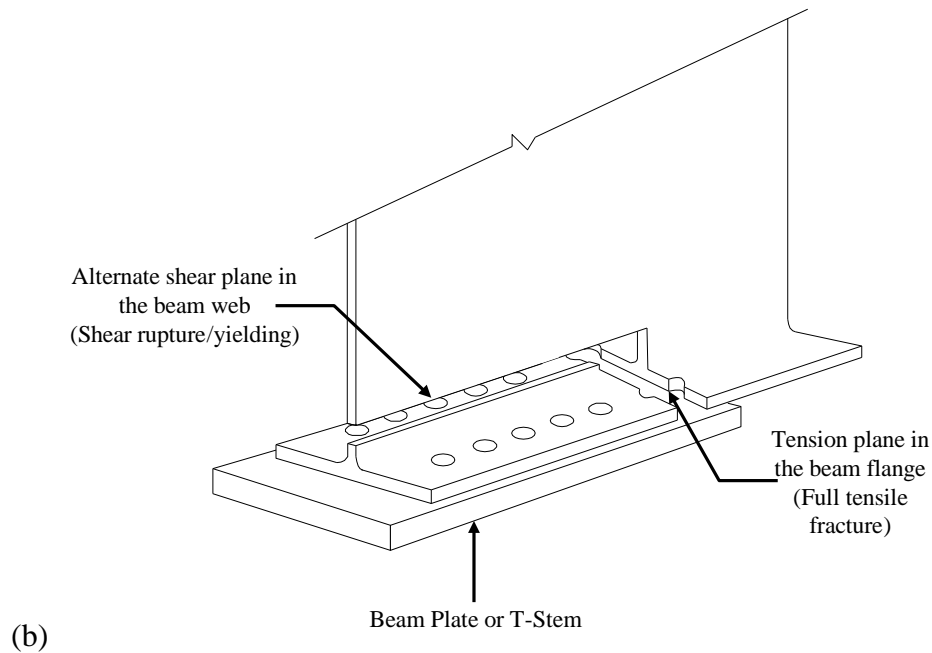


**Figure. 38.** (a) Typical block shear failure path and (b) alternate block shear failure path in W beam section connected to thick plate

## A. FE fracture model

The ductile fracture models explained in Chapter V are used in this chapter to model the ABS and NSF of the tested beam sections.

### 1. Numerical results

The FE models were developed in *ABAQUS* to reproduce the load-deformation response and fracture paths of the experimental program performed as part of this research.

#### a. Geometric, force boundary, and material properties

The four tested specimens were reproduced in *ABAQUS*. The specimens were loaded in two steps. In the first step, bolts were pretensioned by applying a pressure equivalent to the minimum required pretension force. In the second step, a displacement controlled monotonic

load was applied at the tip of the setup plates. During all steps of the analysis, the edge of the beam was fixed. The complete true stress-true strain curve was used for all steel materials with isotropic hardening. Both tension and shear fracture models were specified for all steel material regardless of the expected failure mode. Thus, the failure envelopes were automatically tested at every load increment and the governing one defined the failure pattern.

b. Model discretization

Discretization of all the components of the connection model in *ABAQUS* was performed using explicit *C3D8-R* (eight-node brick elements with reduced integration). At regions where failure was expected to occur and at regions where stress was likely to concentrate (around bolt holes) a finer and a mapped mesh were adopted in order to advance the accuracy of interpolations. Surface-to-surface contact with a finite sliding coefficient was used to reproduce contact surfaces between all components of the specimens. This finite sliding was used to represent a friction coefficient of 0.25. The finite sliding allowed separation, sliding, and rotation of the contact surfaces. A general contact interaction was specified to overcome the excessive distortion issues faced in the explicit fracture modeling. Finally, the *STATUS* field output was activated for the fracture to be visualized.

c. Comparison of FE predictions with experiments

The capability of the FE fracture model to predict the fracture response of beams in steel connections subjected to pure tensile loading was validated against the four tests conducted as part of this research. The load-deformation curves of all specimens are shown in Fig. 39. It can be seen that for all specimens, the FE results predicted well the initial stiffness and both the

yield and ultimate loads. In addition, the developed FE fracture models were able to predict the post-ultimate deformation of beams failing in ABS and NSF.

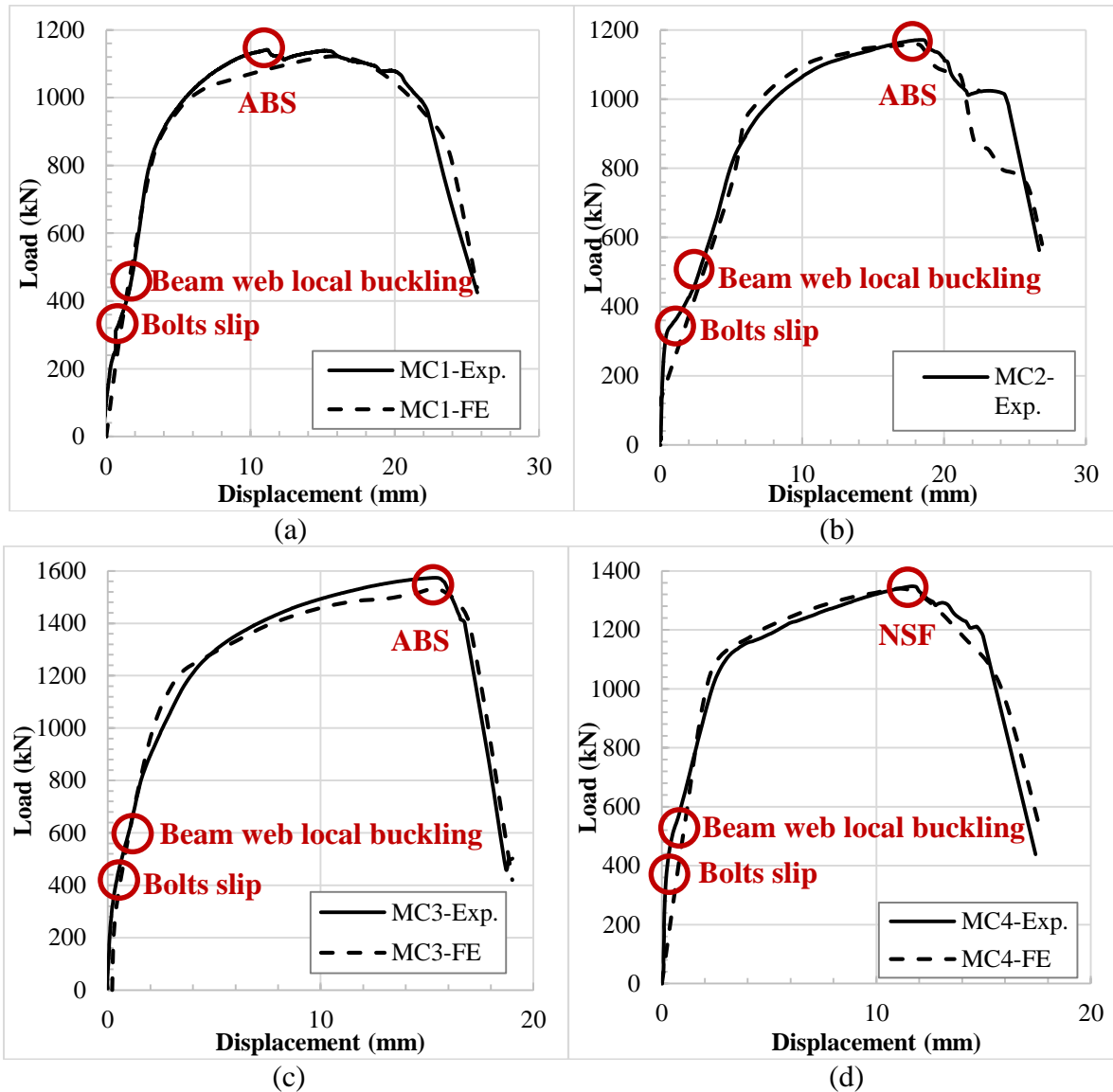


**Figure. 39.** Load-Displacement: Experiment (Exp.) vs. FE fracture: (a) MC1, (b) MC2, (c) MC3, and MC4.

Figure 40 shows a comparison of the failure paths of both ABS and NSF limit states between the FE fracture results and the experimental results. It is shown that the FE fracture path

was similar to the experimental one. For ABS, the tension fracture in the beam flange was followed by shear yielding and fracture in the beam web. For NSF, pure tension fracture developed in the beam section. The FE fracture models predicted well the connection response when compared to experimental results. Thus, the developed FE fracture models can be used in future numerical parametric studies to investigate further the ABS failure mode.

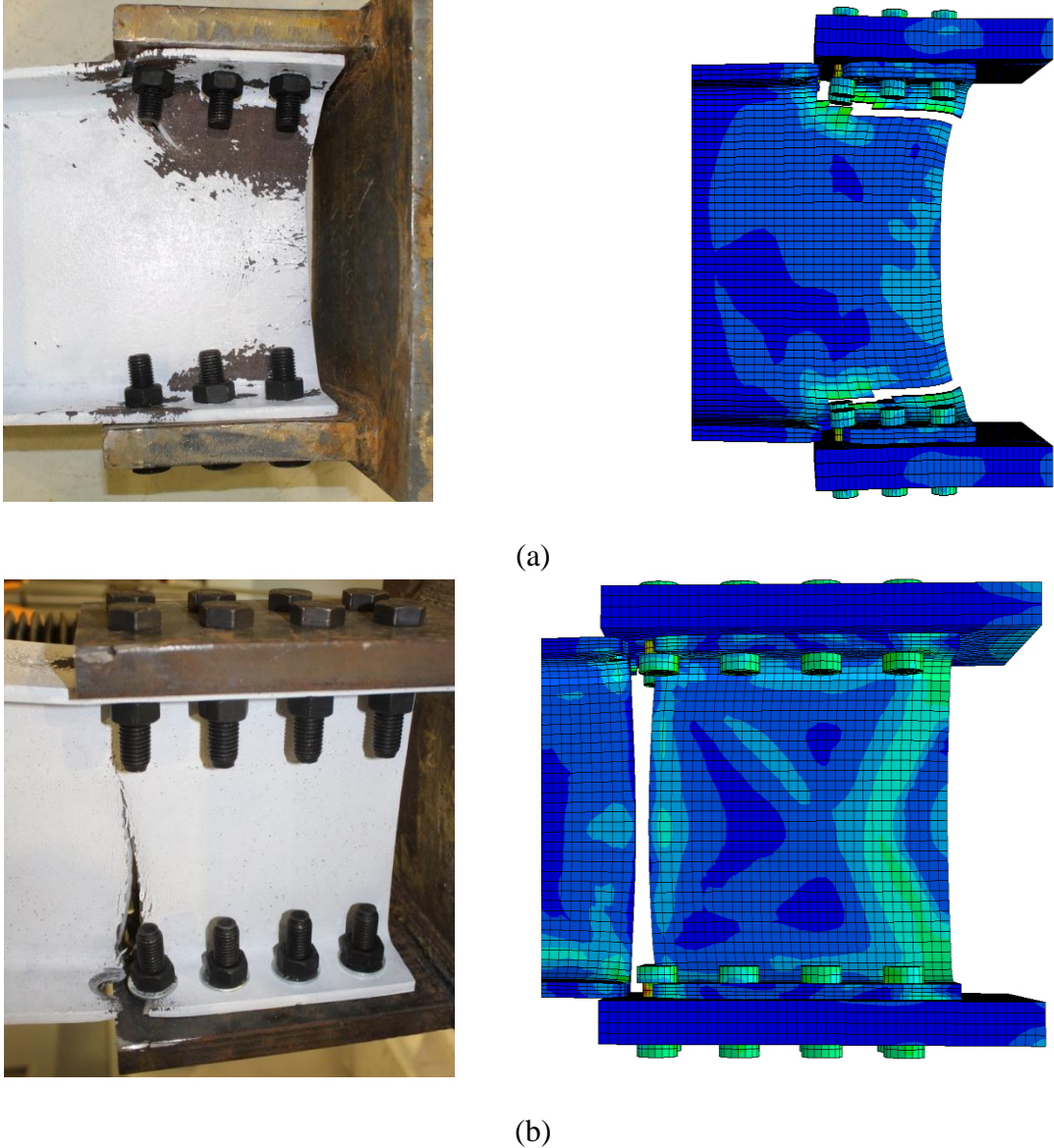


**Figure. 40.** Experiment vs. FE fracture paths: (a) ABS and (b) NSF.



## **B. Conclusions**

In designing steel connections all failure modes are needed to be accounted for including the ABS failure. In fact, when large tensile demands are developed in steel connections, ABS becomes a potential failure mode. That is, ABS failure might occur in the beam section. FE fracture models were developed to predict both pre-yielding and post-yielding responses of the ABS failure mode. Tension and shear ductile fracture models were calibrated for base and bolt steel material. Then, the fracture parameters were implemented in *ABAQUS* to reproduce the experimental results. The developed FE fracture models were validated against experimental results and showed excellent prediction of the load-displacement curves and failure paths and modes in all four specimens. Finally, the performed experimental and analytical investigations are part of an ongoing research that aims at including the ABS failure mode in the current steel design codes to ensure a safe design. Full scale experimental tests of moment connections associated with deep beam sections will be the subject of future research to characterize ABS in these connections. Also, the developed FE fracture models are to be used in future parametric studies to further characterize the ABS failure mode in full scale connections.

## CHAPTER VII

### SEISMIC PERFORMANCE OF FULL SCALE EXTENDED ENDPLATE CONNECTIONS WITH CIRCULAR BOLTS CONFIGURATION AND RBS

Extended endplate connections have become the choice of many structural engineers in designing connections for moment resisting frames in seismic areas. The analytical simulations using *ABAQUS* provide a more extensive data set for analysis. The circular configuration of bolts is thought to eliminate the need for stiffening beam flange plates in moment connections leading to lower fabrication costs.

For the prequalified eight-bolt extended endplate connection, stiffener plates are welded between the end plate and the beam flanges. The presence of stiffeners ensures that beam plastic hinging occurs away from the connection before failure occurs in the protected zone. Since the beam flange stiffeners are omitted in the extended endplate connection with circular bolts configuration, an RBS is used to ensure that beam plastic hinging occurs away from the connection.

The outcome of this research is to validate the proposed design guidelines [65] for engineers to account for the additional forces induced in the tension bolts due to column flange deformation and for the maximum rotational capacity demand in the connection which are required for seismic analysis and design.

Three full scale extended endplate connections with circular bolts configuration using medium to deep beam sections are designed and tested under cyclic loading conditions using FE analysis in *ABAQUS*. The ultimate goal of this research is to incorporate the proposed

connection in the prequalified connections for IMFs and SMFs for seismic applications - *ANSI/AISC 358-16* [2].

A detailed design procedure and a summary of design examples of extended endplate connections with circular bolts configuration and RBS, associated with deep girders ranging from W18 to W24, are presented first. Then, the designed connections are tested under seismic loading using FE analysis and the performance of these connections is evaluated against the seismic provisions of both IMFs and SMFs.

### **A. Design Procedure**

Full-strength extended endplate connections are designed such that plastic hinge formation in the beam is intended to occur at the RBS. Note that the beam and the column are made of A992, the plate is made of A572-50, and the bolts are made of A490 steel material. The procedure presented below is based on equations available in *ANSI/AISC 358-16* [2], Hantouche and Mouannes [19] and El Kalash and Hantouche [65] design recommendations.

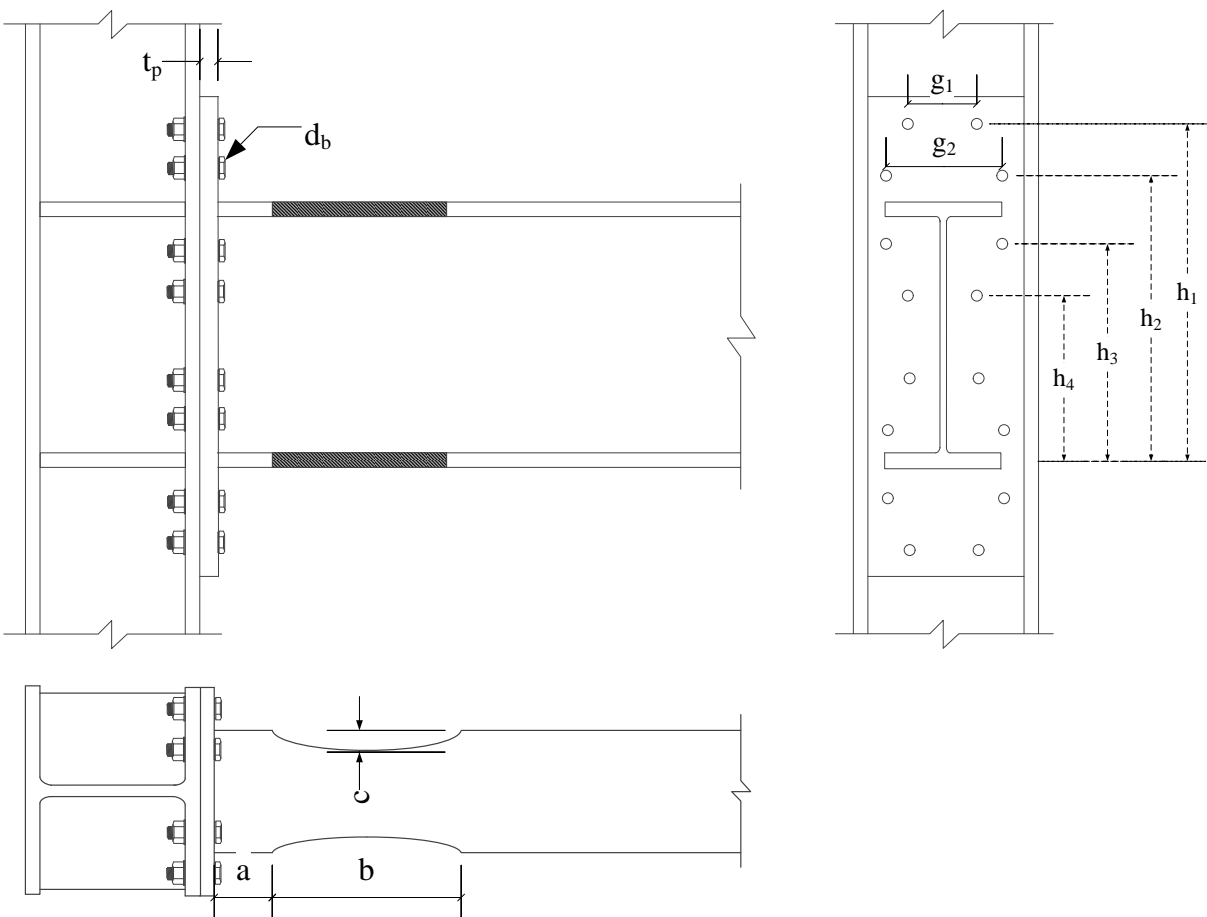
The procedure presented in this chapter includes newly proposed design recommendations and equations. The newly proposed expressions account for new failure mechanisms that might be encountered in endplate and column flange. Specifically, the newly developed expressions that are added to the procedure provide the following:

- The required column flange thickness and endplate for flexural yielding based on yield line theory for the circular bolts configuration, and
- An RBS to account for the lack of beam flange stiffeners and to insure that beam plastic hinge occurs away from the connection.

Not incorporating the aforementioned failure modes and limit states into the design procedure could lead to connection failure.

The following steps provide the design of eight-bolt extended endplate connections with circular bolts configuration using a W24x76 beam section connected to a W14x257 column section. The design and connection details of the remaining two connections are presented in appendix B.

Figure 41 shows the extended endplate connection with circular bolts configuration and RBS. Also, Table 9 shows the geometrical characteristics of the three designed full scale connections and Fig. 42 shows the geometrical characteristics of the connection designed with W24x76 beam section.



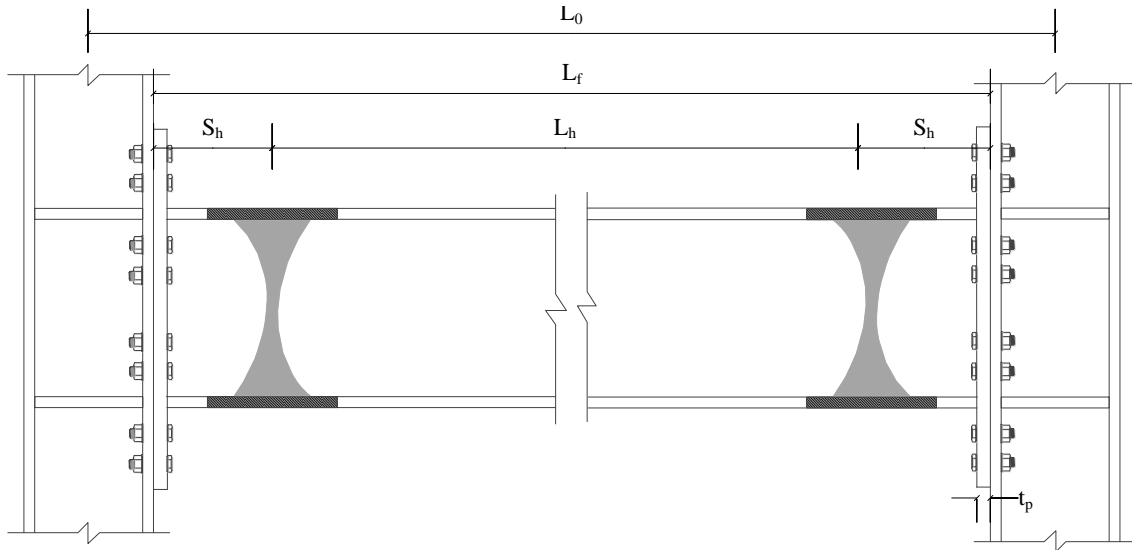


**Figure. 41.** Eight-bolt extended endplate connection with circular bolts configuration and RBS

**Table. 9.** Tests geometrical characteristics

Beam section	Column section	Endplate thickness (in.)	Bolt diameter (in.)	RBS dimensions		
				a (in.)	b (in.)	c (in.)
W24x76	W14x257	1 <sup>1/4</sup>	1	5.6	18	1.6
W21x62		1	1	5.2	15.8	1.5
W18x55		1	7/8	4.7	13.5	1.3

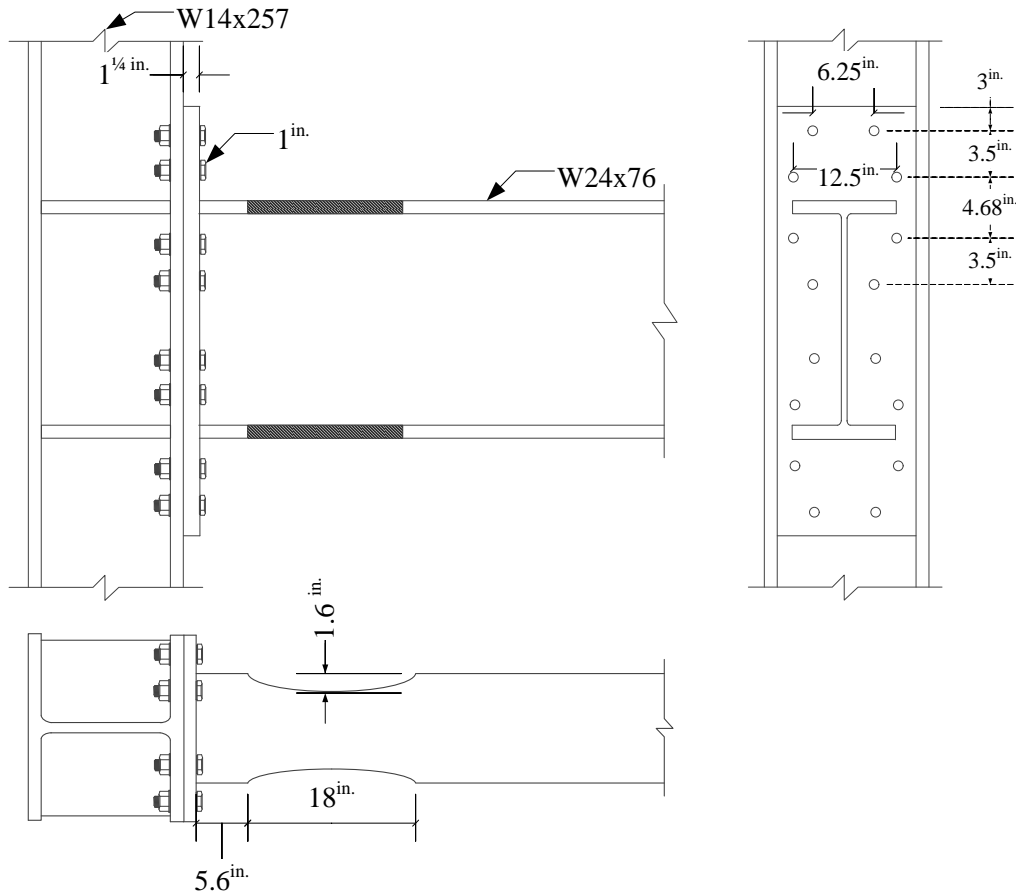


**Figure. 42.** Connection details: W24x76

### 1. Prequalification limits

According to table 6.1 in Chapter 6 in the *ANSI/AISC 358-16* [2], beam and column design parameters should satisfy all prequalification limits as shown below.

#### Beam Limitations

- ✓ Beam is rolled wide flange
- ✓ Beam depth is  $W24 < W36$
- ✓ Beam weight is  $76 \frac{\text{lb}}{\text{ft}} < 150 \frac{\text{lb}}{\text{ft}}$
- ✓ Beam flange thickness:  $t_{\text{bf}} = 0.68^{\text{in.}} < 1^{\text{in.}}$

- ✓ Clear span to depth  $\frac{410}{23.9} = 17.15 > 9$  for SMF
- ✓ Beam flange slenderness:  $\frac{b_{bf}}{2t_{bf}} = 6.61 < 0.3 \sqrt{\frac{E}{F_{yb}}} = 6.89$
- ✓ Beam web slenderness:  $\frac{h}{t_{bw}} = 49 < 2.45 \sqrt{\frac{E}{F_{yb}}} = 56.27$

➤ No local buckling of beam

- ✓ Lateral bracing shall be provided:

Both beam flanges should be laterally braced at intervals not to exceed (*ANSI/AISC 341-16* [3]):

$$L_{bmax} = 0.086r_y \left( \frac{E}{F_y} \right) = 7.98^{ft.}$$

The limiting length:

$$L_p = 1.76r_y \sqrt{\left( \frac{E}{F_y} \right)} = 6.78^{ft.}$$

$$L_r = 1.95r_{ts} \frac{E}{0.7F_y} \sqrt{\left( \frac{JC}{S_x h_0} + \sqrt{\left( \frac{JC}{S_x h_0} \right)^2 + 6.76 \left( \frac{0.7F_y}{E} \right)^2} \right)} = 19.6^{ft.}$$

Provide braces at maximum of 6.5<sup>ft.</sup> outside the protected zone.

The beam is adequate for use in high seismic areas.

### Column Limitations

- ✓ Column is rolled wide flange
- ✓ Beam connected to column flange
- ✓ Column depth is W14 ≤ W14

✓ Column flange slenderness:  $\frac{b_{cf}}{2t_{cf}} = 4.23 < 0.3 \sqrt{\frac{E}{F_{yc}}} = 6.89$

✓ Column web slenderness:  $\frac{h}{t_{cw}} = 9.71 < 2.45 \sqrt{\frac{E}{F_{yc}}} = 56.27$

➤ No local buckling of column

The column is adequate for use in high seismic areas.

## 2. Endplate and bolt design

### Moment at the Face of Column

Compute the probable maximum moment at the beam hinge:

$$M_{pr} = C_{pr} F_y R_y Z_e$$

where:

$$C_{pr} = \frac{F_u + F_y}{2F_y} = \frac{65 + 50}{(2)(50)} = 1.15$$

$$R_y = 1.10 \text{ for A992 steel}$$

$$M_{pr} = (1.15)(1.1)(50)(200) = 12650 \text{ kips.in}$$

Determine the location of the plastic hinge in the beam:

$$S_h = \min \left\{ \begin{array}{l} \frac{d_b}{2} = 11.95 \text{ in.} \\ 3b_{bf} = 26.97 \text{ in.} \end{array} \right\}$$

$$S_h = 11.95 \text{ in.}$$

Determine the beam length between plastic hinges:

$$L_h = L_0 - d_c - 2S_h = 410 - 16.4 - (2)(11.95) = 369.8 \text{ in.}$$



Determine the shear force at the end of the beam:

$$V_u = \frac{2M_{pr}}{L_h} = \frac{(2)(12650)}{369.8} = 68.41^{\text{kips}}$$

Compute the moment expected at the face of the column:

$$M_f = M_{pr} + V_u S_h$$

$$M_f = 12650 + (68.41)(11.95) = 13467.5^{\text{kips.in}}$$

where:

$M_{pr}$  : probable maximum moment at plastic hinge, kips.in.

$S_h$  : distance from face of column to plastic hinge, in.

$V_u$  : shear force at end of beam, kips

$b_{bf}$  : width of beam flange, in.

$d$  : depth of connecting beam, in.

$L_h$  : distance between plastic hinge locations, in.

End-plate moment connection configurations and preliminary values for the connection geometry

*End Plate Configuration:*

The end plate moment connection chosen is the eight-bolt stiffened configuration, with a rectangular bolts configuration initially. Later on, the circular bolts distribution will be adopted.

*End Plate Geometry:*

According to table 6.1 in *ANSI/AISC358-16* [2] , the following four geometric properties of the end plate fall within the acceptable ranges of 8ES:

$$\left\{ \begin{array}{l} bp = 15^{\text{in.}} \in [9, 15]^{\text{in.}} \\ g = 5^{\text{in.}} \in [5, 6]^{\text{in.}} \\ p_{fi}, p_{fo} = 2^{\text{in.}} \in [1.625, 2]^{\text{in.}} \\ p_b = 3.5^{\text{in.}} \in [3.5, 3.75]^{\text{in.}} \\ h_1 = d_b + p_{fi} + p_b - \frac{t_{bf}}{2} = 29.06^{\text{in.}} \\ h_2 = h_1 - p_b = 25.56^{\text{in.}} \\ h_3 = h_2 - 2p_{fi} - t_{bf} = 20.88^{\text{in.}} \\ h_4 = h_3 - p_b = 17.38^{\text{in.}} \\ d_e = 2^{\text{in.}} \end{array} \right.$$

where:

$b_p$  : width of endplate, in.

$g$  : horizontal distance between bolts, in.

$p_{fi}$  : vertical distance from the inside of a beam tension flange to the nearest inside bolt row, in.

$p_{fo}$  : vertical distance from the outside of a beam tension flange to the nearest outside bolt row, in.

$p_b$  : vertical distance between the inner and outer row of bolts in an 8ES connection, in.

The required bolt diameter:

$$d_{\text{req'd}} = \sqrt{\frac{2M_f}{\pi\phi_f F_{nt} (h_1 + h_2 + h_3 + h_4)}}$$

The nominal tensile strength of bolt,  $F_{nt} = 113^{\text{ksi}}$

The reduction factor,  $\phi_f = 0.9$

$$d_{\text{req'd}} = \sqrt{\frac{(2)(13467.5)}{(\pi)(0.9)(113)(29.06 + 25.56 + 20.88 + 17.38)}} = 0.95 \rightarrow \text{use : } 1^{\text{in.}} \text{ bolt}$$

The required end plate thickness

$$t_{p,req'd} = \sqrt{\frac{1.11M_f}{\phi_d F_{yp} Y_p}}$$

$$F_{yp} = 50^{ksi}$$

$$Y_p = \left(\frac{b_p}{2}\right) \left( \frac{h_1}{2d_c} + \frac{h_2}{p_{fi}, p_{fo}} + \frac{h_3}{p_{fi}, p_{fo}} + \frac{h_4}{s} \right) + \left(\frac{2}{g}\right) \left( (h_1) \left( d_c + \frac{p_b}{4} \right) + (h_2) \left( p_{fi}, p_{fo} + \frac{3p_b}{4} \right) + (h_3) \left( p_{fi}, p_{fo} + \frac{p_b}{4} \right) + (h_4) \left( s + \frac{3p_b}{4} \right) + p_b^2 \right) + g = 429.71^{in.}$$

$$t_{p,req'd} = \sqrt{\frac{(1.11)(13467.5)}{(1)(50)(429.71)}} = 0.834 \rightarrow \text{use : } 7 / 8^{in.} \text{ endplate thickness}$$

where:

$F_{yp}$  : specified minimum yield stress of the end-plate material

$Y_p$  : end plate yield line mechanism parameter

The factored beam flange force

$$F_{fu} = \frac{M_f}{d_b - t_{bf}} = \frac{13467.5}{23.9 - 0.68} = 580^{kips}$$

The bolt shear rupture strength of the connection

$$V_u \leq \phi_n R_n = \phi_n (n_b) F_{nv} A_b$$

$$\phi_n R_n = (0.9)(8)(84) \left( \left( \pi \right) \left( \frac{1^2}{4} \right) \right) = 475.01^{kips}$$

$$V_u = 475.01^{kips} \leq 580^{kips}$$

where:

Number of bolts at the compression flange,  $n_b = 8$

Nominal gross area of bolt,  $A_b = \left( \pi \right) \left( \frac{d_b^2}{4} \right)$  , in.<sup>2</sup>

Nominal shear strength of bolt,  $F_{nv} = 84^{\text{ksi}}$

Check bolt-bearing/tear-out failure of the end-plate and column flange

$$V_u \leq \phi_n R_n = \phi_n (n_i) r_{ni} + \phi_n (n_o) r_{no}$$

$$\phi_n R_n = (0.9)(4)(105) + (0.9)(4)(105) = 756^{\text{kips}}$$

*For inner bolts:*

$$r_{ni} = 1.2L_c t F_u = (1.2)(3.5)(0.875)(50) = 183.75^{\text{kips}} < 2.4d_b t F_u = (2.4)(1)(0.875)(50) = 105^{\text{kips}}$$

*For outer bolts:*

$$r_{no} = 1.2L_c t F_u = (1.2)(2)(0.875)(50) = 105^{\text{kips}} < 2.4d_b t F_u = (2.4)(1)(0.875)(50) = 105^{\text{kips}}$$

### 3. Column-side design

Check the column flange for flexural yielding

$$t_{cf} \geq \sqrt{\frac{1.11M_f}{\phi_d F_{yc} Y_c}}$$

$$Y_c = \frac{b_{cf}}{2} \left[ h_1 \left( \frac{1}{s} \right) + h_4 \left( \frac{1}{s} \right) \right] + \frac{2}{g} \left[ h_1 \left( p_b + \frac{c}{s} + s \right) + h_2 \left( \frac{p_b}{2} + \frac{c}{4} \right) + h_3 \left( \frac{p_b}{2} + \frac{c}{2} \right) + h_4(s) \right] + \frac{g}{2} = 580.31^{\text{in.}}$$

$$s = \frac{1}{2} \sqrt{b_{cf} g} = 4.9^{\text{in.}}$$

$$t_{cf} \geq \sqrt{\frac{(1.11)(13467.5)}{(0.9)(50)(580.31)}} = 0.75 < 1.89^{\text{in.}}$$

where:

$F_{yc}$  : specified minimum yield stress of column flange material, ksi

$Y_c$  : unstiffened column flange yield line mechanism parameter from Table 6.6, in.

$t_{cf}$  : column flange thickness, in.

Check the local column web yielding strength of the unstiffened column web at the beam flanges

$$F_{fu} \leq \phi_d R_n$$

$$R_n = C_t (6k_c + t_{bf} + 2t_p) F_{yc} t_{cw}$$

$$R_n = (1)((6)(2.49) + 0.68 + (2)(0.875))(1.18)(50) = 1024.83^{\text{kips}}$$

$$\phi_d R_n = (0.9)(1024.83) = 922.347^{\text{kips}}$$

where:

$C_t$  = 0.5 if the distance from the column top to the top face of the beam flange is less than the depth of the column  
= 1.0 otherwise

$F_{yc}$  : specified yield stress of column web material, ksi

$k_c$  : distance from outer face of the column flange to web toe of fillet (design value) fillet weld, in.

$t_{cw}$  : column web thickness, in.

Check the unstiffened column web buckling strength at the beam compression flange

$$F_{fu} \leq \phi R_n$$

Where  $\phi = 0.75$

$F_{fu}$  is applied at a distance greater than or equal to  $d/2$  from the end of the column:

$$R_n = \frac{24t_{cw}^3 \sqrt{EF_{yc}}}{h}$$

$$h = d - 2t_{bf} = 16.4 - (2)(1.89) = 12.62^{\text{in.}}$$

$$R_n = \frac{(24)(1.18)^3 \sqrt{(29000)(50)}}{12.62} = 3762.5^{\text{kips}}$$

$$\phi R_n = (0.75)(3762.5) = 2821.91^{\text{kips}} > 580^{\text{kips}}$$

Check the unstiffened column web crippling strength at the beam compression flange

$$F_{fu} \leq \phi R_n$$

Where  $\phi = 0.75$

*F<sub>fu</sub> is applied at a distance greater than or equal to d<sub>c</sub>/2 from the end of the column:*

$$R_n = 0.8t_{cw}^2 \left[ 1 + 3 \left( \frac{N}{d_c} \right) \left( \frac{t_{cw}}{t_{cf}} \right)^{1.5} \right] \sqrt{\frac{EF_{yc} t_{cf}}{t_{cw}}}$$

$$N = b_f + 2w + 2t_p = 8.99 + (2)(0.875) = 10.74^{\text{in.}}$$

$$R_n = 0.8(1.18)^2 \left[ 1 + 3 \left( \frac{10.74}{16.4} \right) \left( \frac{1.18}{1.89} \right)^{1.5} \right] \sqrt{\frac{(29000)(1.89)}{1.18}} = 3342.85^{\text{kips}}$$

$$\phi R_n = (0.75)(3342.85) = 2507.14^{\text{kips}} > 580^{\text{kips}}$$

#### **4. Circular bolt pattern**

$$g_1 = \frac{b_p - 2e}{2} = \frac{15 - (2)(1.25)}{2} = 6.25^{\text{in.}}; g_2 = b_p - 2e = 15 - (2)(1.25) = 12.5^{\text{in.}} \quad [19]$$

Prying forces [65]

F1: Endplate flexural mechanism and B1 and B2 fracture:

$$T = 4T_{\text{beam1}} + 4T_{\text{bolt}} = (4)(37.75) + (4)(88.75) = 506^{\text{kips}}$$

$$T_{/beam1} = \frac{(62.8)(1+0.858)}{1.341+1.75} = 37.75^{\text{kips}} ; T_{/bolt} = (113)\left(\frac{\pi}{4}\right)(1^2) = 88.75^{\text{kips}} ;$$

$$M_{pl} = (1/4)(7.5)(7/8)^3(50) = 62.8^{\text{kips.in.}} ; p = (4)(15)/8 = 7.5^{\text{in.}} ; \delta = 1 - (1+1/16)/7.5 = 0.858 ;$$

$$a_1 = \frac{6.25 - 0.68}{2} - (0.8)(1.18) - (1/2) = 1.341^{\text{in.}} ; b_1 = 1.25 + (1/2) = 1.75^{\text{in.}}$$

F2: Column flange/endplate flexural mechanism and B4 fracture:

$$T = 4T_{/beam1} + 4T_{/beam1'} + 2T_{/bolt} = (4)(506) + 4(699.5) + 2(88.75) = 5000^{\text{kips}}$$

$$T_{/beam1'} = \frac{(675)(1+0.858)}{0.043+1.75} = 699.5^{\text{kips}} ; M_{pl}' = (1/4)(8)(1.89)^3(50) = 675^{\text{kips.in.}} ; p' = (4)(16)/8 = 8^{\text{in.}} ;$$

$$\delta' = 0.858^{\text{in.}} ; a_1' = \frac{6.25 - 1.18}{2} - (0.8)(2.49) - (1/2) = 0.043^{\text{in.}} ; b_1' = 1.75^{\text{in.}}$$

F3: Column flange flexural mechanism and B4 fracture:

$$T = 4T_{/beam1'} + 2T_{/bolt} = (4)(699.5) + (2)(88.75) = 2975.5^{\text{kips}}$$

$$\rightarrow T = 506^{\text{kips}} \text{ controls}$$

Total prying forces:

$$Q_{\text{total}} = B_T - T_s = (8)(88.75) - 506 = 204^{\text{kips}}$$

Check the endplate thickness for flexural yielding

$$t_p \geq \sqrt{\frac{1.11M_f}{\phi_d F_{yp} Y_{pc}}}$$

$$Y_{pc} = b_p \left[ h_2 \left( \frac{1}{p_{fi}} \right) + h_3 \left( \frac{1}{p_{fi}} \right) + h_4 \left( \frac{1}{s} \right) \right] + \frac{2}{g_1} \left[ \left( s + \frac{b_p}{4} - \frac{e}{2} \right) h_4 \right] + \frac{2}{g_2} \left[ \left( p_{fi} + \frac{b_p}{2} - e \right) h_3 \right] = 273.48^{\text{in.}}$$

$$s = \frac{1}{2} \sqrt{b_p g} = 4.33^{\text{in.}}$$

Where  $M_f = M_{pr} + (V_u + Q_{\text{total}})S_h = 12650 + (68.41 + 204)(11.95) = 15905.3^{\text{kips.in.}}$

$$t_p \geq \sqrt{\frac{(1.11)(15905.3)}{(0.9)(50)(273.48)}} = 1.19^{\text{in.}} > \frac{7^{\text{in.}}}{8} \text{ use } \rightarrow t_p = 1\frac{1}{4}^{\text{in.}}$$

where:

$Y_{pc}$  : unstiffened endplate yield line mechanism parameter for circular bolts pattern [65], in

Check the column flange thickness for flexural yielding

$$t_{cf} \geq \sqrt{\frac{F_u + Q_{\text{total}}}{\left[ 2\left(\frac{b_{cf}}{2s}\right) + 2(1 + 2p_b)\frac{1}{g_2} + 4(p_b + s)\frac{1}{g_1} \right] F_{yc}}}$$

$$t_{cf} \geq \sqrt{\frac{580 + 204}{\left[ 2\left(\frac{16}{(2)(4.33)}\right) + 2(4.68 + (2)(3.5))\frac{1}{12.5} + 4(3.5 + 4.33)\frac{1}{6.25} \right] (50)}} = 1.217^{\text{in.}} < 1.89^{\text{in.}}$$

### 5. Reduced beam section - RBS

Following is the design of RBS using Chapter 5 of *ANSI/AISC 358-16* [2]:

$$0.5b_{bf} = 4.495^{\text{in.}} \leq a \leq 0.75b_{bf} = 6.7425^{\text{in.}} \rightarrow \text{use : } a = \text{avg}(4.495, 6.7425) = 5.6^{\text{in.}}$$

$$0.65d = 15.535^{\text{in.}} \leq b \leq 0.85d = 20.315^{\text{in.}} \rightarrow \text{use : } b = \text{avg}(15.535, 20.315) = 18^{\text{in.}}$$

$$0.1b_{bf} = 0.899^{\text{in.}} \leq c \leq 0.25b_{bf} = 2.2475^{\text{in.}} \rightarrow \text{use : } c = \text{avg}(0.899, 2.2475) = 1.6^{\text{in.}}$$

$$Z_{\text{RBS}} = Z_x - 2ct_{bf}(d - t_{bf}) = 200 - (2)(1.6)(0.68)(23.9 - 0.68) = 149.47^{\text{in.}^3}$$

$$M_{pr} = (1.15)(1.1)(50)(149.47) = 9453.98^{\text{kips.in}}$$



## B. FE modeling

### 1. Description of the connection model

The three designed extended endplate connections were simulated in *ABAQUS*. The specimens were loaded in two steps. In the first step, the tension bolts were subjected to a pretension force equivalent to the minimum bolt pretension respective to every bolt diameter. The load was modeled by applying a pressure equivalent to the minimum required pretension force. In the second step, a displacement controlled cyclic load, consistent with the seismic load history proposed in the *ANSI/AISC 41-16* [3], was applied at the end of the beam section. During all steps of the analysis, the column was fixed against any translation and rotation at the back section. Discretization of all the components of the connection model in *ABAQUS* was performed using C3D8-R. Surface-to-surface contact with a finite sliding coefficient was used to reproduce the contact surfaces. This finite sliding was used to represent a friction coefficient of 0.25. Figure 43 shows the mesh and boundary conditions applied to the specimens.

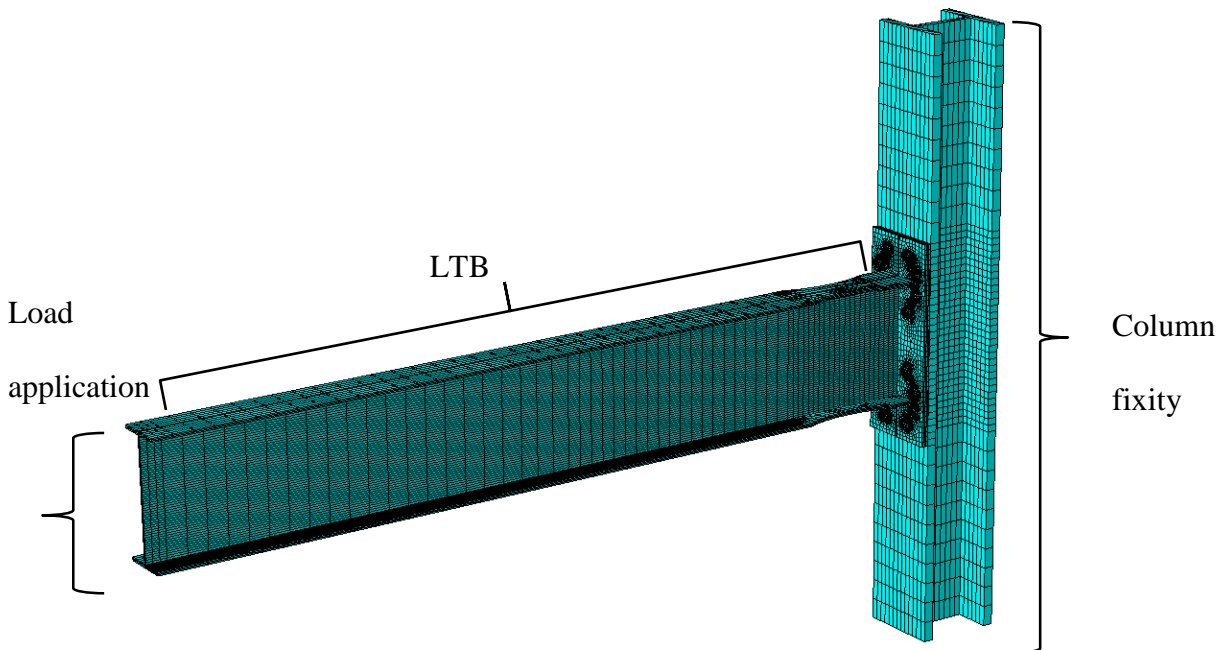


**Figure. 43.** Mesh and boundary conditions

A bilinear true stress-strain material model was used for all steel materials. A kinematic plastic hardening model was specified to account for the *Bauschinger* effect. The A992 material had the following characteristics:  $F_y = 410\text{MPa}$  and  $\epsilon_{py} = 0$  and  $F_u = 720\text{MPa}$  and  $\epsilon_{pu} = 0.41$ . The A572-50 material had the following characteristics:  $F_y = 402\text{MPa}$  and  $\epsilon_{py} = 0$  and  $F_u = 710\text{MPa}$  and  $\epsilon_{pu} = 0.49$ . The A490 bolt material had the following characteristics:  $F_y = 940\text{MPa}$  and  $\epsilon_{py} = 0$  and  $F_u = 1200\text{MPa}$  and  $\epsilon_{pu} = 0.17$ .

## **2. Results**

Figures 44-46 show the moment-rotation curves of the three tested specimens. The strength (0.8Mpr) and rotational capacity (2% for IMF and 4% for SMF) limits specified by the *ANSI/AISC 341-16* [3] for the classification of moment connections are marked in Figs. 44-46. Loading of the specimens was terminated at the 4% rotational demand since the aim of this study is to classify the proposed connection for use in IMFs and SMFs only. The moment-rotation response of the three tested specimens shows the hysteretic behavior of the steel material under cyclic loading. The specimens reached a tensile strength and rotation higher in absolute value to the compressive strength and rotation due to the *Bauschinger* effect. The energy dissipation capacity of the connection designed with the deep beam (W24x76) is in the order of 458000 kips.in while the energy dissipation capacities of the smaller beam sections are in the order of 243000 kips.in for the W21x62 beam section and 197000 kips.in for the W18x55 beam section. This proves that the connection designed with deep beam section has higher plastic capacity under seismic loading. Furthermore, all three connections have manifested a hysteretic behavior capable of resisting highly seismic activity.

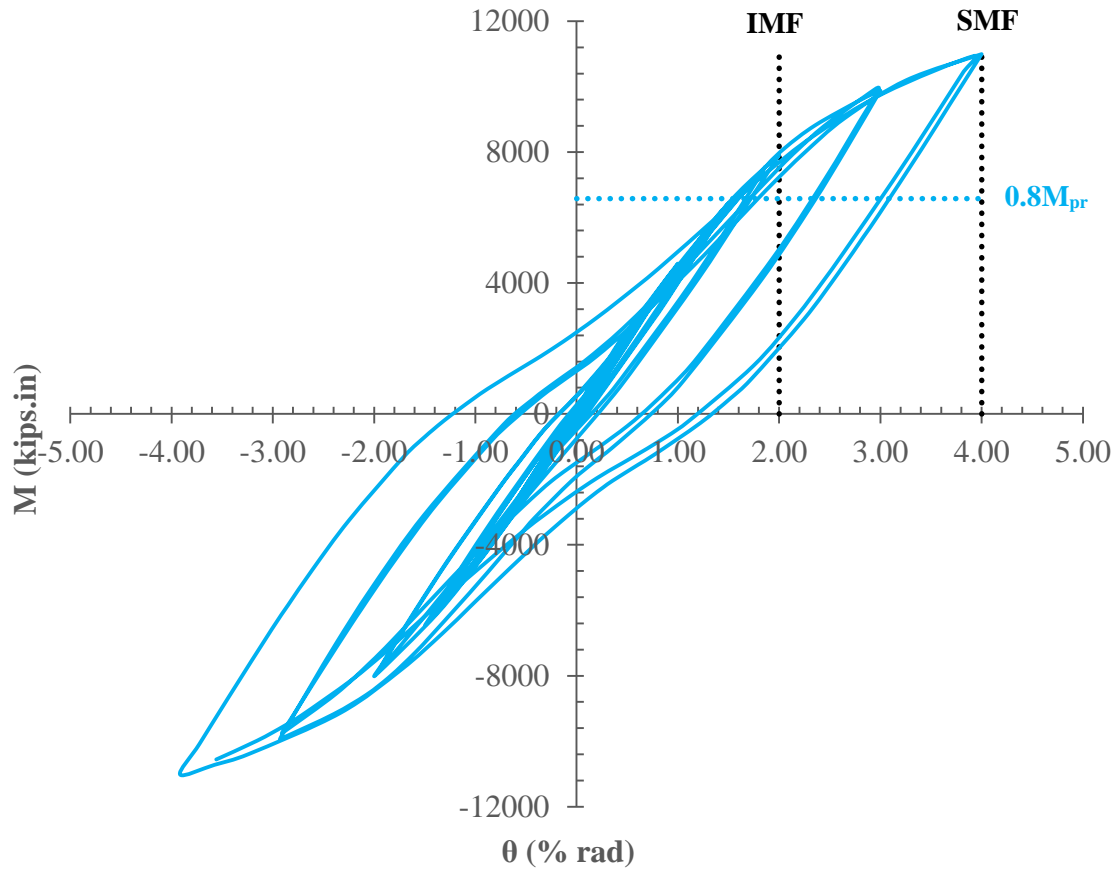


**Figure. 44.** Moment-rotation: W24x76 beam

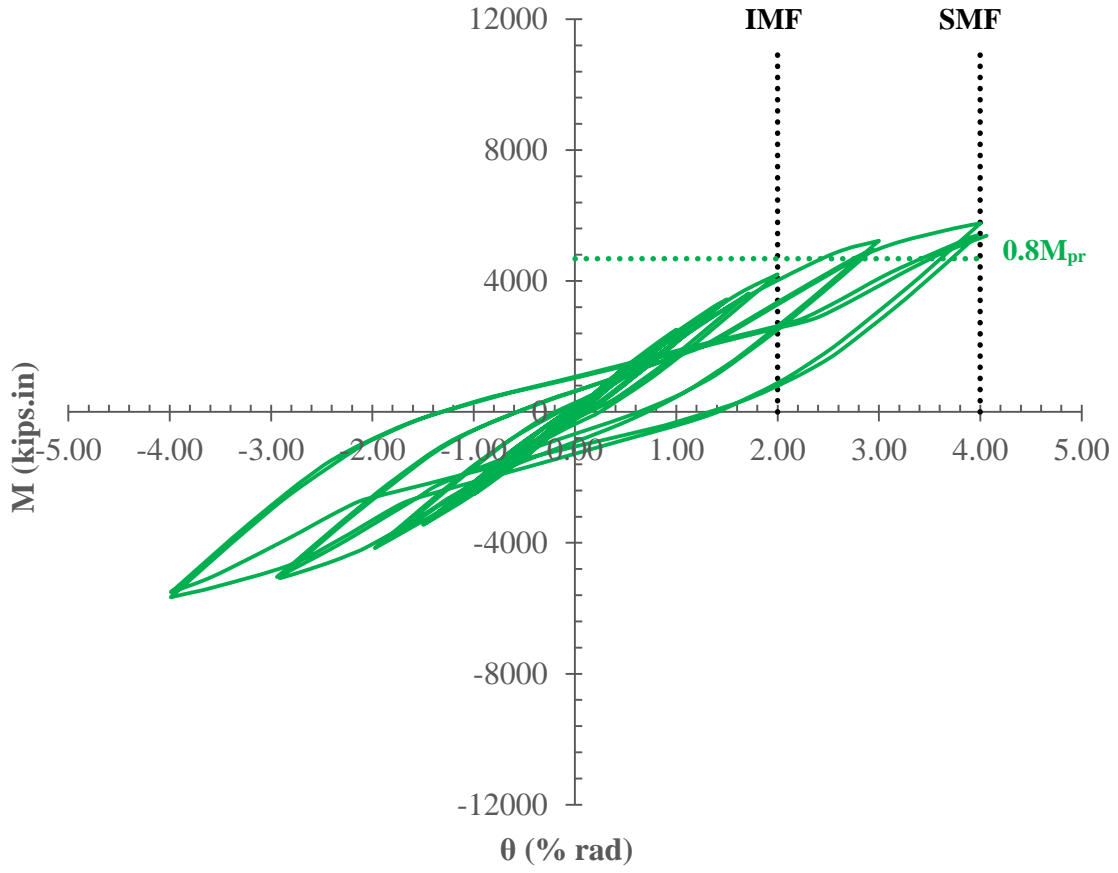


**Figure. 45.** Moment-rotation: W21x62 beam

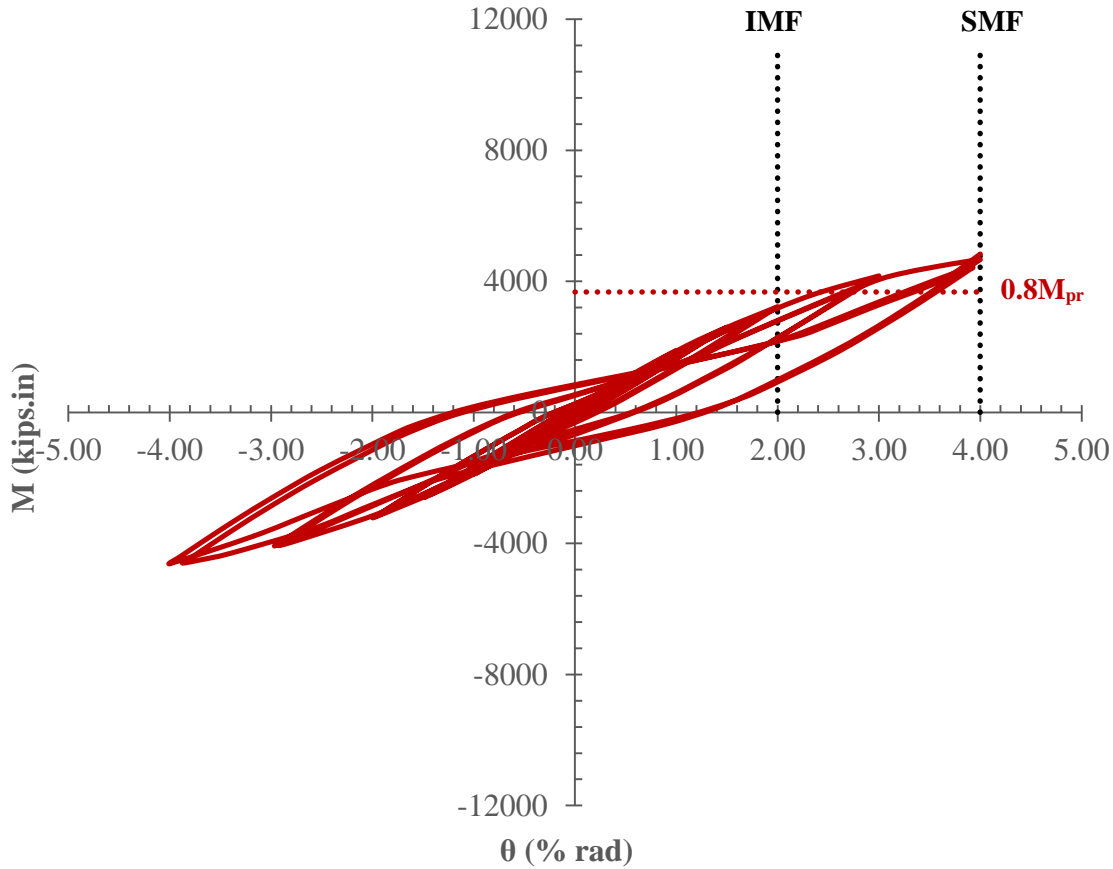


**Figure. 46.** Moment-rotation: W18x55 beam

Figures 44-46 also show that the connections stiffness and strength increase with the increase in the beam section. That is, the connection designed with the W18x55 beam section (Fig. 46) has the lowest stiffness and strength capacities and the connection designed with the W24x76 (Fig. 44) has the highest stiffness and strength capacities. Analysis of the results show that all designed specimens bypassed the  $0.8M_{pr}$  strength limit indicating that the connections have a full strength capacity. Similarly, the designed connections were able to withstand a 4% rotational capacity, due to the seismic loading applied, without failure. This indicates that the proposed eight-bolt extended endplate connection with circular bolt configuration and RBS can

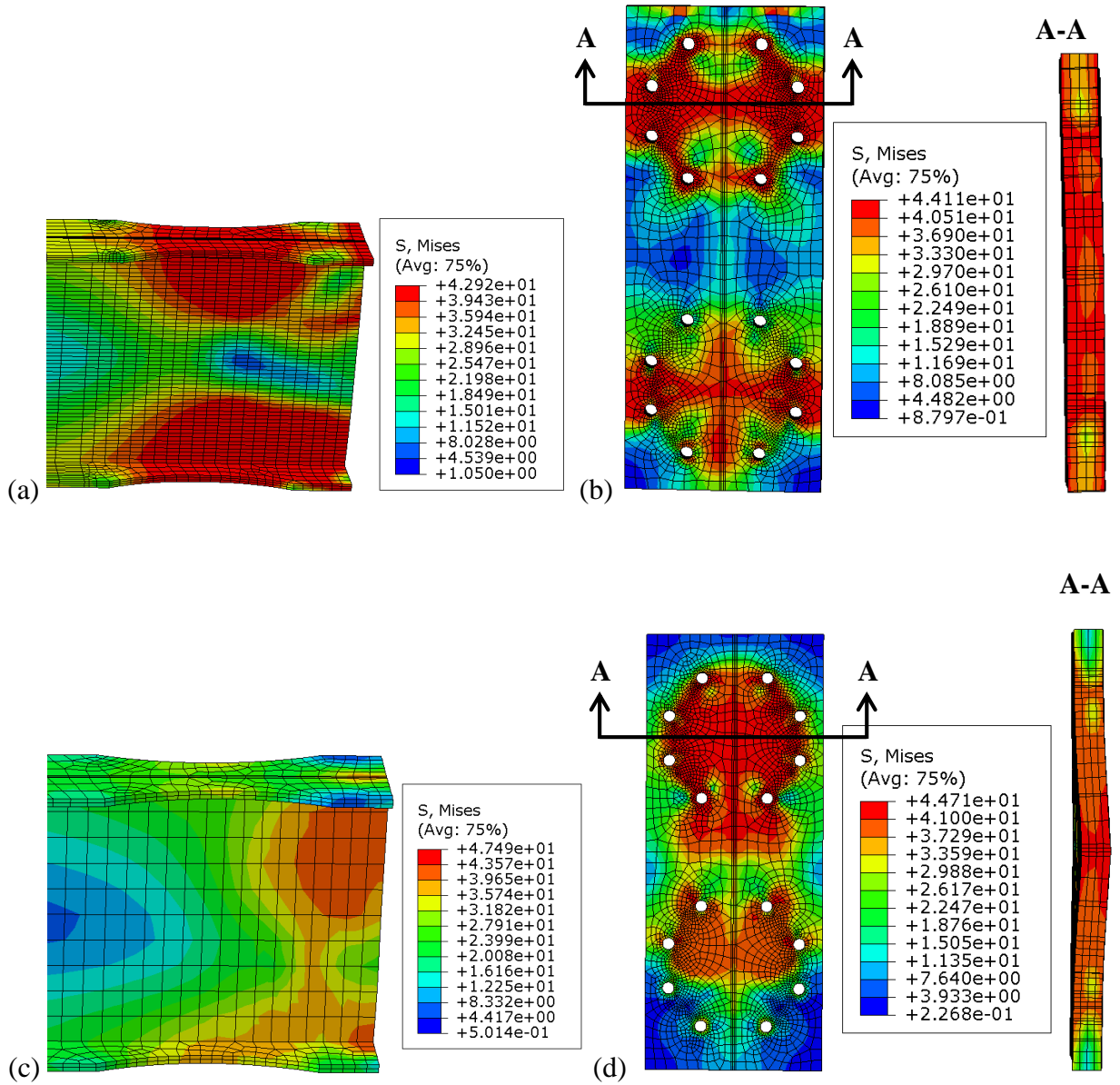
be qualified for use in IMFs and SMFs. This also indicates that the proposed design procedure is accurate.

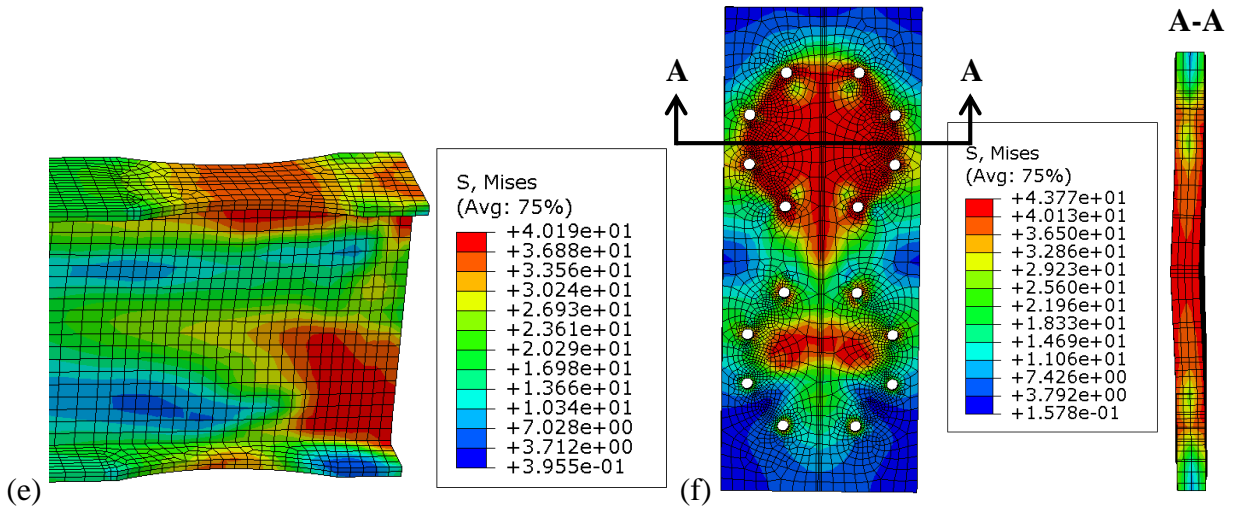
Apparent pinching is observed in the response of the three tested connections as shown in Figs. 44-46. The pinching phenomenon is caused by the yielding of the bolts or endplate. In fact, the elongation of the bolts reduces the pre-tensioning force of the bolts. That is, the strength of the connection is reduced in the subsequent loading cycle. Similarly, if the endplate yields before the bolts are fully welded, pinching may occur [68]. The circular bolt configuration ensures that the tensile force demand is equally distributed among all bolts [65]. Thus, the bolts are not fully loaded and do not yield as early as the connection with rectangular bolt pattern. That is, the pinching effect due to bolts yielding is reduced for the circular bolt configuration.

Figure 47 shows the von Mises stress state of the beam section at the RBS of all tested specimens at the last cycle of 4% rotational demand. All tested specimens showed partial yielding of the steel material at the RBS indicating that further loading will cause a plastic hinge to form at the RBS prior to any failure in the connection zone or in the protected zone of the column section. That is, reducing the beam section acts as an alternative to supplying beam flange stiffeners in securing that beam plastic hinging occurs first and away from the connection area. It is shown from Fig. 47 that the connection designed with the deep beam section have an apparent plastic hinge at the RBS when compared to the connections designed with medium beam sections. That is, the deep beam section reaches a high percentage of its plastic capacity which complies with the seismic design approach of the *ANSI/AISC 358-16* [2].

Figure 47 also shows the von Mises stress state of the endplates at the last cycle of 4% rotational demand. The yield line that is forming across the endplates indicates that further loading of the specimens might cause endplate flexural mechanism to occur right after beam

plastic hinging. The stress contour across the endplate thickness indicates that no full yielding of the endplate occurs. However, for the endplate associated with the deep beam section (Fig. 47 (b)), the yielding capacity of the endplate is almost reached along with the beam plastic hinging.





**Figure. 47.** Von Mises stress contours: (a) W24x76-beam, (b) W24x76-plate, (c) W21x62-beam, (d) W21x62-plate, (e) W18x55-beam, (f) W18x55-plate



## CHAPTER IX

### SUMMARY, CONCLUSIONS, AND RECOMMENDATIONS

#### A. Summary and conclusions

Steel beam-to-column connections used in SMFs and IMFs must be prequalified by testing prior to their use. The primary goal of this research is to investigate the behavior of eight-bolted double Tees and extended endplate connections with circular bolts configuration for use in MRFs for seismic application. The results of experimental tests and FE fracture simulations were used to provide the data set needed to develop mechanical-based models and design guidelines to describe their behavior under seismic actions.

Despite all experimental tests and analytical models conducted on double Tees and extended endplate connections, very few investigated the influence of column size (thin, medium, and thick), and bolt arrangements (circular and rectangular) on their response. Also, FE fracture modeling has not been thoroughly investigated on Tees and extended endplate connections and very few have predicted the post-yielding behavior of steel connections.

A summary of the performed research and the drawn conclusions is presented below:

- Seven component tests were conducted on Tee connections/column flange subjected to monotonic and cyclic loadings. Various column flange thicknesses were tested to quantify the stiffness, strength, and ductility associated with eight-bolted Tees. This study specifically aimed to provide insight as to whether continuity plates are necessary in columns when designing and detailing those types of connections. The results showed that increasing the column flange thickness decreases the secondary prying forces, ductility, energy dissipation capacities, and increases the strength and stiffness

capacities of the connection. Detailing columns without continuity plates reduces the fabrication cost and eliminates the need to weld in regions of low notch toughness. Adding the secondary prying failure mode check to the current *ANSI/AISC 358-16* and *Eurocode 3 part 1-8* guidelines is recommended to ensure a safe design.

- Eight monotonic and cyclic component tests were conducted on extended endplates with circular bolts configuration. The aim was to particularly identify the changes in the behavioral characteristics and prying tensile forces in bolts associated with circular configuration. Three failure modes were identified. The results showed that a minimum of 7.4 bolts out of the 8 bolts present in the investigated connections were effective in carrying the applied load and reached their full capacity at the point of ultimate. This lead to a higher design capacity of the connection. Compared to the rectangular bolt configuration, the circular configuration requires less fabrication due to the omission of stiffener plates but thicker endplates.
- FE fracture models that incorporate material damage and plasticity were developed, calibrated, and validated against the experimental results of the tested connections and tests available in the literature to predict the post-yielding behavior. The results showed that the proposed FE fracture model is able to predict the failure modes and load-displacement responses of double Tees, extended endplates, and ABS in steel beams with excellent accuracy. The FE fracture model predicted the post-ultimate strength and ductility required for seismic applications. Also, the FE fracture model was able to predict crack initiation in base or bolt material due to tensile and/or shear loadings. The proposed FE fracture model can be considered a first step towards including the

fracture characteristics (load and plastic displacement at fracture point) in the current design guidelines of steel connections.

- Three full scale analytical tests for eight-bolt unstiffened extended endplate connections with circular bolt configuration and RBS, subjected to cyclic loading, were conducted using FE analysis. This allowed the prediction of full assembly behavioral characteristics under seismic activity. The objective was to ultimately prequalify this type of connections for use in MRFs in seismic areas. The results showed that the proposed connection can be classified for use in both IMFs and SMFs. Also, that the RBS ensures that beam plastic hinging occurs first and away from the connection.

## **B. Recommendations**

More research work is still needed in order to develop a full understanding of the connections response to seismic loading.

- Full scale experimental tests of eight-bolt extended endplate connections with circular bolts configuration and RBS are needed to be tested under seismic loading.
- Full scale experimental tests of double Tee moment connections are needed to be tested to investigate the effect of continuity plates removal and column flange thickness on the overall seismic behavior of the connection and to check if the connection under study can meet the prequalification requirements for use in IMFs and SMFs.
- The fracture of steel base, bolt, and weld material under elevated temperature is needed to be investigated using FE fracture analysis.

## BIBLIOGRAPHY

- [1] "FEMA 350: Recommended seismic design criteria for new steel moment-frame buildings," Federal Emergency Management Agency, Washington DC, USA., 2000.
- [2] Prequalified connections for special and intermediate steel moment frames for seismic applications - ANSI/AISC358-16, Chicago, US: American Institute of Steel Construction, 2016.
- [3] Seismic Provisions for Structural Steel Buildings ANSI/AISC 341-16, Chicago, US, 2016.
- [4] An American National Standard: Specification for Structural Steel Buildings-ANSI/AISC 360-16, Chicago, US, 2016.
- [5] "Part 1-8: Design of joints," in *Eurocode 3: Design of steel structures*, Brussels, Belgium, European committee for standardization, 2005.
- [6] E. Hantouche, A. Kukreti and G. Rassati, "Investigation of secondary prying in thick built-up T-stub connections using nonlinear finite element modeling," *Engineering Structures*, vol. 36, pp. 113-122, 2012.
- [7] R. Hamburger, H. Krawinkler, J. Malley and S. Adan, Seismic design of steel special moment frames: a guide for practicing engineers, National Institute of Standards and Technology, 2009.
- [8] E. Hantouche and N. Abboud, "Stiffness modeling of bolted thick built-up T-stub connections including secondary prying," *Journal of Constructional Steel Research*, vol. 95, pp. 279-289, 2014.
- [9] Z. Pisarek and A. Kozlowski, "End-plate steel joint with four bolts in the row," *Progress in*

- Steel, Composite and Aluminium Structures*, pp. 257-266, 2008.
- [10] J. Demonceau, K. Weynand, J. Jaspart and C. Müller, "Application of Eurocode 3 to steel connections with four bolts per horizontal row," in *SDSS'Rio 2010 Stability and Ductility of Steel Structures*, Rio de Janeiro, Brazil, 2010.
- [11] G. R. A. S. a. L. d. S. M. Latour, "Experimental analysis and mechanical modeling of T-stubs with four bolts per row," *Journal of Constructional Steel Research* , vol. 101, pp. 158-174, 2014.
- [12] R. Kiamanesh, A. Abolmaali and M. Razavi, "Effect of circular bolt pattern on behavior of extended end-plate connection," *Journal of Structional Engineering*, Vols. 10.1061/(ASCE)ST.1943-541X.0000765, 2013.
- [13] L. Massimo, G. Rizzano , A. Santiago and L. Simoes da Silva, "Experimental analysis and mechanical modeling of T-stubs with four bolts per row," *Journal of Constructional Steel Research*, vol. 101, pp. 158-174, 2014.
- [14] F. McClintock, "A criterion for ductile fracture by the growth of holes," *Journal of Applied Mechanics*, vol. 35, no. 2, pp. 363-371, 1968.
- [15] J. Rice and D. Tracey, "On the enlargement of voids in triaxial stress fields," *Journal of the Mechanics and Physics of Solids*, vol. 17, no. 3, pp. 201-217, 1969.
- [16] J. Hancock and A. Mackenzie, "On the mechanisms of ductile failure in high-strength steels subjected to multi-axial stress-states," *Journal of the Mechanics and Physics of Solids*, vol. 24, no. 2, pp. 147-160, 1976.
- [17] G. Johnson and W. Cook, "Fracture characteristics of three metals subjected to various strains, strain rates, temperatures and pressures," *Engineering Fracture Mechanics*, vol. 21,

- pp. 31-48, 1985.
- [18] D. Schweizer, Experimental investigation of innovative seismic performance enhancement techniques for steel building beam to column moment connections - PhD Dissertation, Raleigh, NC, USA: North Carolina State University, 2013.
- [19] E. Hantouche and E. Mouannes, "Strength and Stiffness modeling of extended endplate connections with circular and rectangular bolt configurations," *Steel and Composite Structures*, vol. 22, no. 2, pp. 323-352, 2016.
- [20] M. Morrison, S. Quayyum and T. Hassan, "Performance enhancement of eight bolt extended end-plate moment connections under simulated seismic loading," *Engineering Structures*, vol. 151, pp. 444-458, 2017.
- [21] W. Chi, A. Kanvinde and G. Deierlein, "Prediction of ductile fracture in steel connections using SMCS criterion," *Journal of Structural Engineering*, vol. 132, no. 2, pp. 171-181, 2006.
- [22] F. McClintock, "A criterion for ductile fracture by the growth of holes," *Journal of Applied Mechanics*, vol. 35, no. 2, pp. 363-371, 1968.
- [23] J. Rice and D. Tracey, "On the enlargement of voids in triaxial stress fields," *Journal of the Mechanics and Physics of Solids*, vol. 17, no. 3, pp. 201-217, 1969.
- [24] J. Hancock and A. Mackenzie, "On the mechanisms of ductile failure in high-strength steels subjected to multi-axial stress-states," *Journal of the Mechanics and Physics of Solids*, vol. 24, no. 2, pp. 147-160, 1976.
- [25] G. Johnson and W. Cook, "Fracture characteristics of three metals subjected to various strains, strain rates, temperatures and pressures," *Engineering Fracture Mechanics*, vol. 21,

- no. 1, pp. 31-48, 1985.
- [26] H. Hooputra, H. Gese, H. Dell and H. Werner, "A comprehensive failure model for crashworthiness simulation of aluminum extrusions," *International Journal of Crashworthiness*, vol. 9, no. 5, pp. 449-464, 2004.
- [27] A. Kanvinde and G. Deierlein, "Micromechanical simulation of earthquake induced fractures in steel structures," Blume Center TR145, Stanford Univ., Stanford, California, 2004.
- [28] A. Kanvinde and G. Deierlein, "The void growth model and the stress modified critical strain model to predict ductile fracture in structural steels," *Journal of Structural Engineering*, vol. 132, no. 12, pp. 1907-1918, 2006.
- [29] T. Wierzbicki, Y. Bao, Y. Lee and Y. Bai, "Calibration and evaluation of seven fracture models," *International Journal of Mechanical Sciences*, vol. 47, pp. 719-743, 2005.
- [30] Y. Bao, "Dependence of ductile crack formation in tensile tests on stress triaxiality, stress and strain ratios," *Engineering Fracture Mechanics*, vol. 72, pp. 505-522, 2005.
- [31] A. Myers, A. Kanvinde and G. Deierlein, "Calibration of the SMCS criterion for ductile fracture in steels: specimen size dependence and parameter assessment," *Journal of Engineering Mechanics*, vol. 136, no. 11, pp. 1401-1410, 2010.
- [32] Y. Wang, H. Zhou, Y. Shi and J. Xio, "Fracture prediction of welded steel connections using traditional fracture mechanics and calibrated micromechanics based models," *International Journal of Steel Structures*, vol. 11, no. 3, pp. 351-366, 2011.
- [33] R. Kiran and K. Khandelwal, "A micromechanical model for ductile fracture prediction in ASTM A992 steels," *Engineering Fracture Mechanics*, vol. 102, pp. 101-117, 2013.

- [34] W. Cai, *Steel Fracture Modeling at Elevated Temperature for Structural-Fire Engineering Analysis*, Austin, Texas, US: The University of Texas at Austin, 2015.
- [35] L. Jia, H. Ge, K. Shinohara and H. Kato, "Experimental and numerical study on ductile fracture of structural steels under combined shear and tension," *Journal of Bridge Engineering*, vol. 21, no. 5, 2016.
- [36] L. Jia, T. Ikai, K. Shinohara and H. Ge, "Ductile crack initiation and propagation of structural steels under cyclic combined shear and normal stress loading," *Construction and Building Materials*, vol. 112, pp. 69-83, 2016.
- [37] C. Oh, N. Kim, Y. Kim, J. Baek, Y. Kim and W. Kim, "A finite element ductile failure simulation method using stress-modified fracture strain model," *Engineering Fracture Mechanics*, vol. 78, pp. 124-137, 2011.
- [38] H. Zhou, Y. Wang, Y. Shi, J. Xiong and L. Yang, "Extremely low cycle fatigue prediction of steel beam-to-column connection by using a micro-mechanics based fracture model," *International Journal of Fatigue*, vol. 48, pp. 90-100, 2013.
- [39] L. Jia and H. Kuwamura, "Ductile fracture simulation of structural steels under monotonic tension," *Journal of Structural Engineering*, vol. 140, no. 5, 2014.
- [40] L. Jia and H. Kuwamura, "Ductile fracture model for structural steel under cyclic large strain loading," *Journal of Constructional Steel Research*, vol. 106, pp. 110-121, 2015.
- [41] L. Kang, H. Ge and X. Fang, "An improved ductile fracture model for structural steels considering effect of high stress triaxiality," *Construction and Building Materials*, vol. 115, pp. 634-650, 2016.
- [42] H. Wen, *Predicting ductile fracture in steel connections*, Colorado, US: Colorado State



University, 2016.

- [43] X. Wang, B. Sun and Z. Li, "Damage-induced material softening and its effect on seismic performance of steel structures," *Technological Sciences*, vol. 59, no. 10, pp. 1559-1572, 2016.
- [44] E. Hantouche, A. Kukreti, G. Rassati and J. Swanson, "Prying Models for Strength in Thick-Flange Built-Up T-Stubs with Complete Joint Penetration and Fillet Welds," *Journal of Structural Engineering*, Vols. 10.1061/(ASCE)ST.1943-541X.0001051, 2015.
- [45] "Part 1-1: General rules and rules for buildings," in *Eurocode 3: Design of steel structures*, Brussels, Belgium, European committee for standardization, 2005.
- [46] J. Swanson and R. Leon, "Stiffness modeling of bolted T-stub connection components," *Journal of Structural Engineering*, vol. 127, no. 5, pp. 498-505, 2001.
- [47] "Part 9: System HR or HV - Direct tension indicators for bolt and nut assemblies - BS EN 14399-9," in *High strength structural bolting for preloading*, Brussels, European committee for standardization, 2009.
- [48] "Guidelines for seismic testing of components of steel structures," Applied Technology Council, Report No 24, ATC, Redwood City, CA, USA, 1992.
- [49] M. Morrison, S. Quayyum and T. Hassan, "Performance enhancement of eight bolt extended end-plate moment connections under simulated seismic loading," *Engineering Structures*, vol. 151, pp. 444-458, 2017.
- [50] T. Murray, "Recent development for the design of moment end-plate connections," *Journal of Constructional Steel Research*, vol. 10, pp. 133-162, 1988.
- [51] Optimizing the seismic performance of steel and steel-concrete structures by standardising

- material quality control (OPUS) - EUR 25893, Luxembourg: European Commission, 2013.
- [52] A. Daryan and M. Yahyai, "Modeling of bolted angle connections in fire," *Fire Safety Journal*, vol. 44, no. 7, pp. 976-988, 2009.
- [53] "Lecture 9: Material Damage and Failure," ABAQUS/Explicit: Advanced Topics, 2005.
- [54] Y. Ling, "Uniaxial true stress-strain after necking," *AMP Journal of Technology*, vol. 5, pp. 37-48, 1996.
- [55] H. Hooputra, H. Gese, H. Dell and H. Werner, " A Comprehensive Failure Model for Crashworthiness Simulation of Aluminum Extrusions," *International Journal of Crashworthiness*, vol. 9, no. 5, pp. 449-464, 2004.
- [56] K. Adewole and L. Teh, "Predicting steel tensile responses and fracture using the phenomenological ductile shear fracture model," *Journal of Materials in Civil Engineering*, vol. 29, no. 12, p. 06017019, 2017.
- [57] W. Cai, Steel Fracture Modeling at Elevated Temperature for Structural-Fire Engineering Analysis - PhD Thesis, Austin, TX, USA : The University of Texas at Austin, 2015.
- [58] G. Hu , Behavior of Beam Shear Connections in Steel Buildings Subject to Fire - PhD Thesis, Austin, TX, USA: The University of Texas at Austin, 2011.
- [59] J. Ribeiro , A. Santiago and C. Rigueiro , "Damage model calibration and application for S355," in *21st European Conference on Fracture- ECF21* , Catania, Italy, EU, 2016.
- [60] P. Versailot, Effect of cyclic loading on the mechanical properties of steel - PhD Thesis, Romania: Universitatea Politehnica Timisoara, 2015.
- [61] J. Brnic, G. Turkalj and G. Vukelic, "Importance of experimental research in the design of structures," in *Annals of DAAAM for 2012 & Proceedings of the 23rd International DAAAM*

*Symposium*, Vienna, Austria, EU, 2012.

- [62] A. Moore, G. Rassati and J. Swanson, "Evaluation of the Current Resistance Factors for High-Strength Bolts," in *Research Council on Structural Connections*, 2008.
- [63] R. Christopher , Calibration of alloy steel bolts - Master's Thesis, PA, USA: Lehigh University, 1964.
- [64] S. El Kalash and E. Hantouche, "Secondary prying of column flange in Tee-connections: Experimental investigation and mechanical modeling," *Journal of Constructional Steel Research*, vol. 145, pp. 518-528, 2018.
- [65] S. El Kalash and E. Hantouche, "Prying effect in unstiffened extended endplate connection," *Journal of Constructional Steel Research*, vol. 160, pp. 402-410, 2019.
- [66] A. Coelho, F. Bijlaard , N. Gresnigt and L. Simoes da Silva, "Experimental assessment of the behaviour of bolted T-stub connections made up of welded Plates," *Journal of Constructional Steel Research*, vol. 60, pp. 269-311, 2004.
- [67] V. Piluso and G. Rizzano, "Experimental analysis and modelling of bolted T-stubs under cyclic loads," *Journal of Constructional Steel Research*, vol. 64, pp. 655-669, 2008.
- [68] R. Kiamanesh, On the effect of circular bolt patterns on the behavior of the extended end-plate connections - PhD Thesis, TX, US: The University of Texas at Arlington, 2011.
- [69] L. Massimo, G. Rizzano , A. Santiago and L. Simoes da Silva, "Experimental analysis and mechanical modeling of T-stubs with four bolts per row," *Journal of Constructional Steel Research*, vol. 101, pp. 158-174, 2014.
- [70] F. Sun, X. Xue, Y. Xiao, Y. Le and G. Li, "Effect of welding and complex loads on the high-strength steel T-stub connection," *Journal of Constructional Steel Research*, vol. 150,

pp. 76-86, 2018.

# APPENDIX A

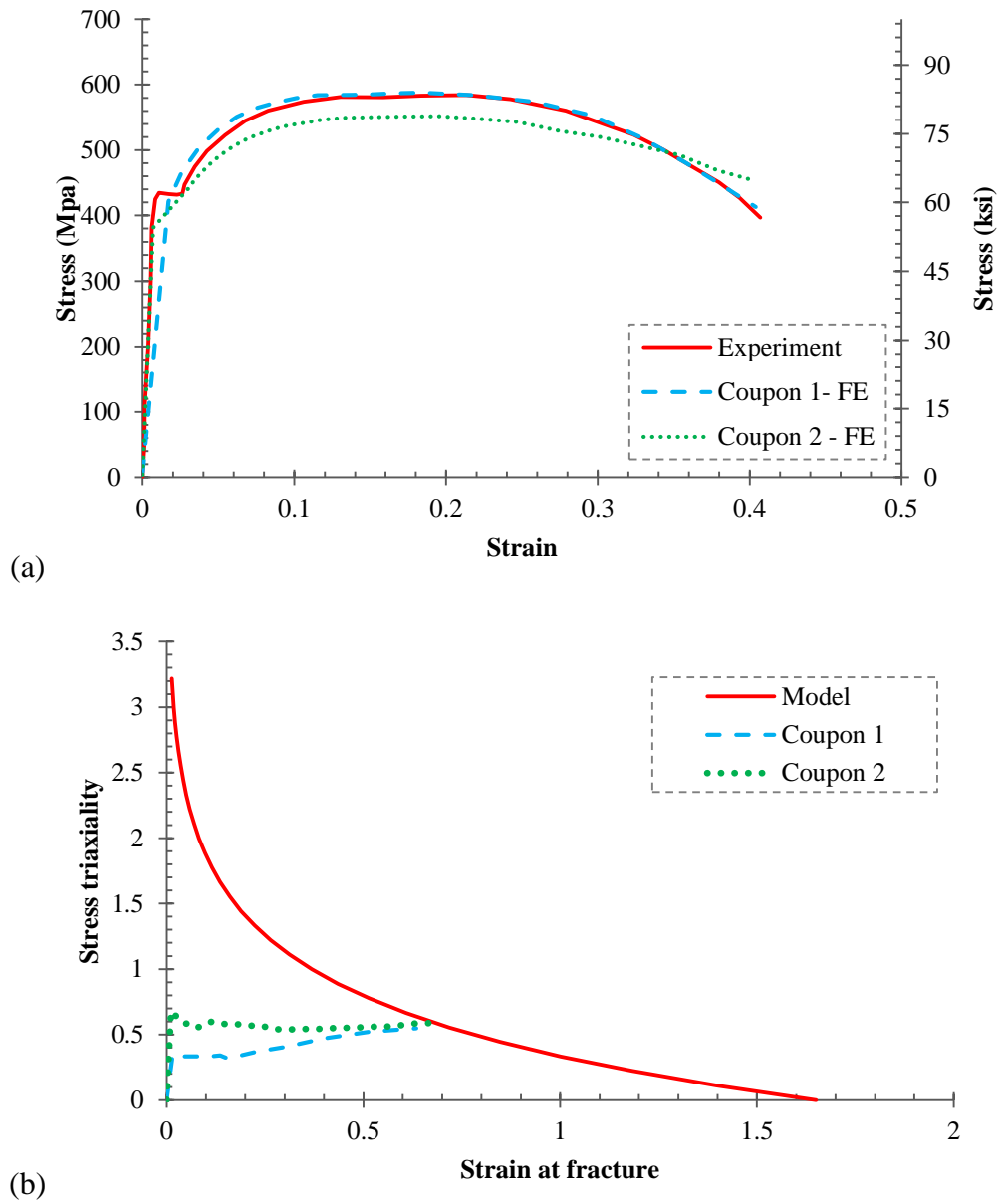
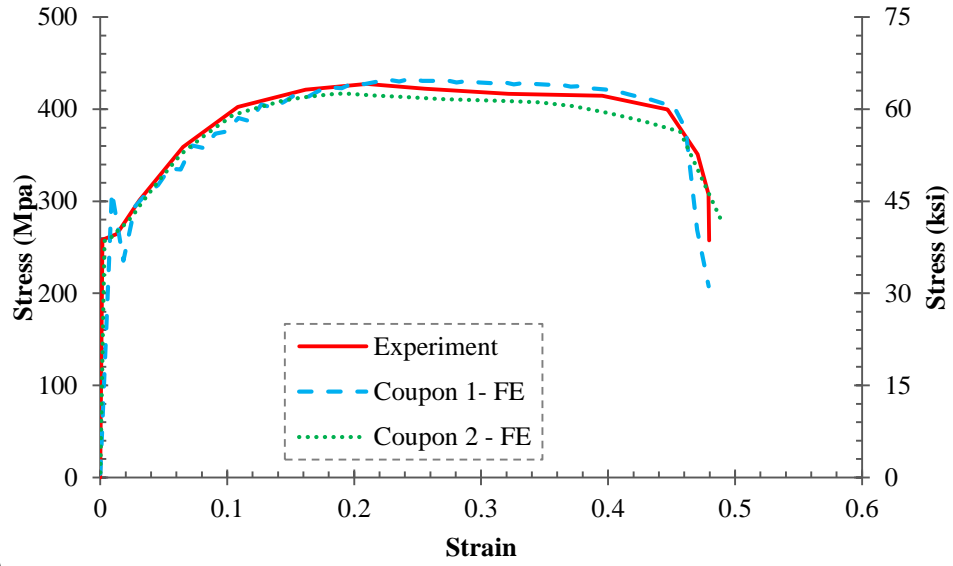
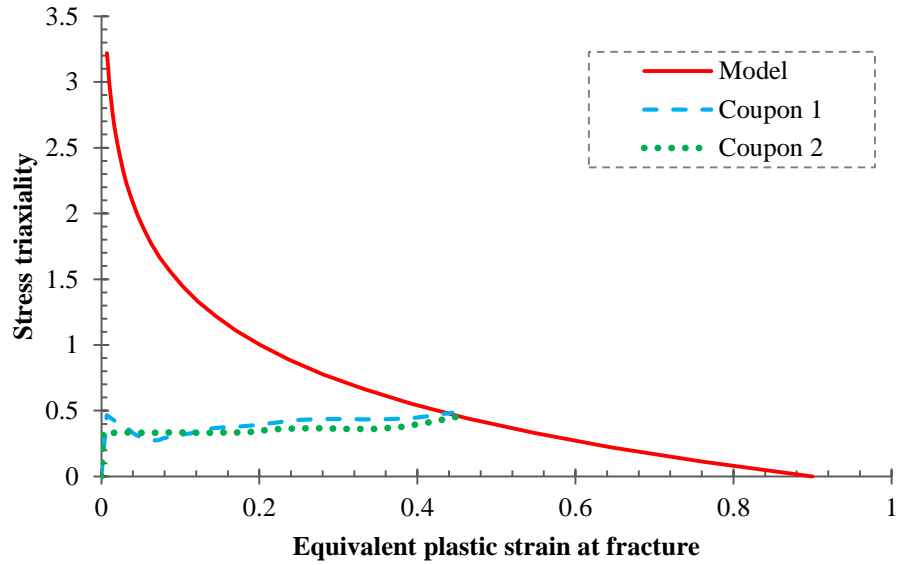


**Figure. 48.** A572-50 & S355: (a) stress vs. strain, (b) stress-triaxiality vs. strain at fracture

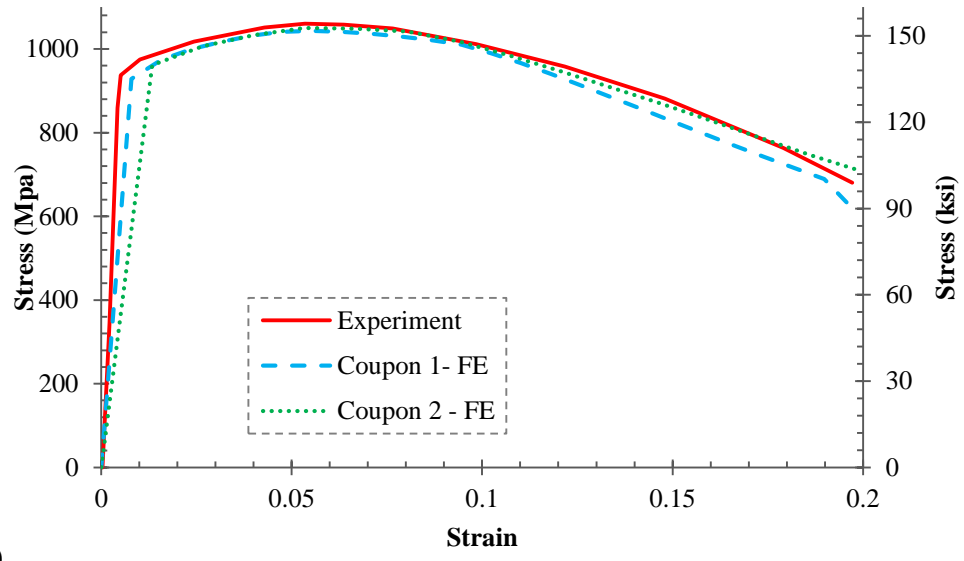


(a)

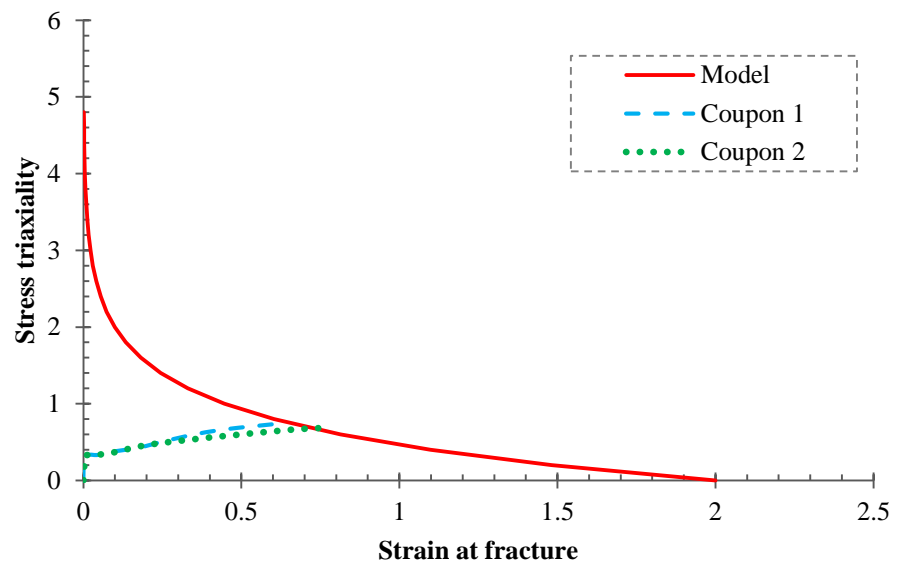


(b)

**Figure. 49.** A36 & S275: (a) stress vs. strain, (b) stress-triaxiality vs. strain at fracture

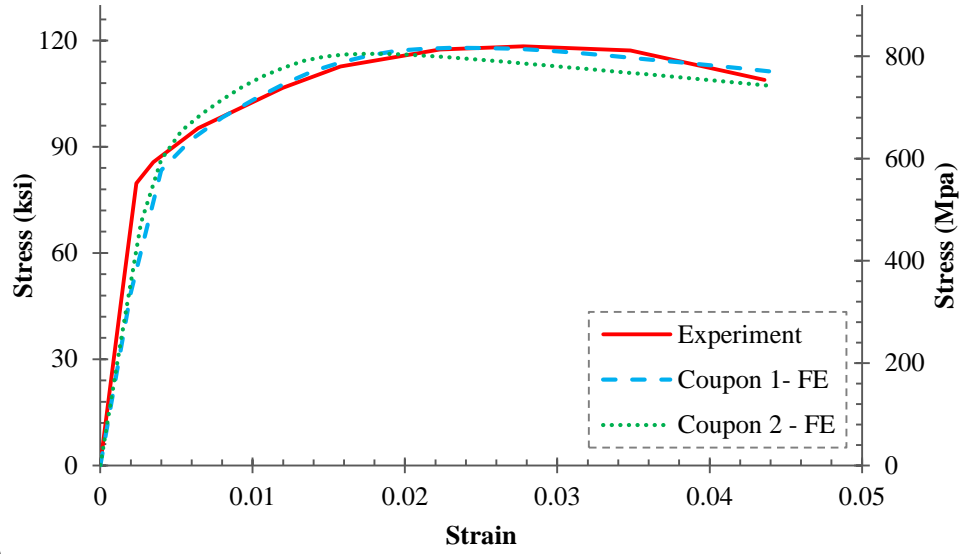


(a)

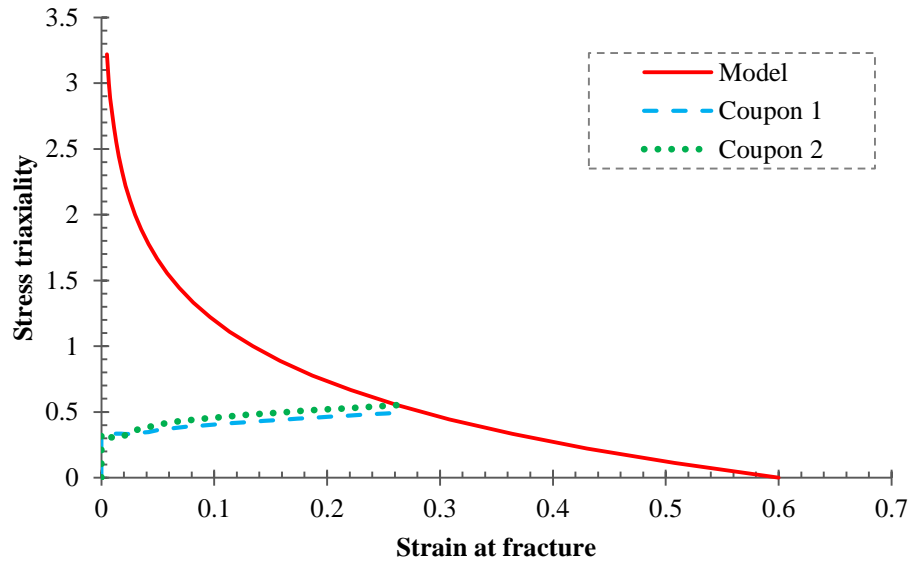


(b)

**Figure. 50.** A490 & Grade 10.9: (a) stress vs. strain, (b) stress-triaxiality vs. strain at fracture



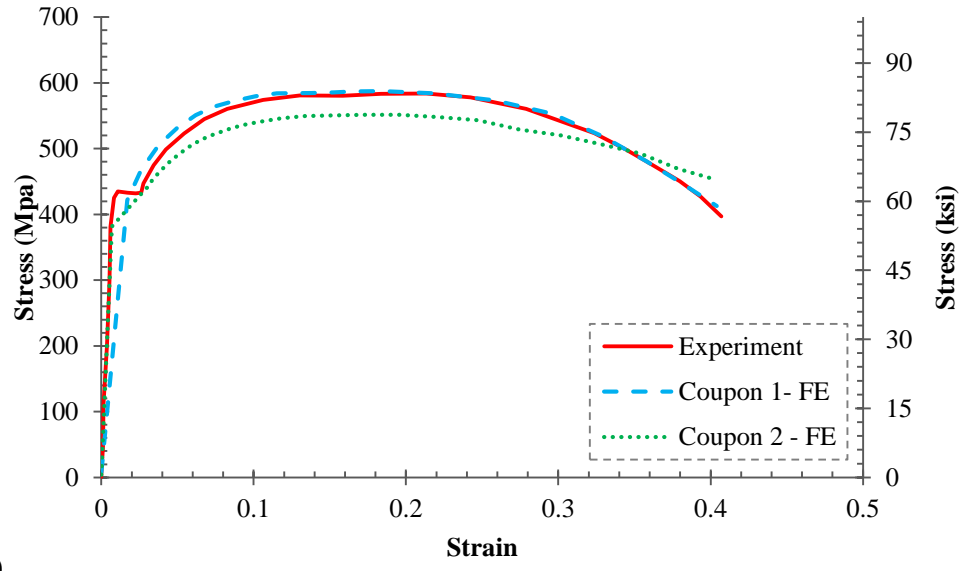
(a)



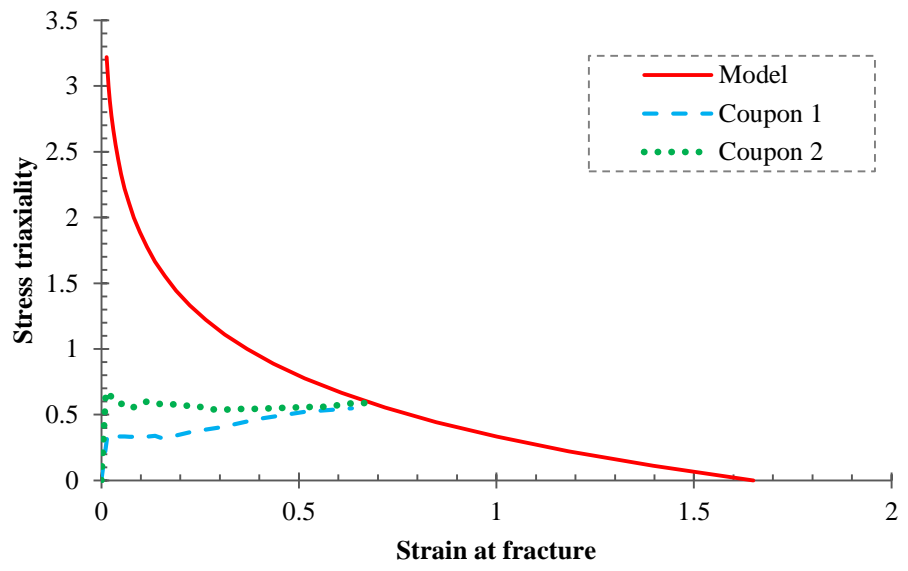
(b)

**Figure. 51.** A325 & Grade 8.8: (a) stress vs. strain, (b) stress-triaxiality vs. strain at fracture



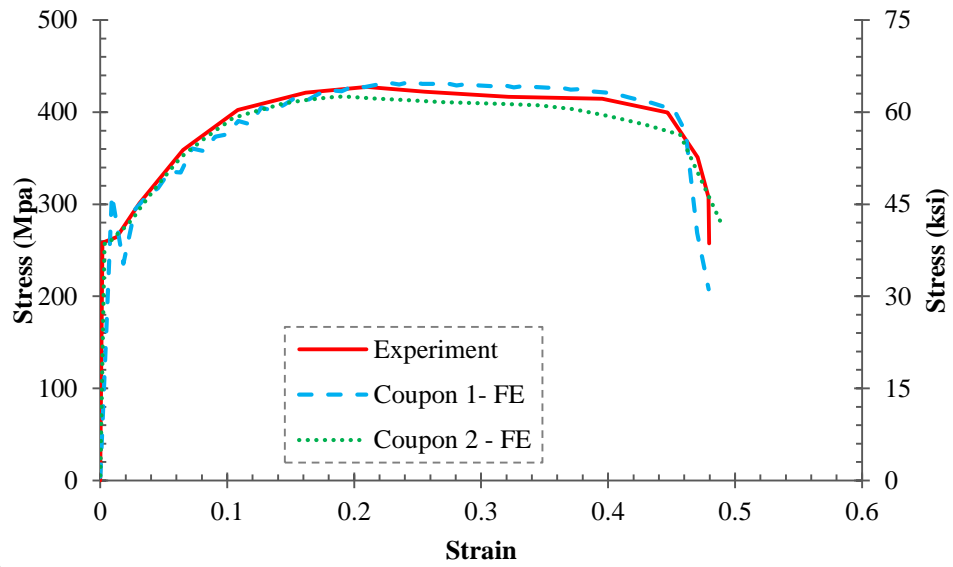


(a)

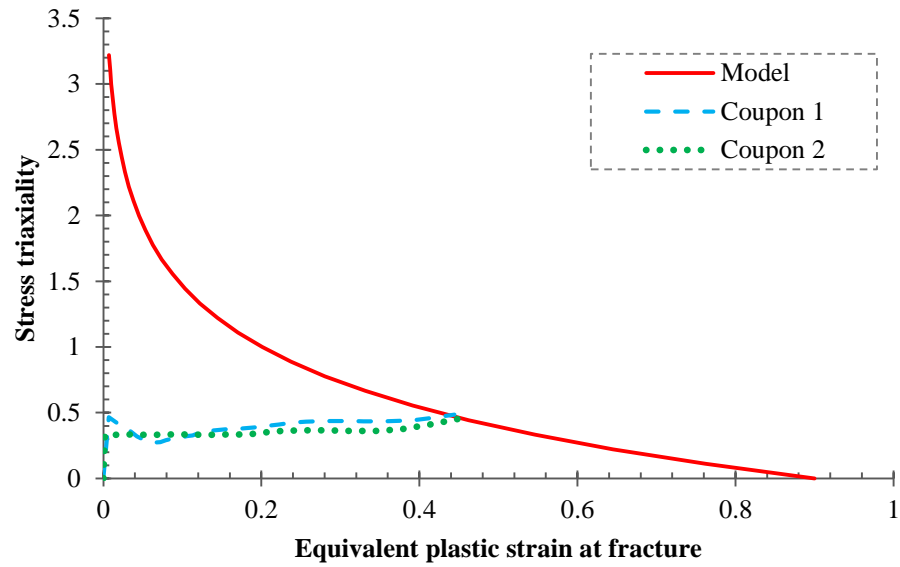


(b)

**Figure. 52.** A572-50 & S355: (a) stress vs. strain, (b) stress-triaxiality vs. strain at fracture

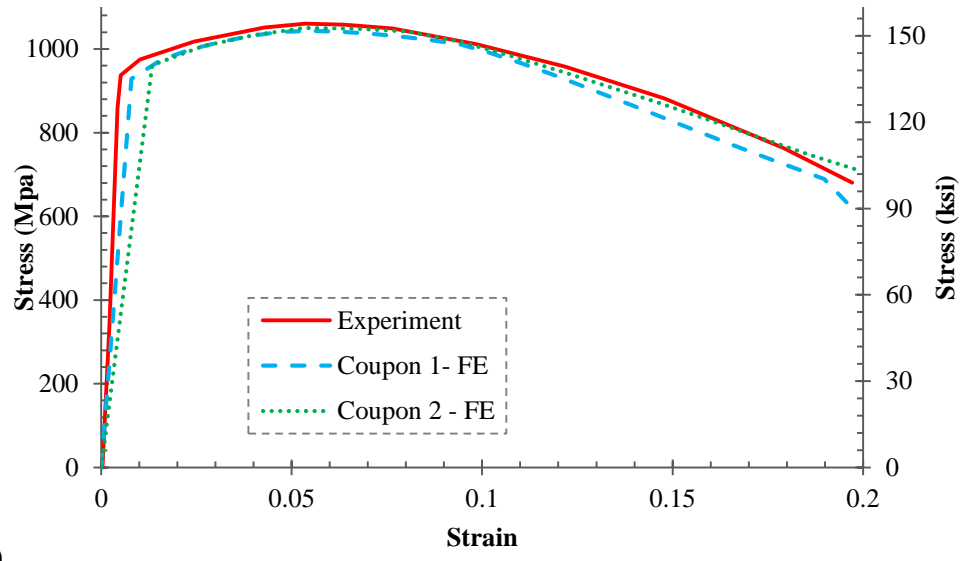


(a)

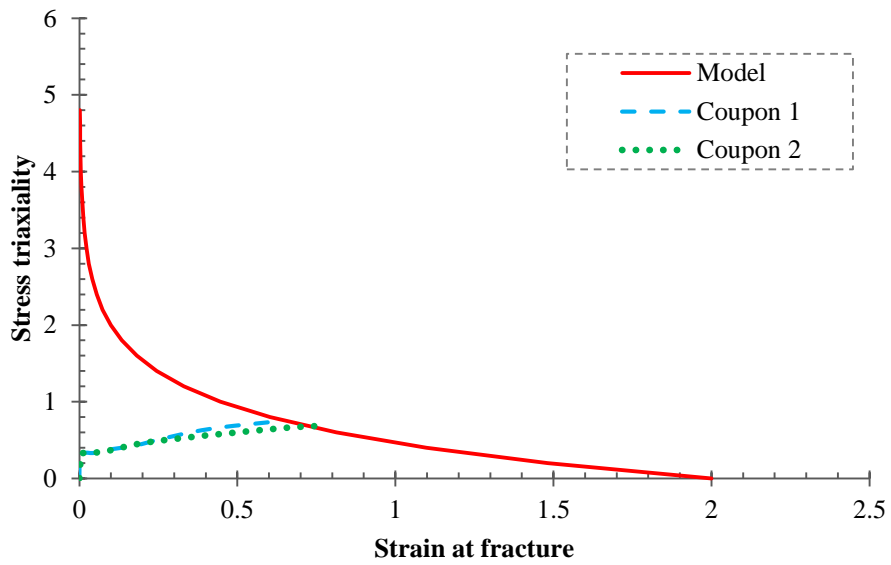


(b)

**Figure. 53.** A36 & S275: (a) stress vs. strain, (b) stress-triaxiality vs. strain at fracture

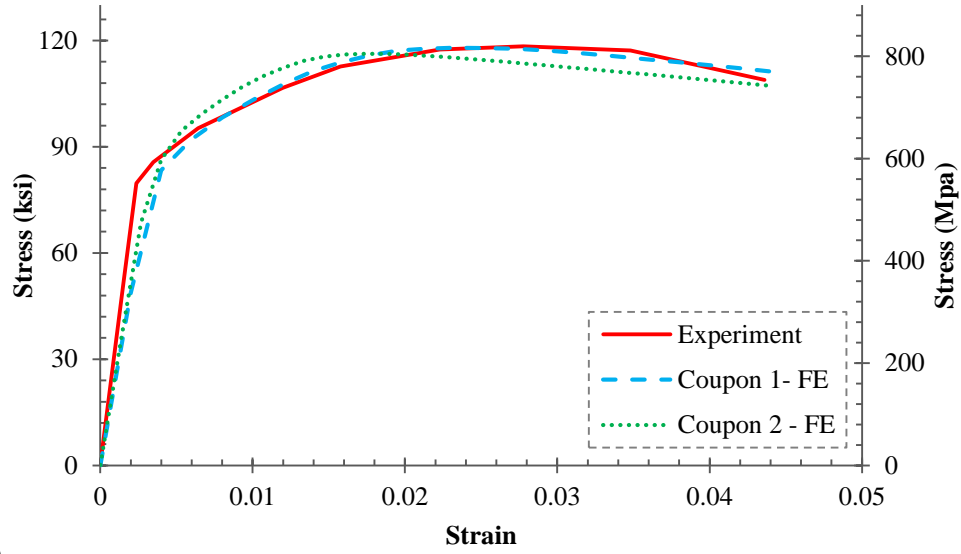


(a)

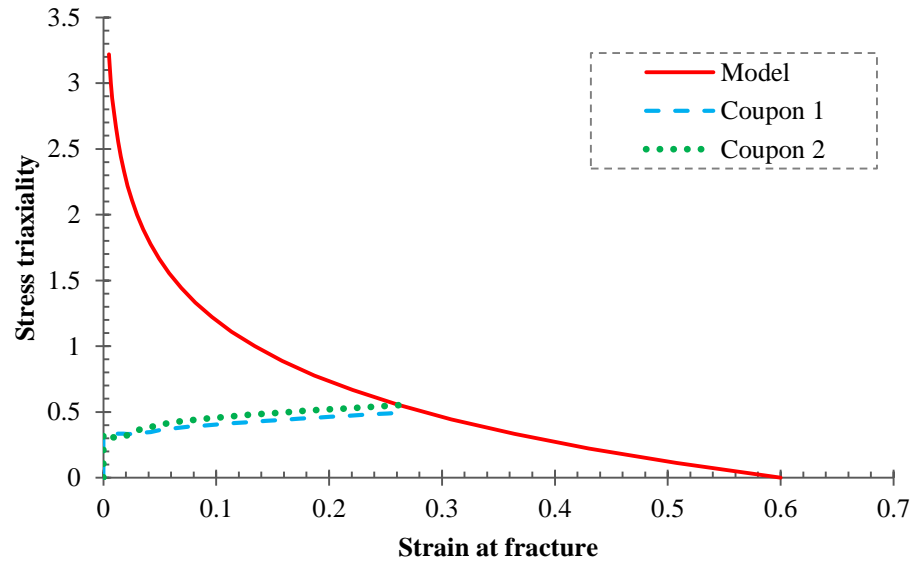


(b)

**Figure. 54.** A490 & Grade 10.9: (a) stress vs. strain, (b) stress-triaxiality vs. strain at fracture



(a)



(b)

**Figure. 55.** A325 & Grade 8.8: (a) stress vs. strain, (b) stress-triaxiality vs. strain at fracture

## APPENDIX B

### A. W21x62 beam section

#### 1. Prequalification limits

##### Beam Limitations

- ✓ Beam is rolled wide flange
  - ✓ Beam depth is W21 < W36
  - ✓ Beam weight is  $62 \frac{\text{lb}}{\text{ft.}} < 150 \frac{\text{lb}}{\text{ft.}}$
  - ✓ Beam flange thickness:  $t_{\text{bf}} = 0.615^{\text{in.}} < 1^{\text{in.}}$
  - ✓ Clear span to depth  $\frac{410}{21} = 19.52 > 9$  for SMF
  - ✓ Beam flange slenderness:  $\frac{b_{\text{bf}}}{2t_{\text{bf}}} = 6.7 < 0.3 \sqrt{\frac{E}{F_{\text{yb}}}} = 6.89$
  - ✓ Beam web slenderness:  $\frac{h}{t_{\text{bw}}} = 46.9 < 2.45 \sqrt{\frac{E}{F_{\text{yb}}}} = 56.26$
- No local buckling of beam
- ✓ Lateral bracing shall be provided:

Both beam flanges should be laterally braced at intervals not to exceed (ANSI/AISC 341-16 [3]):

$$L_{\text{bmax}} = 0.086r_y \left( \frac{E}{F_y} \right) = 7.36^{\text{ft.}}$$

The limiting length:

$$L_p = 1.76r_y \sqrt{\left( \frac{E}{F_y} \right)} = 6.25^{\text{ft.}}$$

$$L_r = 1.95r_{ts} \frac{E}{0.7F_y} \sqrt{\left( \frac{JC}{S_x h_0} + \sqrt{\left( \frac{JC}{S_x h_0} \right)^2 + 6.76 \left( \frac{0.7F_y}{E} \right)^2} \right)} = 13.9 \text{ ft.}$$

Provide braces at maximum of 6<sup>ft.</sup> outside the protected zone.

The beam is adequate for use in high seismic areas.

### Column Limitations

- ✓ Column is rolled wide flange
  - ✓ Beam connected to column flange
  - ✓ Column depth is W14 ≤ W14
  - ✓ Column flange slenderness:  $\frac{b_{cf}}{2t_{cf}} = 4.23 < 0.3 \sqrt{\frac{E}{F_{yc}}} = 6.89$
  - ✓ Column web slenderness:  $\frac{h}{t_{cw}} = 9.71 < 2.45 \sqrt{\frac{E}{F_{yc}}} = 56.27$
- No local buckling of column

The column is adequate for use in high seismic areas.

## **2. Endplate and bolt design**

### Moment at the Face of Column

Compute the probable maximum moment at the beam hinge:

$$M_{pr} = C_{pr} F_y R_y Z_e$$

where:

$$C_{pr} = \frac{F_u + F_y}{2F_y} = \frac{65 + 50}{(2)(50)} = 1.15$$

$$R_y = 1.10 \text{ for A992 steel}$$

$$M_{pr} = (1.15)(1.1)(50)(144) = 9108^{\text{kips.in}}$$

*Determine the location of the plastic hinge in the beam:*

$$S_h = \min \left\{ \begin{array}{l} \frac{d_b}{2} = 10.5^{\text{in.}} \\ 3b_{bf} = 24.72^{\text{in.}} \end{array} \right\}$$

$$S_h = 10.5^{\text{in.}}$$

*Determine the beam length between plastic hinges:*

$$L_h = L_0 - d_c - 2S_h = 410 - 16.4 - (2)(10.5) = 372.6^{\text{in.}}$$

*Determine the shear force at the end of the beam:*

$$V_u = \frac{2M_{pr}}{L_h} = \frac{(2)(9108)}{372.6} = 48.89^{\text{kips}}$$

*Compute the moment expected at the face of the column:*

$$M_f = M_{pr} + V_u S_h$$

$$M_f = 9108 + (48.89)(10.5) = 9621.35^{\text{kips.in}}$$

End-plate moment connection configurations and preliminary values for the connection geometry

$$\left\{ \begin{array}{l} bp = 15^{\text{in.}} \in [9, 15]^{\text{in.}} \\ g = 5^{\text{in.}} \in [5, 6]^{\text{in.}} \\ p_{fi}, p_{f0} = 2^{\text{in.}} \in [1.625, 2]^{\text{in.}} \\ p_b = 3.5^{\text{in.}} \in [3.5, 3.75]^{\text{in.}} \\ h_1 = d_b + p_{fi} + p_b - \frac{t_{bf}}{2} = 26.2^{\text{in.}} \\ h_2 = h_1 - p_b = 22.7^{\text{in.}} \\ h_3 = h_2 - 2p_{fi} - t_{bf} = 18.085^{\text{in.}} \\ h_4 = h_3 - p_b = 14.585^{\text{in.}} \\ d_c = 2^{\text{in.}} \end{array} \right.$$

### The required bolt diameter

$$d_{\text{req'd}} = \sqrt{\frac{2M_f}{\pi\phi_f F_{nt} (h_1 + h_2 + h_3 + h_4)}}$$

The nominal tensile strength of bolt,  $F_{nt} = 113^{\text{ksi}}$

The reduction factor,  $\phi_f = 0.9$

$$d_{\text{req'd}} = \sqrt{\frac{(2)(9126.5)}{(\pi)(0.9)(113)(26.2 + 22.7 + 18.085 + 14.585)}} = 0.837 \rightarrow \text{use: } \frac{7}{8} \text{ bolt}$$

### The required end plate thickness

$$t_{\text{p,req'd}} = \sqrt{\frac{1.11M_f}{\phi_d F_{yp} Y_p}}$$

$$F_{yp} = 50^{\text{ksi}}$$

$$Y_p = \left(\frac{b_p}{2}\right) \left( \frac{h_1}{2d_e} + \frac{h_2}{p_n, p_{r0}} + \frac{h_3}{p_n, p_{r0}} + \frac{h_4}{s} \right) + \left(\frac{2}{g}\right) \left( (h_1) \left( d_e + \frac{p_b}{4} \right) + (h_2) \left( p_n, p_{r0} + \frac{3p_b}{4} \right) + (h_3) \left( p_n, p_{r0} + \frac{p_b}{4} \right) + (h_4) \left( s + \frac{3p_b}{4} \right) + p_b^2 \right) + g = 326.55^{\text{in.}}$$

$$t_{\text{p,req'd}} = \sqrt{\frac{(1.11)(9126.5)}{(1)(50)(326.55)}} = 0.787 \rightarrow \text{use: } 7/8^{\text{in.}} \text{ endplate thickness}$$

### The factored beam flange force

$$F_{fu} = \frac{M_f}{d_b - t_{bf}} = \frac{9126.5}{21 - 0.615} = 447.71^{\text{kips}}$$

### The bolt shear rupture strength of the connection

$$V_u \leq \phi_n R_n = \phi_n (n_b) F_{nv} A_b$$

$$\phi_n R_n = (0.9)(8)(84) \left( (\pi) \left( \frac{(7/8)^2}{4} \right) \right) = 363.68^{\text{kips}}$$

$$V_u = 363.68^{\text{kips}} \leq 447.71^{\text{kips}}$$



Check bolt-bearing/tear-out failure of the end-plate and column flange

$$V_u \leq \phi_n R_n = \phi_n (n_i) r_{ni} + \phi_n (n_o) r_{no}$$

$$\phi_n R_n = (0.9)(4)(91.875) + (0.9)(4)(91.875) = 661.5^{\text{kips}}$$

*For inner bolts:*

$$r_{ni} = 1.2L_c t F_u = (1.2)(3.5)(0.875)(50) = 183.75^{\text{kips}} < 2.4d_b t F_u = (2.4)(7/8)(0.875)(50) = 91.875^{\text{kips}}$$

*For outer bolts:*

$$r_{no} = 1.2L_c t F_u = (1.2)(2)(0.875)(50) = 105^{\text{kips}} < 2.4d_b t F_u = (2.4)(7/8)(0.875)(50) = 91.875^{\text{kips}}$$

### 3. Column-side design

Check the column flange for flexural yielding

$$t_{cf} \geq \sqrt{\frac{1.11M_f}{\phi_d F_{yc} Y_c}}$$

$$Y_c = \frac{b_{cf}}{2} \left[ h_1 \left( \frac{1}{s} \right) + h_4 \left( \frac{1}{s} \right) \right] + \frac{2}{g} \left[ h_1 \left( p_b + \frac{c}{s} + s \right) + h_2 \left( \frac{p_b}{2} + \frac{c}{4} \right) + h_3 \left( \frac{p_b}{2} + \frac{c}{2} \right) + h_4(s) \right] + \frac{g}{2} = 238.09^{\text{in.}}$$

$$s = \frac{1}{2} \sqrt{b_{cf} g} = 4.33^{\text{in.}}$$

$$t_{cf} \geq \sqrt{\frac{(1.11)(9126.5)}{(0.9)(50)(238.09)}} = 0.97 < 1.89^{\text{in.}}$$

Check the local column web yielding strength of the unstiffened column web at the beam flanges

$$F_u \leq \phi_d R_n$$

$$R_n = C_t (6k_c + t_{bf} + 2t_p) F_{yc} t_{cw}$$

$$R_n = (1)((6)(2.49) + 0.68 + (2)(0.875))(1.18)(50) = 1024.83^{\text{kips}}$$

$$\phi_d R_n = (0.9)(1024.83) = 922.347^{\text{kips}}$$

Check the unstiffened column web buckling strength at the beam compression flange

*F<sub>tu</sub> is applied at a distance greater than or equal to d<sub>c</sub>/2 from the end of the column:*

$$R_n = \frac{24t_{cw}^3 \sqrt{EF_{yc}}}{h}$$

$$h = d - 2t_{bf} = 16.4 - (2)(1.89) = 12.62^{\text{in.}}$$

$$R_n = \frac{(24)(1.18)^3 \sqrt{(29000)(50)}}{12.62} = 3762.5^{\text{kips}}$$

$$\phi R_n = (0.75)(3762.5) = 2821.91^{\text{kips}} > 580^{\text{kips}}$$

Check the unstiffened column web crippling strength at the beam compression flange

*F<sub>tu</sub> is applied at a distance greater than or equal to d<sub>c</sub>/2 from the end of the column:*

$$R_n = 0.8t_{cw}^2 \left[ 1 + 3 \left( \frac{N}{d_c} \right) \left( \frac{t_{cw}}{t_{cf}} \right)^{1.5} \right] \sqrt{\frac{EF_{yc} t_{cf}}{t_{cw}}}$$

$$N = b_f + 2w + 2t_p = 8.99 + (2)(0.875) = 10.74^{\text{in.}}$$

$$R_n = 0.8(1.18)^2 \left[ 1 + 3 \left( \frac{10.74}{16.4} \right) \left( \frac{1.18}{1.89} \right)^{1.5} \right] \sqrt{\frac{(29000)(1.89)}{1.18}} = 3342.85^{\text{kips}}$$

$$\phi R_n = (0.75)(3342.85) = 2507.14^{\text{kips}} > 580^{\text{kips}}$$

#### **4. Circular bolt pattern**

$$g_1 = \frac{b_p - 2e}{2} = \frac{15 - (2)(1.125)}{2} = 8.625^{\text{in.}}; g_2 = b_p - 2e = 15 - (2)(1.125) = 12.75^{\text{in.}} \quad [19]$$

Prying forces [65]

F1: Endplate flexural mechanism and B1 and B2 fracture:

$$T = 4T_{/beam1} + 4T_{/bolt} = (4)(27.81) + (4)(67.95) = 383.04^{\text{kips}}$$

$$T_{/beam1} = \frac{(62.8)(1+0.875)}{2.672+1.5625} = 27.81^{\text{kips}}; T_{/bolt} = (113)\left(\frac{\pi}{4}\right)\left(\left(\frac{7}{8}\right)^2\right) = 67.95^{\text{kips}};$$

$$M_{pl} = (1/4)(7.5)(7/8)^3(50) = 62.8^{\text{kips.in.}}; p = (4)(15)/8 = 7.5^{\text{in.}}; \delta = 1 - (0.875 + 1/16)/7.5 = 0.875$$

$$; a_1 = \frac{8.625 - 0.615}{2} - (0.8)(1.12) - ((7/8)/2) = 2.672^{\text{in.}}; b_1 = 1.125 + ((7/8)/2) = 1.5625^{\text{in.}}$$

F2: Column flange/endplate flexural mechanism and B4 fracture:

$$T = 4T_{/beam1} + 4T_{/beam1'} + 2T_{/bolt} = (4)(27.81) + 4(415.91) + 2(67.95) = 1910.78^{\text{kips}}$$

$$T_{/beam1'} = \frac{(675)(1+0.875)}{1.293+1.75} = 415.91^{\text{kips}}; M_{pl}' = (1/4)(8)(1.89)^3(50) = 675^{\text{kips.in.}}; p' = (4)(16)/8 = 8^{\text{in.}}$$

$$; \delta' = 0.875^{\text{in.}}; a_1' = \frac{8.625 - 1.18}{2} - (0.8)(2.49) - ((7/8)/2) = 1.293^{\text{in.}}; b_1' = 1.75^{\text{in.}}$$

F3: Column flange flexural mechanism and B4 fracture:

$$T = 4T_{/beam1'} + 2T_{/bolt} = (4)(415.91) + (2)(67.95) = 1799.54^{\text{kips}}$$

$$\rightarrow T = 383.05^{\text{kips}} \text{ controls}$$

Total prying forces:

$$Q_{\text{total}} = B_T - T_s = (8)(67.95) - 383.05 = 160.55^{\text{kips}}$$

Check the endplate thickness for flexural yielding

$$t_p \geq \sqrt{\frac{1.11M_f}{\phi_d F_{yp} Y_{pc}}}$$

$$Y_{pc} = b_p \left[ h_2 \left( \frac{1}{p_{fi}} \right) + h_3 \left( \frac{1}{p_{fi}} \right) + h_4 \left( \frac{1}{s} \right) \right] + \frac{2}{g_1} \left[ \left( s + \frac{b_p}{4} - \frac{e}{2} \right) h_4 \right] + \frac{2}{g_2} \left[ \left( p_{fi} + \frac{b_p}{2} - e \right) h_3 \right] = 302.6^{\text{in.}}$$

$$s = \frac{1}{2} \sqrt{b_p g} = 4.33^{\text{in.}}$$

Where  $M_f = M_{pr} + (V_u + Q_{total})S_h = 9126.5 + (48 + 160.55)(10.5) = 11325.62^{\text{kips.in.}}$

$$t_p \geq \sqrt{\frac{(1.11)(11325.56)}{(0.9)(50)(302.6)}} = 0.96^{\text{in.}} > \frac{7^{\text{in.}}}{8} \text{ use } \rightarrow t_p = 1^{\text{in.}}$$

where:

$Y_{pc}$  : unstiffened endplate yield line mechanism parameter for circular bolts pattern [65], in

Check the column flange thickness for flexural yielding

$$t_{cf} \geq \sqrt{\frac{F_u + Q_{total}}{\left[ 2\left(\frac{b_{cf}}{2s}\right) + 2(1 + 2p_b)\frac{1}{g_2} + 4(p_b + s)\frac{1}{g_1} \right] F_{yc}}}$$

$$t_{cf} \geq \sqrt{\frac{447.71 + 160.55}{\left[ 2\left(\frac{16}{(2)(4.33)}\right) + 2(4.615 + (2)(3.5))\frac{1}{12.75} + 4(3.5 + 4.33)\frac{1}{8.625} \right] (50)}} = 1.291^{\text{in.}} < 1.89^{\text{in.}}$$

### 5. Reduced beam section - RBS

$$0.5b_{bf} = 4.12^{\text{in.}} \leq a \leq 0.75b_{bf} = 6.18^{\text{in.}} \rightarrow \text{use : } a = \text{avg}(4.12, 6.18) = 5.15^{\text{in.}}$$

$$0.65d = 13.65^{\text{in.}} \leq b \leq 0.85d = 17.85^{\text{in.}} \rightarrow \text{use : } b = \text{avg}(13.65, 17.85) = 15.75^{\text{in.}}$$

$$0.1b_{bf} = 0.824^{\text{in.}} \leq c \leq 0.25b_{bf} = 2.06^{\text{in.}} \rightarrow \text{use : } c = \text{avg}(0.824, 2.06) = 1.442^{\text{in.}}$$

$$Z_{RBS} = Z_x - 2ct_{bf}(d - t_{bf}) = 144 - (2)(1.442)(0.615)(21 - 0.615) = 107.84^{\text{in.}^3}$$

$$M_{pr} = (1.15)(1.1)(50)(107.84) = 6820.88^{\text{kips.in}}$$

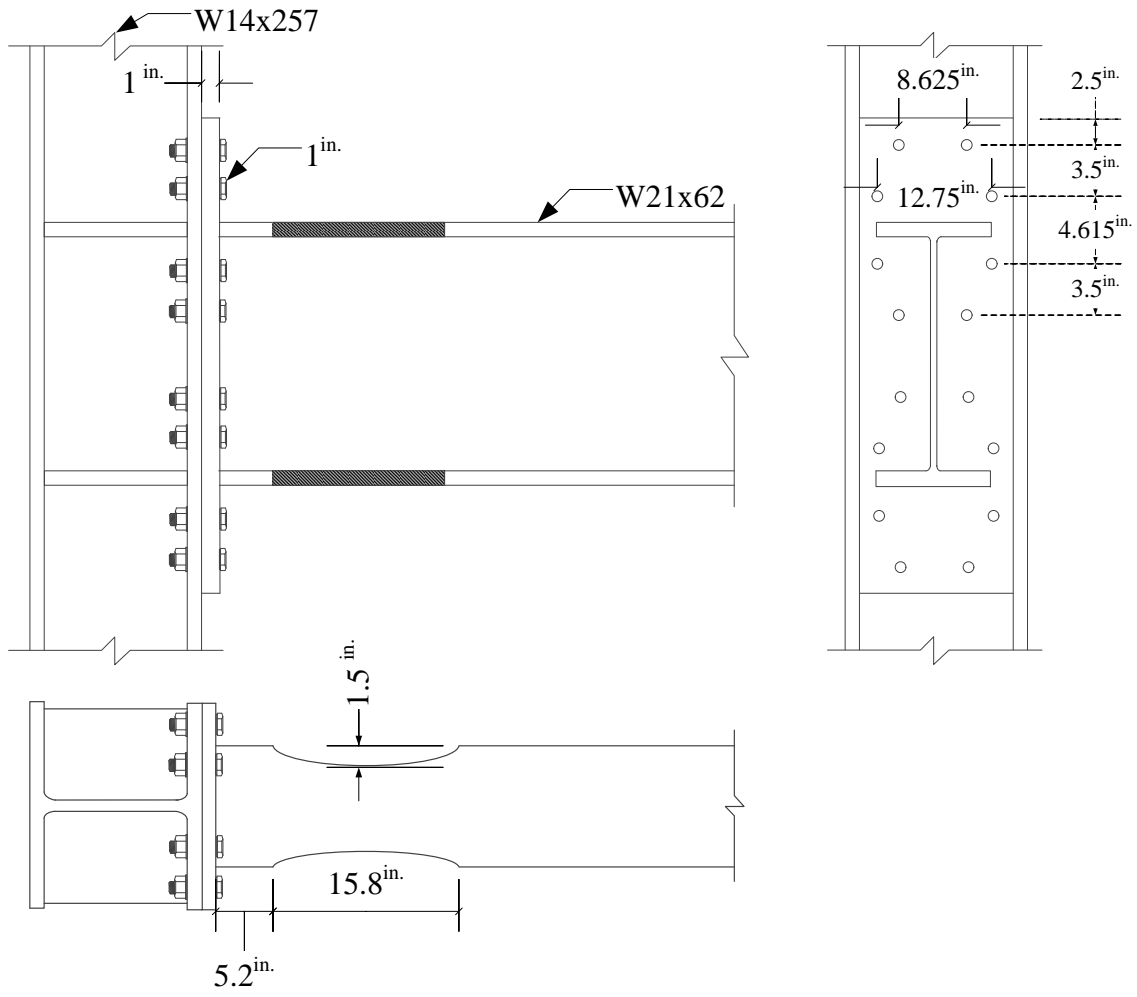


**Figure. 56.** Connection details: W21x62

## B. W18x55 beam section

### 1. Prequalification limits

#### Beam Limitations

- ✓ Beam is rolled wide flange
  - ✓ Beam depth is W18 < W36
  - ✓ Beam weight is  $55 \frac{\text{lb}}{\text{ft.}} < 150 \frac{\text{lb}}{\text{ft.}}$
  - ✓ Beam flange thickness:  $t_{bf} = 0.63^{\text{in.}} < 1^{\text{in.}}$
  - ✓ Clear span to depth  $\frac{410}{18.1} = 22.65 > 9$  for SMF
  - ✓ Beam flange slenderness:  $\frac{b_{bf}}{2t_{bf}} = 5.98 < 0.3 \sqrt{\frac{E}{F_{yb}}} = 6.89$
  - ✓ Beam web slenderness:  $\frac{h}{t_{bw}} = 41.1 < 2.45 \sqrt{\frac{E}{F_{yb}}} = 56.26$
- No local buckling of beam
- ✓ Lateral bracing shall be provided:

Both beam flanges should be laterally braced at intervals not to exceed (ANSI/AISC 341-16 [3]):

$$L_{b\max} = 0.086r_y \left( \frac{E}{F_y} \right) = 6.31^{\text{ft.}}$$

The limiting length:

$$L_p = 1.76r_y \sqrt{\left( \frac{E}{F_y} \right)} = 5.62^{\text{ft.}}$$

$$L_r = 1.95r_{ts} \frac{E}{0.7F_y} \sqrt{\left(\frac{JC}{S_x h_0}\right)^2 + \sqrt{\left(\frac{JC}{S_x h_0}\right)^2 + 6.76 \left(\frac{0.7F_y}{E}\right)^2}} = 17.5\text{ft.}$$

Provide braces at maximum of 5.5<sup>ft.</sup> outside the protected zone.

The beam is adequate for use in high seismic areas.

### Column Limitations

- ✓ Column is rolled wide flange
  - ✓ Beam connected to column flange
  - ✓ Column depth is W14 ≤ W14
  - ✓ Column flange slenderness:  $\frac{b_{cf}}{2t_{cf}} = 4.23 < 0.3 \sqrt{\frac{E}{F_{yc}}} = 6.89$
  - ✓ Column web slenderness:  $\frac{h}{t_{cw}} = 9.71 < 2.45 \sqrt{\frac{E}{F_{yc}}} = 56.27$
- No local buckling of column

The column is adequate for use in high seismic areas.

## **2. Endplate and bolt design**

### Moment at the Face of Column

Compute the probable maximum moment at the beam hinge:

$$M_{pr} = C_{pr} F_y R_y Z_e$$

where:

$$C_{pr} = \frac{F_u + F_y}{2F_y} = \frac{65 + 50}{(2)(50)} = 1.15$$

$$R_y = 1.10 \text{ for A992 steel}$$

$$M_{pr} = (1.15)(1.1)(50)(112) = 7084^{\text{kips.in}}$$

Determine the location of the plastic hinge in the beam:

$$S_h = \min \left\{ \begin{array}{l} \frac{d_b}{2} = 9.05^{\text{in.}} \\ 3b_{bf} = 22.59^{\text{in.}} \end{array} \right\}$$

$$S_h = 9.05^{\text{in.}}$$

Determine the beam length between plastic hinges:

$$L_h = L_0 - d_c - 2S_h = 410 - 16.4 - (2)(9.05) = 375.5^{\text{in.}}$$

Determine the shear force at the end of the beam:

$$V_u = \frac{2M_{pr}}{L_h} = \frac{(2)(7084)}{375.5} = 37.73^{\text{kips}}$$

Compute the moment expected at the face of the column:

$$M_f = M_{pr} + V_u S_h$$

$$M_f = 7084 + (37.73)(9.05) = 7425.5^{\text{kips.in}}$$

End-plate moment connection configurations and preliminary values for the connection geometry

$$\left\{ \begin{array}{l} bp = 15^{\text{in.}} \in [9, 15]^{\text{in.}} \\ g = 5^{\text{in.}} \in [5, 6]^{\text{in.}} \\ p_{fi}, p_{fo} = 2^{\text{in.}} \in [1.625, 2]^{\text{in.}} \\ p_b = 3.5^{\text{in.}} \in [3.5, 3.75]^{\text{in.}} \\ h_1 = d_b + p_{fi} + p_b - \frac{t_{bf}}{2} = 23.29^{\text{in.}} \\ h_2 = h_1 - p_b = 19.79^{\text{in.}} \\ h_3 = h_2 - 2p_{fi} - t_{bf} = 15.155^{\text{in.}} \\ h_4 = h_3 - p_b = 11.66^{\text{in.}} \\ d_c = 2^{\text{in.}} \end{array} \right.$$



### The required bolt diameter

$$d_{\text{req'd}} = \sqrt{\frac{2M_f}{\pi\phi_f F_{nt} (h_1 + h_2 + h_3 + h_4)}}$$

The nominal tensile strength of bolt,  $F_{nt} = 113^{\text{ksi}}$

The reduction factor,  $\phi_f = 0.9$

$$d_{\text{req'd}} = \sqrt{\frac{(2)(7425.5)}{(\pi)(0.9)(113)(23.29 + 19.79 + 15.155 + 11.66)}} = 0.815 \rightarrow \text{use : } \frac{7}{8}^{\text{in.}} \text{ bolt}$$

### The required end plate thickness

$$t_{\text{p,req'd}} = \sqrt{\frac{1.11M_f}{\phi_d F_{yp} Y_p}}$$

$$F_{yp} = 50^{\text{ksi}}$$

$$Y_p = \left(\frac{b_p}{2}\right) \left( \frac{h_1}{2d_e} + \frac{h_2}{p_n, p_{r0}} + \frac{h_3}{p_n, p_{r0}} + \frac{h_4}{s} \right) + \left(\frac{2}{g}\right) \left( (h_1) \left( d_e + \frac{p_b}{4} \right) + (h_2) \left( p_n, p_{r0} + \frac{3p_b}{4} \right) + (h_3) \left( p_n, p_{r0} + \frac{p_b}{4} \right) + (h_4) \left( s + \frac{3p_b}{4} \right) + p_b^2 \right) + g = 280.4^{\text{in.}}$$

$$t_{\text{p,req'd}} = \sqrt{\frac{(1.11)(7425.5)}{(1)(50)(280.4)}} = 0.767 \rightarrow \text{use : } 7/8^{\text{in.}} \text{ endplate thickness}$$

### The factored beam flange force

$$F_{fu} = \frac{M_f}{d_b - t_{bf}} = \frac{7425.5}{18.1 - 0.63} = 425.04^{\text{kips}}$$

### The bolt shear rupture strength of the connection

$$V_u \leq \phi_n R_n = \phi_n (n_b) F_{nv} A_b$$

$$\phi_n R_n = (0.9)(8)(84) \left( (\pi) \left( \frac{(7/8)^2}{4} \right) \right) = 363.68^{\text{kips}}$$

$$V_u = 363.68^{\text{kips}} \leq 425.04^{\text{kips}}$$

Check bolt-bearing/tear-out failure of the end-plate and column flange

$$V_u \leq \phi_n R_n = \phi_n (n_i) r_{ni} + \phi_n (n_o) r_{no}$$

$$\phi_n R_n = (0.9)(4)(91.875) + (0.9)(4)(91.875) = 661.5^{\text{kips}}$$

*For inner bolts:*

$$r_{ni} = 1.2L_c t F_u = (1.2)(3.5)(0.875)(50) = 183.75^{\text{kips}} < 2.4d_b t F_u = (2.4)(7/8)(0.875)(50) = 91.875^{\text{kips}}$$

*For outer bolts:*

$$r_{no} = 1.2L_c t F_u = (1.2)(2)(0.875)(50) = 105^{\text{kips}} < 2.4d_b t F_u = (2.4)(7/8)(0.875)(50) = 91.875^{\text{kips}}$$

### 3. Column-side design

Check the column flange for flexural yielding

$$t_{cf} \geq \sqrt{\frac{1.11M_f}{\phi_d F_{yc} Y_c}}$$

$$Y_c = \frac{b_{cf}}{2} \left[ h_1 \left( \frac{1}{s} \right) + h_4 \left( \frac{1}{s} \right) \right] + \frac{2}{g} \left[ h_1 \left( p_b + \frac{c}{s} + s \right) + h_2 \left( \frac{p_b}{2} + \frac{c}{4} \right) + h_3 \left( \frac{p_b}{2} + \frac{c}{2} \right) + h_4(s) \right] + \frac{g}{2} = 173.5^{\text{in.}}$$

$$s = \frac{1}{2} \sqrt{b_{cf} g} = 3.07^{\text{in.}}$$

$$t_{cf} \geq \sqrt{\frac{(1.11)(7425.5)}{(0.9)(50)(173.5)}} = 1.03 < 1.89^{\text{in.}}$$

Check the local column web yielding strength of the unstiffened column web at the beam flanges

$$F_u \leq \phi_d R_n$$

$$R_n = C_t (6k_c + t_{bf} + 2t_p) F_{yc} t_{cw}$$

$$R_n = (1)((6)(2.49) + 0.68 + (2)(0.875))(1.18)(50) = 1024.83^{\text{kips}}$$

$$\phi_d R_n = (0.9)(1024.83) = 922.347^{\text{kips}}$$

Check the unstiffened column web buckling strength at the beam compression flange

*F<sub>fu</sub> is applied at a distance greater than or equal to d<sub>c</sub>/2 from the end of the column:*

$$R_n = \frac{24t_{cw}^3 \sqrt{EF_{yc}}}{h}$$

$$h = d - 2t_{bf} = 16.4 - (2)(1.89) = 12.62^{\text{in.}}$$

$$R_n = \frac{(24)(1.18)^3 \sqrt{(29000)(50)}}{12.62} = 3762.5^{\text{kips}}$$

$$\phi R_n = (0.75)(3762.5) = 2821.91^{\text{kips}} > 580^{\text{kips}}$$

Check the unstiffened column web crippling strength at the beam compression flange

*F<sub>fu</sub> is applied at a distance greater than or equal to d<sub>c</sub>/2 from the end of the column:*

$$R_n = 0.8t_{cw}^2 \left[ 1 + 3 \left( \frac{N}{d_c} \right) \left( \frac{t_{cw}}{t_{cf}} \right)^{1.5} \right] \sqrt{\frac{EF_{yc} t_{cf}}{t_{cw}}}$$

$$N = b_f + 2w + 2t_p = 8.99 + (2)(0.875) = 10.74^{\text{in.}}$$

$$R_n = 0.8(1.18)^2 \left[ 1 + 3 \left( \frac{10.74}{16.4} \right) \left( \frac{1.18}{1.89} \right)^{1.5} \right] \sqrt{\frac{(29000)(1.89)}{1.18}} = 3342.85^{\text{kips}}$$

$$\phi R_n = (0.75)(3342.85) = 2507.14^{\text{kips}} > 580^{\text{kips}}$$

#### **4. Circular bolt pattern**

$$g_1 = \frac{b_p - 2e}{2} = \frac{15 - (2)(1.125)}{2} = 8.625^{\text{in.}}; g_2 = b_p - 2e = 15 - (2)(1.125) = 12.75^{\text{in.}} \quad [19]$$

Prying forces [65]

F1: Endplate flexural mechanism and B1 and B2 fracture:

$$T = 4T_{/beam1} + 4T_{/bolt} = (4)(27.39) + (4)(67.95) = 381.36^{\text{kips}}$$

$$T_{/beam1} = \frac{(62.8)(1+0.875)}{2.736+1.5625} = 27.39^{\text{kips}}; T_{/bolt} = (113)\left(\frac{\pi}{4}\right)\left(\left(\frac{7}{8}\right)^2\right) = 67.95^{\text{kips}};$$

$$M_{pl} = (1/4)(7.5)(7/8)^3(50) = 62.8^{\text{kips.in.}}; p = (4)(15)/8 = 7.5^{\text{in.}}; \delta = 1 - (0.875 + 1/16)/7.5 = 0.875$$

$$; a_1 = \frac{8.625 - 0.63}{2} - (0.8)(1.03) - ((7/8)/2) = 2.736^{\text{in.}}; b_1 = 1.125 + ((7/8)/2) = 1.5625^{\text{in.}}$$

F2: Column flange/endplate flexural mechanism and B4 fracture:

$$T = 4T_{/beam1} + 4T_{/beam1'} + 2T_{/bolt} = (4)(27.39) + 4(415.91) + 2(67.95) = 1909.1^{\text{kips}}$$

$$T_{/beam1'} = \frac{(675)(1+0.875)}{1.293+1.75} = 415.91^{\text{kips}}; M_{pl}' = (1/4)(8)(1.89)^3(50) = 675^{\text{kips.in.}}; p' = (4)(16)/8 = 8^{\text{in.}}$$

$$; \delta' = 0.875^{\text{in.}}; a_1' = \frac{8.625 - 1.18}{2} - (0.8)(2.49) - ((7/8)/2) = 1.293^{\text{in.}}; b_1' = 1.75^{\text{in.}}$$

F3: Column flange flexural mechanism and B4 fracture:

$$T = 4T_{/beam1'} + 2T_{/bolt} = (4)(415.91) + (2)(67.95) = 1799.54^{\text{kips}}$$

$$\rightarrow T = 381.36^{\text{kips}} \text{ controls}$$

Total prying forces:

$$Q_{\text{total}} = B_T - T_s = (8)(67.95) - 381.36 = 162.24^{\text{kips}}$$

Check the endplate thickness for flexural yielding

$$t_p \geq \sqrt{\frac{1.11M_f}{\phi_d F_{yp} Y_{pc}}}$$

$$Y_{pc} = b_p \left[ h_2 \left( \frac{1}{p_{fi}} \right) + h_3 \left( \frac{1}{p_{fi}} \right) + h_4 \left( \frac{1}{s} \right) \right] + \frac{2}{g_1} \left[ \left( s + \frac{b_p}{4} - \frac{e}{2} \right) h_4 \right] + \frac{2}{g_2} \left[ \left( p_{fi} + \frac{b_p}{2} - e \right) h_3 \right] = 286.93^{\text{in.}}$$

$$s = \frac{1}{2} \sqrt{b_p g} = 3.07^{\text{in.}}$$

Where  $M_f = M_{pr} + (V_u + Q_{total})S_h = 7425.5 + (37.73 + 162.24)(9.05) = 9235.23 \text{ kips.in.}$

$$t_p \geq \sqrt{\frac{(1.11)(9235.23)}{(0.9)(50)(286.93)}} = 0.891 \text{ in.} > \frac{7}{8} \text{ use } \rightarrow t_p = 1 \text{ in.}$$

where:

$Y_{pc}$  : unstiffened endplate yield line mechanism parameter for circular bolts pattern [65], in

d. Check the column flange thickness for flexural yielding

$$t_{cf} \geq \sqrt{\frac{F_u + Q_{total}}{\left[ 2 \left( \frac{b_{cf}}{2s} \right) + 2(1 + 2p_b) \frac{1}{g_2} + 4(p_b + s) \frac{1}{g_1} \right] F_{yc}}}$$

$$t_{cf} \geq \sqrt{\frac{425.04 + 162.24}{\left[ 2 \left( \frac{16}{(2)(3.07)} \right) + 2(4.63 + (2)(3.5)) \frac{1}{12.75} + 4(3.5 + 3.07) \frac{1}{8.625} \right] (50)}} = 1.08 \text{ in.} < 1.89 \text{ in.}$$

### 5. Reduced beam section - RBS

$$0.5b_{bf} = 3.77 \text{ in.} \leq a \leq 0.75b_{bf} = 5.65 \text{ in.} \rightarrow \text{use : } a = \text{avg}(3.77, 5.65) = 4.7 \text{ in.}$$

$$0.65d = 11.77 \text{ in.} \leq b \leq 0.85d = 15.39 \text{ in.} \rightarrow \text{use : } b = \text{avg}(11.77, 15.39) = 13.6 \text{ in.}$$

$$0.1b_{bf} = 0.753 \text{ in.} \leq c \leq 0.25b_{bf} = 1.88 \text{ in.} \rightarrow \text{use : } c = \text{avg}(0.753, 1.88) = 1.35 \text{ in.}$$

$$Z_{RBS} = Z_x - 2ct_{bf}(d - t_{bf}) = 112 - (2)(1.35)(0.63)(18.1 - 0.63) = 82.28 \text{ in.}^3$$

$$M_{pr} = (1.15)(1.1)(50)(82.28) = 5204.43 \text{ kips.in}$$

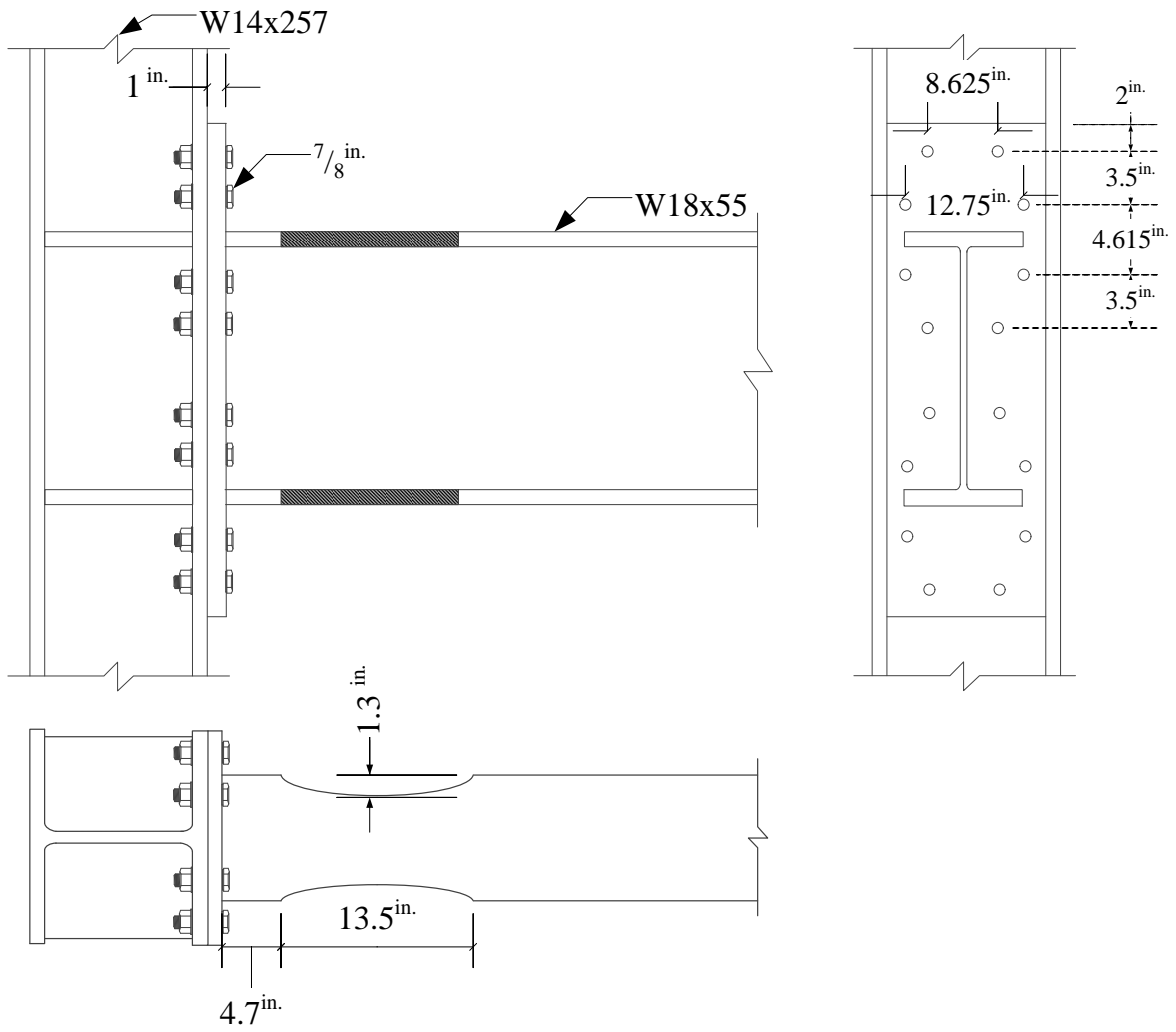


**Figure. 57.** Connection details: W18x55

